GAZİ ÜNİVERSİTESİ

Gazi

1926

NONLINEAR FE ANALYSIS OF BOND-SLIP BEHAVIOR OF CONCRETE STRENGTHENED WITH ANCHORAGED CFRP STRIP

A THESIS SUBMITTED TO
THE GRADUATE SCHOOL OF NATURAL AND APPLIED SCIENCES
OF
GAZİ UNIVERSITY

BY

Shaimaa Tariq Sakin SAKIN

IN PARTIAL FULFILLMENT OF THE REQUIREMENTS
FOR
THE DEGREE OF DOCTOR OF PHILOSOPHY
IN
CIVIL ENGINEERING

JUNE 2018

The thesis study titled "NONLINEAR FE ANALYSIS OF BOND-SLIP BEHAVIOR OF CONCRETE STRENGTHENED WITH ANCHORAGED CFRP STRIP" is submitted by Shaimaa Tariq Sakin SAKIN in partial fulfillment of the requirements for the degree of Doctor of Philosophy in the Department of Civil Engineering, Gazi University by the following committee.

Supervisor: Prof. Dr. Özgür ANIL
Civil Engineering, Gazi University
I certify that this thesis is a graduate thesis in terms of quality and content …..………..…………..

Chairman: Prof. Dr. Mustafa ŞAHMARAN Civil
Engineering Department, Hacettepe University
I certify that this thesis is a graduate thesis in terms of quality and content …..………..…………..

Member: Prof. Dr. Kurtuluş SOYLUK
Civil Engineering Department, Gazi University
I certify that this thesis is a graduate thesis in terms of quality and content …..………..…………..

Member: Assoc. Prof. Dr. Mehmet BARAN
Civil Engineering Department, Yıldırım Beyazıt University
I certify that this thesis is a graduate thesis in terms of quality and content …..………..…………..

Member: Lecturer Dr. Yağmur KOPRAMAN
Civil Engineering Department, Gazi University
I certify that this thesis is a graduate thesis in terms of quality and content …..………..…………..

Date: 08/06/2018

I certify that this thesis, accepted by the committee, meets the requirements for being a Doctor of Philosophy Thesis.

………………………..…….
Prof. Dr. Sena YAŞYERLİ
Dean of Graduate School of Natural and Applied Sciences

ETHICAL STATEMENT

I hereby declare that in this thesis study I prepared in accordance with thesis writing rules of Gazi University Graduate School of Natural and Applied Sciences;

- All data, information and documents presented in this thesis have been obtained within the scope of academic rules and ethical conduct,
- All information, documents, assessments and results have been presented in accordance with scientific ethical conduct and moral rules,
- All material used in this thesis that are not original to this work have been fully cited and referenced,
- No change has been made in the data used,
- The work presented in this thesis is original,

or else, I admit all loss of rights to be incurred against me.

Shaimaa Tariq Sakin SAKIN

08/06/2018

NONLINEAR FE ANALYSIS OF BOND-SLIP BEHAVIOR OF CONCRETE STRENGTHENED WITH ANCHORAGED CFRP STRIP

(Ph. D. Thesis)

Shaimaa Tariq Sakin SAKIN

GAZİ UNIVERSITY

GRADUATE SCHOOL OF NATURAL AND APPLIED SCIENCES

June 2018

ABSTRACT

The last decades have witnessed an increasing interest in using carbon fiber reinforced polymer (CFRP) for the strengthening of structural members. This could be ascribed to the distinctive properties of (CFRP) which contributed to improve the strength and the ductility of the strengthened elements without adding stiffness. But, the occurrence of debonding failure causes the loss of composite action between CFRP strip and concrete substrate at early stage and that leads to a brittle failure at low loading and prevent the CFRP from reaching its full strength. Many researchers have been studied this phenomenon and they found that the usage of anchorage systems can prevent or delay the process of debonding, increase the bonding strength or in some cases provide a ductile failure instead of the sudden, brittle failure. The current study aimed to create a bond-slip model for anchored CFRP strip and propose an equation for calculating the bonding strength of anchored CFRP strip. Therefore, three-dimensional finite element simulation via ANSYS (version 15) was conducted to understand the complex behavior of the structural members strengthened with anchored CFRP strip. The existence of proper finite element model for CFRP anchor will allow to accurately simulate the behavior of the anchored system. Therefore, a new approach to represent the CFRP anchors in finite element analysis is produced. The CFRP anchor effect is represented by increasing the bonding strength at the interface over a specific area where the CFRP anchors penetrate the concrete by using the bond-slip model proposed by Mertoğlu et al. after modification. The parameters of the modified bond-slip model were estimated by fitting of the finite element analysis results to available experimental results from the literature. Then, the analytical model was used for further analyses to investigate the influence of several parameters which were not examined experimentally such as concrete strength, strip width, number of anchorages and bond length. Finally, the overall results were used for proposing an equation to calculate the bond strength of the anchored system.

Science Code	:	91120
Key Words	:	CFRP strip; CFRP anchor; Debonding; Bond-slip model; CZM model.
Page Number	:	92
Supervisor	:	Prof. Dr. Özgür ANIL

ANKRAJLI CFRP ŞERİTLER İLE BETON YÜZEY ARASINDAKİ GERİLME DEFORMASYON DAĞILIMININ LİNEER OLMAYAN SONLU ELEMAN ANALİZİ

(Doktora Tezi)

Shaimaa Tariq Sakin SAKIN

GAZİ ÜNİVERSİTESİ

FEN BİLİMLERİ ENSTİTÜSÜ

Haziran 2018

ÖZET

Yapı elemanlarının güçlendirilmesi konusunda karbon fiber takviyeli polimerin (CFRP) kullanımına olan ilgi, son yıllarda artmıştır. Bu ilgi, rijitliği arttırılmadan güçlendirilen elemanın, dayanımının ve sünekliğinin iyileştirilmesine katkıda bulunan CFRP'nin ayırt edici özelliklerine bağlanabilir. Ancak, erken aşamalarda sıyrılma probleminin oluşması, beton yüzey ile CFRP şerit arasında kompozit davranışın kaybına ve CFRP'nin tam dayanıma ulaşmadan küçük yüklerde gevrek bir göçmeye neden olur. Bir çok araştırmacı bu olgu hakkında çalışmalar yürütmüştür ve araştırmacılar, sıyrılma dayanımını arttıran ve bazı durumlarda, ani gevrek bir göçme yerine daha sünek bir göçme temin eden, sıyrılma sürecini erteleyebilen ya da önleyebilen ankraj sistemlerinin kullanımını keşfetmişlerdir. Bu çalışma kapsamında ankrajlı CFRP şeritler için bir bond-slip modelinni oluşturlması amaçlanmış ve ankrajlı CFRP şerltleri taşıma gücünün hesaplanabilmesi için bir eşitlik önerilmiştir. Bu nedenle, ankrajlı CFRP şerit ile güçlendirilmiş yapısal elemanların karmaşık davranışını kavramak için, ANSYS (versiyon 15) aracılığı ile 3 boyutlu sonlu eleman modeli oluşturulmuştur. Sonlu eleman analizinde CFRP ankrajları temsil etmek için yeni bir yaklaşım üretilmiştir. CFRP ankraj için uygun sonlu eleman modelinin varlığı ise ankraj sisteminin davranışını doğru bir şekilde simüle etmeyi sağlamıştır. CFRP ankrajın etkisi, Mertoğlu ve arkadaşları tarafından değişikliklerden sonra önerilen sıyrılma-kayma modeli kullanılarak, CFRP ankrajların beton içerisine yerleştirildiği belirli bir alandaki ara yüzde sıyrılma mukavemetinin arttırılması aracılığıyla temsil edilmiştir. Değiştirilen sıyrılma-kayma modelinin parametreleri, sonlu elemanlar analizi sonuçlarının literatürden elde edilen deneysel sonuçlarla doğrulanması ile tahmin edilmiştir. Sonrasında analitik model, beton mukavemeti, şerit genişliği, ankraj sayısı, yapışma uzunluğu gibi deneysel olarak incelenmeyen çeşitli parametrelerin etkisini araştırmak için daha ileri analizlerde kullanılmıştır. Son olarak, tüm sonuçlardan, ankraj sisteminin sıyrılma mukavemetinin hesaplanması konusunda, bir denklem önermek için faydalanılmıştır.

Bilim Kodu	:	91120
Anahtar Kelimeler	:	CFRP şeritler, CFRP ankraj, Sıyrılma, Sıyrılma-kayma modeli, CZM modeli.
Sayfa Adedi	:	92
Danışman	:	Prof. Dr. Özgür ANIL

ACKNOWLEDGMENTS

I would like to express my sincere thanks and deep gratitude to my supervisor Prof. Dr. Özgür ANIL for his advice, kindness, guidance, and encouragement throughout this work. Thanks are also expressed to the Head and staff of the Department for providing facilities and assistance throughout the duration of the study. I also wish to thank my parents and my dear sister Dunia SAKIN for their patience and care during the research period.

Shaimaa Tariq Sakin SAKIN

TABLE OF CONTENTS

Page

Page

LIST OF TABLES

Table **Page**

LIST OF FIGURES

Figure **Page**

Figure **Page**

SYMBOLS AND ABBREVIATIONS

The notations and abbreviations along with their explanations used in the current study are presented below

Symbol	Explanation
$\boldsymbol{E_c}$	Modulus of elasticity of concrete; MPa
$\boldsymbol{E_f}$	Modulus of elasticity of CFRP; GPa
$\boldsymbol{G_f}$	Interfacial fracture energy of unanchored system; N/mm
$\boldsymbol{G_{f-anchor}}$	Interfacial fracture energy of anchored system; N/mm
$\boldsymbol{K_0}$	Initial stiffness of bond slip curve of unanchored system; N/mm^3
$\boldsymbol{K_{0\_anchor}}$	Initial stiffness of bond slip curve of anchored system; N/mm^3
$\boldsymbol{b_c}$	Width of concrete prism; mm
$\boldsymbol{b_f}$	Width of CFRP strip; mm
$\boldsymbol{f'_c}$	Concrete cylinder compressive strength; MPa
$\boldsymbol{f_c}$	Stress of concrete at any strain; Mpa
$\boldsymbol{f_t}$	Concrete tensile strength; MPa
$\boldsymbol{t_f}$	Thickness of CFRP strip; mm
$\boldsymbol{\beta_w}$	Width ratio factor
$\boldsymbol{\varepsilon}$	Strain of concrete at any stress
$\boldsymbol{\varepsilon_o}$	Strain of concrete at the ultimate compressive strength
$\boldsymbol{\tau_{max}}$	Maximum local shear stress of unanchored system, MPa
$\boldsymbol{\tau_{max-anchor}}$	Maximum local shear stress of anchored system, MPa
L	Bonding length; mm
Le	Effective bonding length; mm
$\mathbf{L_{end}}$	The distance from anchor to the plate free end; mm
N	Number of anchors
Pn	Average normalized bond strength
$\mathbf{P_u}$	Ultimate bonding strength; KN
$\boldsymbol{s_0}$	Local slip at maximum shear stress; mm

Symbol	Explanation
s_f	Local slip at completion of debonding; mm
$s_{f\text{-}anchor}$	Local slip at completion of debonding; mm

Abbreviations	Explanation
CBDD	Bilinear material behavior with traction and separation distance
CBDE	Bilinear material behavior with traction and critical fraction energy
CFRP	Carbon fiber reinforced polymer
CZM	Cohesive zone model
FE	Finite element
RC	Reinforced concrete

1. INTRODUCTION

Fiber-reinforced polymer (FRP) is a composite laminate that consisting of small diameter fibers embedded in a polymer matrix as shown in Figure 1.1 below. The fibers provide the main reinforcement while the polymer matrix acts as a binder holding the fibers in the composite, protecting fibers from direct exposure to the environment, transferring the stresses through the fiber–matrix interface to the fibers, and resisting some of the applied load, especially transverse normal stresses and interlaminar shear stresses. The fibers are typically made of glass, carbon, and aramid. The most widely used fibers in industry are carbon fibers or graphite fibers due to their high stiffness and strength as well as environmental stability (ACI 440.2R-02, 2002; Rasheed, 2015).

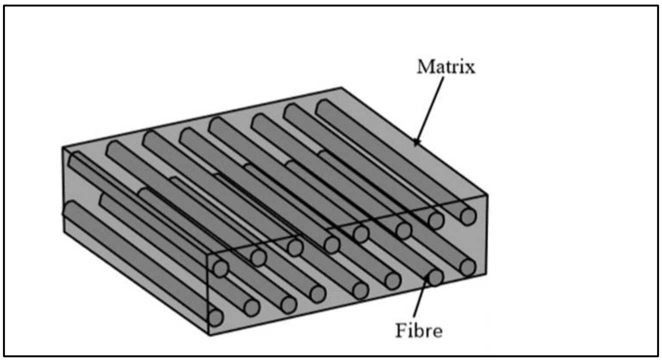

Figure 1.1. A typical unidirectional FRP plate (Obaidat, 2011)

The development of FRP started in the aerospace industry in the mid-1950s (Rasheed, 2015). Since 1980, the designers started to consider this material as a good alternative for strengthening and retrofitting of the concrete members which are subjected to heavier loading, environmental degradation or for correcting the deficiency in construction or design. The selective of the FRP material for the previously mentioned purposes could be attributed to its high tensile strength, light weight, ease of installation specially in limited area where the using of the traditional techniques is difficult, corrosion resistance, flexibility to apply on surfaces having different shapes as well as its ability to improve the strength and ductility of the structural elements (ACI 440.2R-08, 2008; Mertoğlu, Anıl and Durucan, 2016; Kalfat, Al-Mahaidi and Smith, 2013; Hosseini and Mostofinejad, 2013).

The externally bonded FRP strengthening system is one of the strengthening techniques used for repairing and retrofitting of the reinforced concrete (RC) structures, in which the FRP strips are attached to exterior tensile faces of structural members via adhesives or epoxies in order to increase the shear and flexural capacity as shown in Figure 1.2. (Belarba and Acun, 2013; Khalifa, 2016).

Figure 1.2. Concrete beam strengthened with CFR (Rasheed, 2015)

But this strengthening technique is prone to premature debonding failure as observed in several cases and reported in the literature (Figure 1.3). This type of failure is occurred due to the generation of high shear and normal stresses at FRP- concrete interface at the plate ends or at the areas around the flexural and shear cracks which are known as intermediate crack debonding (IC debonding) (Smith and Teng, 2002). The high shear stress at the end of the FRP plate lead to generate micro crack in the adjacent concrete layer and this crack will propagate to the level of tensile reinforcement and extend horizontally along the bottom of the tension steel reinforcement while the normal stresses causes the FRP sheets to pull away from the concrete until most of the FRP sheets is no longer attached to the reinforced concrete beam leading to the loss of composite action between CFRP strip and concrete substrate at low load and prevents the CFRP from reaching its full strength (Niemitz, James, and Breña, 2010; Grelle and Sneed, 2013; Buyukozturk, Gunes and Karaca, 2004).

Figure 1.3. Debonding Failure

The debonding at a shear or flexural cracks occur in a similar manner, where the debonding started from such cracks and then propagates toward the plate end. The surface level offset in shrear crack leading to the generation of the normall stresses while the crack widening drive debonding in flexural cracks (Obaidat, 2011). Figure 1.4 shows types of debonding modes. The debonding failure mode was not observed in beams retrofitted with complete FRP wrap while it was the main failure mode for beams strengthened on sides only (Belarba and Acun, 2013).

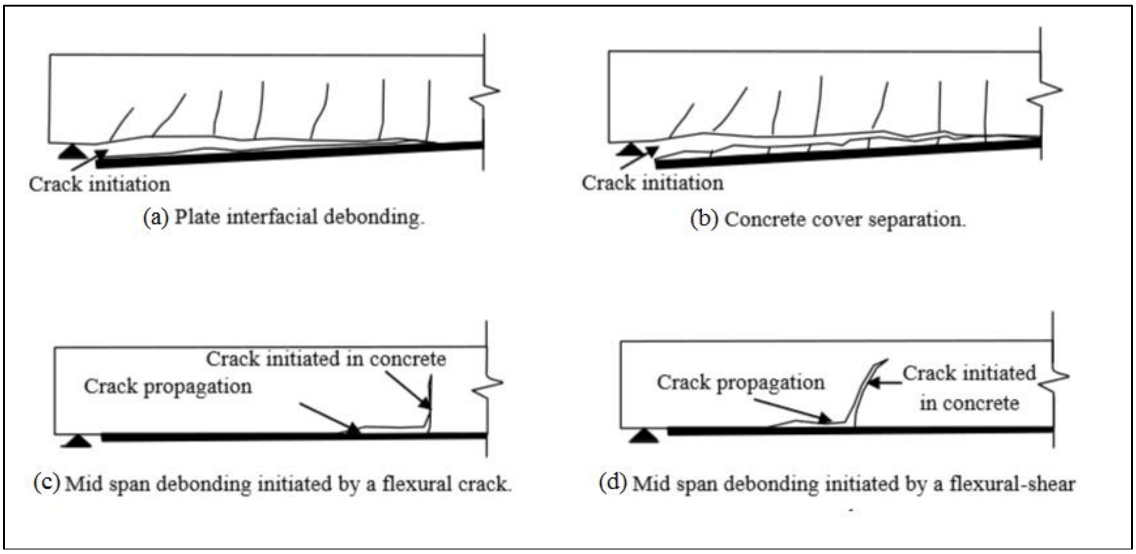

Figure 1.4. Debonding types in concrete beams (Obaidat, 2011).

A large number of experimental and theoretical studies which had been conducted to understand this phenomenon concluded that the use of anchorages improve the efficiency of the strengthening system. The using of anchorage systems can prevent or delay the process of debonding, by providing an alternate stress transfer mechanism at critical locations of structural members (Ceroni, Pecce, Matthys and Taerwe, 2008), provides higher levels of fiber utilization prior to debonding failure and in some cases provide a ductile failure instead of the typical sudden, brittle failure mode (Kalfat, Al-Mahaidi and Smith, 2013). Some of the studies connected the increment in ductility or in the bonding strength to the position of anchors. For instance, an experimental study conducted by Brena et al. (Brena and McGuirk, 2013) showed that increasing the spacing between the anchors in the longitudinal direction increases the ductility, on the contrary, decreasing the distance between anchors especially within the effective area of the FRP strip can increase the bonding strength significantly. Where in the first case, the anchor/ anchors placed in the second-row will not contribute in developing force in the FRP strip unless the debonding passing the leading anchors (the anchor/anchors placed in the first row). Whereas, in the second case, both the bond and anchor will work together to increase the stress transmitted through the concrete-FRP interface, thereby increasing the bonding strength.

The previous studies presented several methods for anchoring the FRP strips to concrete which have been tested experimentally such as the using of U- shape anchor, transverse FRP warps, steel bolts anchor, mechanical anchor and CFRP anchor (Grelle and Sneed, 2013). The CFRP anchor also known as spike anchor was originally developed by the Shimizu Corporation in Japan (Orton, 2007). It is made from rolled fibres sheets inserted into predrilled holes in concrete substrate and fanned out over the CFRP sheets, Figure 1.5. Among the previously mentioned anchors' types, the CFR anchor has acquired a special attention by researchers because of its characteristics and applications. This type of anchor is a non-metalik, has high strength and high modulus of elasticity. Also, it increases the ultimate load, bonding strength between concrete and CFR sheets (Mertoğlu, Anıl and Durucan, 2016), and the strain in the FRP strips (Ozbakkaloglu, Fang and Gholampour, 2017); beside it could be applied for different structural members such as slabs and walls.

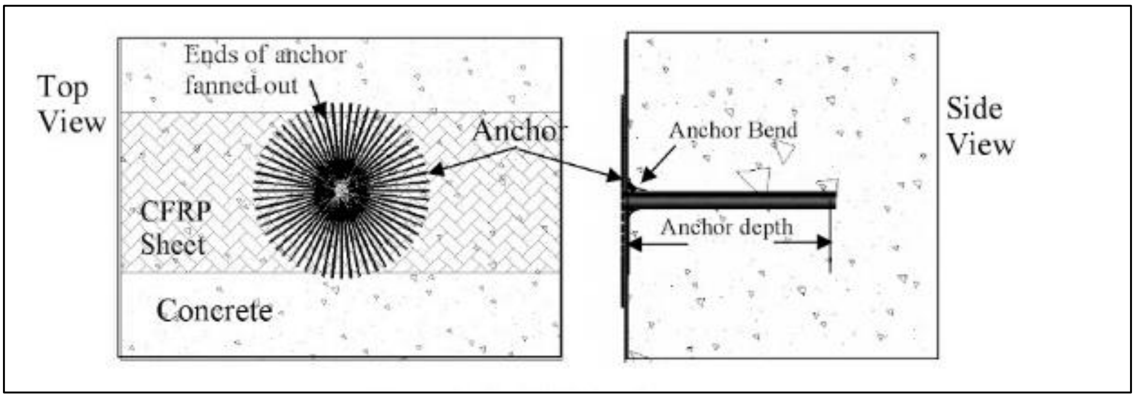

Figure 1.5. Carbon fiber anchors (Orton, 2007)

The effect of this type of anchor on the ultimate load capacity of the strengthening system is related to several parameters such as the CFR anchor's embedment depth, splay's diameter, the angle between anchor dowel and splay, quality of the workmanship during installation method, the number of anchors, anchor's configuration and position.

Although the anchoring of CFRP strips with CFRP anchors has shown promising results, the failure of anchors may limit the strength of the strengthening system. Generally, the failure of anchored strengthening system can be classified to (i) CFRP strip rupture which is a sudden and brittle failure results from the increment in the local stress concentrations imposed by the CFRP anchor (Grelle and Sneed, 2013),(ii) the global anchorage failure which includes: the seperation of the CFRP anchor splay from the CFRP strip surface, the CFRP anchor shear rupture just below the CFRP strip surface with keeping of the CFRP splay attached to CFRP strip upper face, and finally the CFRP anchor pullout which is a rare failure that occurres when the insertion holes in the concrete are improperly cleaned (Niemitz, James and Breña, 2010).

In literature, many experimental studies have been conducted to consider the effect of anchors by using different test setups. The test method plays a major role in determining the design strength of the anchored system. In general, there are three types of test procedure as shown in Figure 1.6: (İ) Pullout test: can be used to evaluate the anchorage's strength without including the bonded FRP length; (ii) Direct shear test includes single-shear and double-shear tests, it has the advantage of including the bonded length of FRP-to-concrete. This test is suitable for studying the interfacial shear debonding propagation for instance in a beam-footing interface, or the interface between a T-beam web and flange;

(iii) Bending test is used to evaluate the effect of applying the FRP strengthening system and anchorage on a beam strengthened in flexural (Grelle and Sneed, 2013).

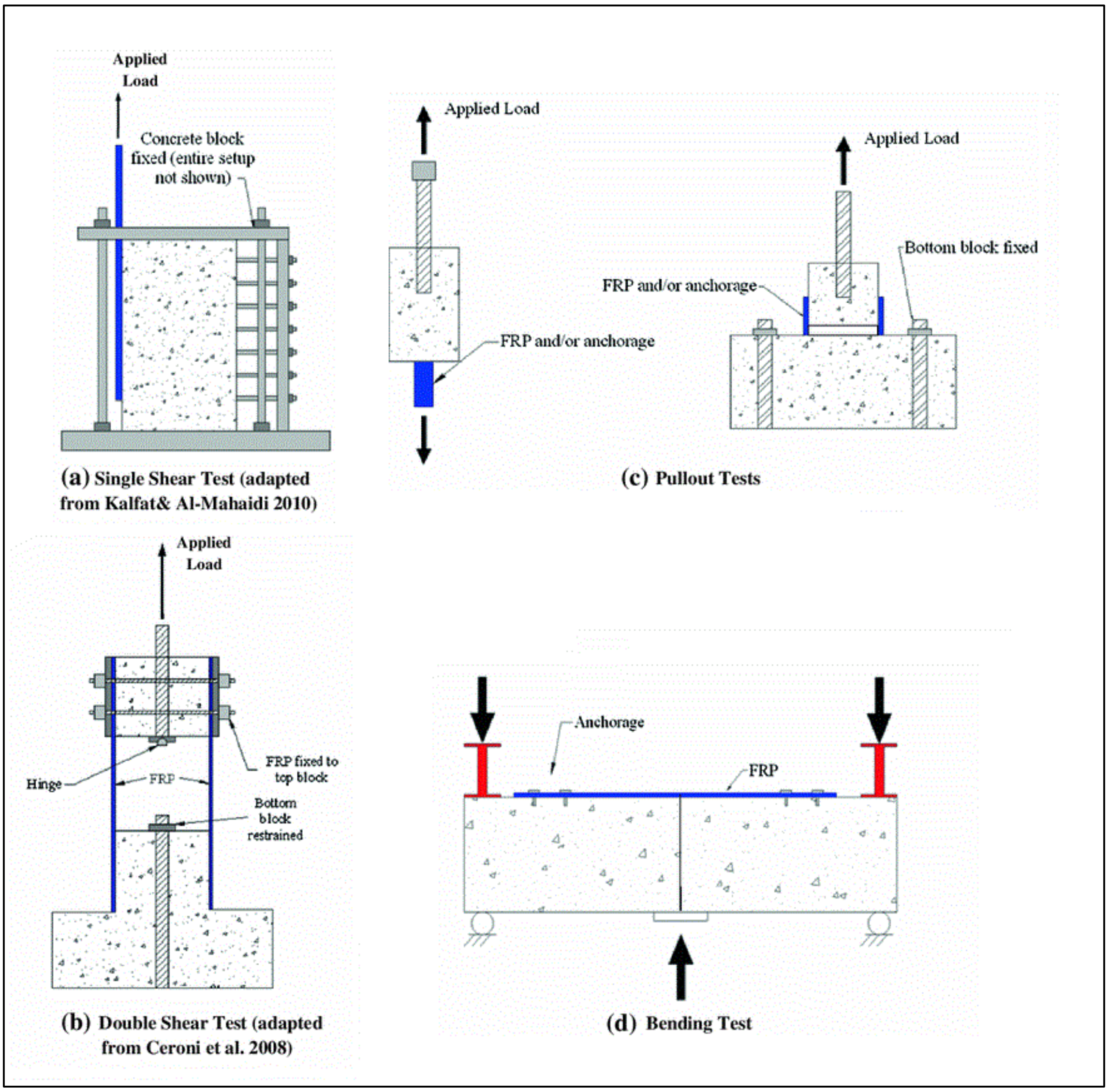

Figure 1.6. Test setup of FRP strengthened system (Grelle and Sneed, 2013)

Until today, most of the conducted studies about the anchored systems were concentrated on experimental programs compared to limited numerical studies that were implemented in this area. Nowadays, the provision of modern, fast computers made the engineering research increasingly sophisticated. With these computers, the finite element analysis (FEA) became an integral part of the structural analysis. Where it is allowed to create a virtual environment to simulate, analyze and obtain an approximate yet accurate solution to a wide variety of engineering problems. It is also allowing to test many design variations quickly and provided a complete engineering information which is not easy to obtain experimentally and that will help in saving time and effort.

Accordingly, in the current study, a three-dimensional finite element simulation via ANSYS (version 15) was conducted to understand the complex behavior of the structural members strengthened with anchored CFRP strip. The existence of proper FE model for CFRP anchor will allow to accurately simulate the behavior of the anchored system. Therefore, a new approach to represent the CFRP anchors in finite element analysis is produced. The CFRP anchor effect is represented by increasing the bond strength between CFRP strip and concrete over a specific area where the CFRP anchors penetrate the concrete. This was implemented by using the bond- slip model proposed by Mertoğlu after modification. The parameters of the modified bond-slip model were estimated by fitting of the finite element analysis results to available experimental results from the literature. Then after, further analyses were made to investigate the influence of several parameters which were not examined experimentally such as concrete strength, strip width, number of anchorages, bond length. Finally, the overall results were used for proposing an equation to calculate the bond strength of the anchored system.

2. LITERATURE REVIEW

For many years, the debonding in structural members strengthened with externally bonded reinforcement has become researchers main concern due to its ability to reduce the efficiency of the CFRP strengthening system. Consequently, many of the analytical and experimental studies were conducted to understanding the causes and mechanisms of debonding failures and finding out methods to prevent the debonding failure. This chapter will highlight the previous experimental and numerical main studies concerning the unanchored and anchored CFRP.

2.1. Experimental Studies on Unanchored and Anchored FRP Strengthening System

An experimental study was conducted by Orton et al. (Orton, Jirsa and Bayrak, 2008) to investigate the ability of the CFRP anchor for increasing the strain in the CFRP strips and to improve the material usage. Forty specimens with different surface level offsets were prepared and strengthened with various CFRP laminate types. The differences in CFRP anchors size, numbers, and distribution spaces were also considered in that study. The study showed that using a great number of smaller anchors contribute to distribute the forces evenly across the width of CFRP strip thereby, obtaining highest tensile capacity. Further, using a slop of 1:4 eliminates the effect of offset in the surface level and the surface preparations was not important if the CFRP strips are anchored properly.

Niemitz et. al. (Niemitz, James and Breña, 2010) conducted an experimental study to investigate the behavior concrte blocks strengthened with of CFRP sheets by using epoxy or CFRP anchor or by epoxy and CFRP anchors together. The main variables in the latest group were the FRP anchor number, pattern, anchor diameter, and splay diameter. The predicted experimental results supported the usage of FRP anchors with bonding as alternative load transfer mechanisms to improve the efficiency of the FRP strengthening system. The results also showed that, the force transferred into the FRP anchors is proportional to the anchor splay diameter and the thickness of the FRP sheet. Where using larger anchor splay diameters allowed to engage a wider sheet region.

Zang and Smith (Zhang and Smith, 2012) studied the effect of using FRP anchors on the concrete members strengthened externally by using CFRP strips. A series of experimental programs were conducted. They included 43 specimens with various number of anchors installed in different locations and methods (flexible and rigid anchor). The results showed that, the strain developed in FRP plate in specimens with multiple anchors was greater than the strain developed in FRP plate for unanchored specimens. Although the specimens with rigid anchors showed higher strength, the flexible anchors were recommended because the inability of the rigid anchor to deform in the bend region resulted in a premature anchor rapture failure. The study also presented an analytical modal to estimate the ultimate load capacity for the FRP strengthened system with multiple FRP anchors depending on the location of the anchor.

Koutas and Triantafillou (Koutas and Triantafillou, 2013) studied the strengthening of reinforced concrete T-beam in shear with the combination of U-jacket and spike anchors experimentally. Six beams with the same geometry were constructed and tested. The main variables were the number and orientation of the spike anchors and the material of both the U-jacket and the spike anchor (carbon fiber and glass fiber). The results indicated that placing the spike anchor vertically within the slab was more effective than those placed horizontally within the web. Increasing the number of anchors did not show proportional increment in the shear resistance because some anchors were not above a shear crack. Also, the specimens with the same anchor geometrical characteristic, changing the material of the U-jacket and anchor from carbon fiber to glass fiber showed similar effectiveness.

Mostafa and Razaqpur (Mustafa and Razaqpur, 2013) developed a new CFRP anchor (π anchor) which is consisted of two legs and a wide head plate to delay or prevent the debonding of externally bonded CFRP laminate from concrete substrate. The study included the testing of 21 simply supported T-beams which were strengthened in flexure by using CFRP strips with different thickness and anchored with various anchors number and distribution to find out the most effective configuration. The results showed that the π anchor was able to prevent the debonding failure efficiently in beams strengthened with up to eight layers of CFRP laminates. Also, the new anchor was able to increase the beams strength without effecting the ductility. For achieving this results, the π anchors must be placed uniformly along the CFRP strip so that the CFRP strip passes between the anchor legs. Furthermore, the π anchor showed the highest efficiency factor regarding the efficient utilization of the FRP strength in retrofit works in comparison to other types of anchors.

Ko et al. (Ko, Matthys, Palmieri and Sato, 2014) conducted a double bonding test for 18 concrete specimens strengthened with FRP to study the bonding behavior between concrete and CFRP. The main variables in the experimental program were the FRP tensile strength, modulus of elasticity, thickness, and width. Based on the experimental results and the assessment of the database for the available bond-slip model in literature, a new bilinear bond-slip model was suggested which taking into account the concrete strength and FRP stiffness.

Issa et al. (Issa, Rahma and Alrousan, 2016) studied the bond behavior between concrete and CFRP by conducting double shear test for 30 concrete specimens having a different compressive strength and strengthened with CFRP strips having a different width. The results showed that increasing the concrete compressive strength and CFRP width, increases the ultimate bonding strength. Also, the brittle failure mode was observed by increasing the concrete compressive strength and decreasing the CFRP width. Finally, the study proposed an analytical model for estimating the ultimate load and the corresponding slip. The proposed model was a modification of the model proposed by Chen and Teng.

Çelebi et al. (Mertoğlu, Anıl and Durucan, 2016) conducted an experimental study to investigate the strain distribution and bond-slip behavior in concrete strengthened with anchored CFRP strips. 14 concrete specimens strengthened with CFRP strips having different length and width in the existence of various numbers of anchor were tested. The result showed that, the using anchors effecting significantly on the ultimate load capacity, strain distribution and energy dissipation capacity. The study also proposed a bond-slip model for anchored CFRP strengthened system. The model can estimate the ultimate shear stress and the corresponding slip for the anchored CFRP strengthened system depending on the ultimate shear stress and corresponding slip for specimens without anchor which could be calculated by using any bond strength model or experimental data.

An experimental study was carried out by Ozbakkaloglu et.al. (Ozbakkaloglu, Fang and Gholampour, 2017) to investigate the effect of FRP anchors configuration, numbers, and embedment depth on the behavior of FRP plate externally bonded on concrete member. 33 specimens were prepared for this purpose. The results showed that, all the investigated parameters exhibited significant effect on the ultimate load capacity of the FRP plate. The presence of the FRP anchor with increasing the embedment depth and number of anchors results in increasing the ductility, maximum longitudinal strain, and the ultimate load capacity of the FRP strengthening system. The study also showed that placing the leading anchor near the loaded end leading to delay the debonding. Finally, the longitudinal anchor pattern developed higher strain in FRP plate in comparison to the transverse anchor pattern.

2.2. Numerical Studies on Unanchored and Anchored FRP Strengthening System

The numerical analysis is an integral part of most structural analysis because it can provide some engineering information which are difficult to obtain experimentally. Most of the available numerical studies were conducted on the unanchored CFRP strengthening system whereas limited studies are available for the anchored CFRP strengthening system. Below are some of the studies for both unanchored and anchored CFRP systems:

Holmer (Holmer, 2010) developed a two-dimensional FE model using ANSYS program to investigate the effect of changing geometrical dimensions, material properties, and cohesive properties on the behaviour of FRP- concrete interface and maximum peel load capacity of the modified double cantilever beam test (MDCB). The calibration of the proposed model was conducted by using available experimental data. The results showed that increasing the thickness of FRP, adhesive and residual thickness of concrete (RTC) leading to increase the peeling load. In the same way, increasing the modulus of elasticity for FRP and concrete leaded to increase the peeling load too. While increasing the modulus of elasticity for adhesive had little effect on the maximum peeling load. Furthermore, the study showed that the stress and displacement involved in the energy equation for cohesive element which was proposed by Ouyang has a greater impact on the maximum peel load and the flexibility of the model respectively.

Zidani et al. (Zidani, Belakhdar, Tounsi and Bedia, 2015) presented a three-dimensional finite element model to simulate the flexural behaviour of initially damaged concrete beams repaired with FRP plates by using Ansys program. Solid65, link8, solid45 and inter205 with zero initial thickness are selected to represent concrete, steel reinforcement, CFRP plate and CFRP- concrete interface respectively. The validation of the proposed model was examined by the comparison of the analytical results with the experimental data of the selected 12 beams. The analysis was performed in two stages: first the beams were loaded to introduce damage and after bonding the FRP plate, the beams were reloaded until failure. The model could simulate the full history of the tested beams. After that further analysis were conducted by using the proposed model to study the effect of the CFRP plate thickness on the load carrying capacity, interfacial shear stress distribution, crack pattern, and failure mechanism. The predicted results showed that using the CFRP plate increases the load capacity of all repaired beams in comparison to the control beams for any damage degree. Also, the most likely failure mode for any CFRP plate thickness was the debonding mode.

Al- Musawe et al. (Al-Musawe, Al-Mahaidi and Zaho, 2015) conducted experimental and numerical study to investigate the bond behaviour of steel members strengthened with CFRP laminates which having two CFRP cross sectional areas (10x 1,4 mm and 20x 1,4mm) and different modulus of elasticity (low, normal, and ultra-high CFRP modulus) under quasi- static load. The three-dimensional nonlinear finite element model was developed by using ABAQUS 6.13 program. The numerical results were in good agreement with the experimental results. The predicted results showed that the modulus of elasticity of CFRP effecting the strain distribution while the tensile strength of CFRP effecting the joint capacity. Also, The failure mode and effective length for the specimens with low and normal modulus of elasticity were similar; the failure mode was debonding and the effective length was 110mm. Whereas, the specimens with ultra- high CFRP modulus showed different behavior, the effective bond length was 70mm and the failure mode for the specimens with bonding length equal or greater than the effective length was FRP rupture. While the specimens with bonding length below the effective length was FRP delamination. In specimens with 10mm CFRP width the adhesive size was very small thereby its ability to resist load was very sensitive to any movement and did not give accurate results.

Kim et al. (Kim, Shin, Choi and Kim, 2015) conducted experimental and numerical study included the testing of 165 strengthened concrete beams to investigate the effect of using a tapered and non-tapered layers of CFRP or hybrid FRP strips on the moment capacity for concrete beams. Also, the relationships between maximum moment capacity and interfacial stress were investigated depending on the maximum loads and strain distributions obtained from the tests. The experimental results showed that the tapered CFRPs had larger load capacity than the non-tapered CFRPs because the stress concentration at the end of the CFRP sheet was distributed over the tapered area which leading to delay the beam failure due to debonding. On the other hand, using GFRP sheet between two CFRPs sheets prevents the transformation of the large stress developed in CFRP sheets to the concrete interface due to the low modulus of elasticity of the GFRP. The study also adopted a modification factor for the equation used for calculating the moment capacity of concrete beams strengthened with FRP which was suggested by the ACI repair manual to include the effect of using the tapered layered FRP sheets. Finally, the relationships between the interfacial shear stress and maximum load capacity for the reinforced concrete beam strengthened with tapered FRP sheets was verified by implementing finite element analysis via ABAQUS 6.10.

Sun and Ghannoum (Sun and Ghannoum, 2015) developed a three-dimensional model using Ansys for simulating the load transfer mechanisms from CFRP strips to CFRP fan anchors. The eight-node element was selected to model the concrete and the steel loading plates. The CFRP fibers in the strip and anchors were represented by using the truss element. Four node plate elements were selected to model the epoxy resin matrix. The CFRP fan anchor was modeled using fanning truss elements which was rigidly connected to the concrete elements at the point of insertion. The nonlinear spring elements were used to simulate the bond behavior between concrete and CFRP. The nonlinear spring elements were given an undeformed length equal to the CFRP strip thickness. Since the spring elements cannot transfer moments at their ends, bond shear force can only be developed across the interface. A parametric study was also conducted to study the effect of changing the CFRP anchor material ratio, the concrete strength, the length of anchor fan and the bond condition between CFRP and concrete. The simulation could estimate the failure load and the load - deflection responses of tested beams. The proposed model showed limited sensitivity to the modulus of elasticity of CFRP strips in the direction of the fibre, the modulus of elasticity of the epoxy as well as the descending slope of the selected bond stress-slip model.

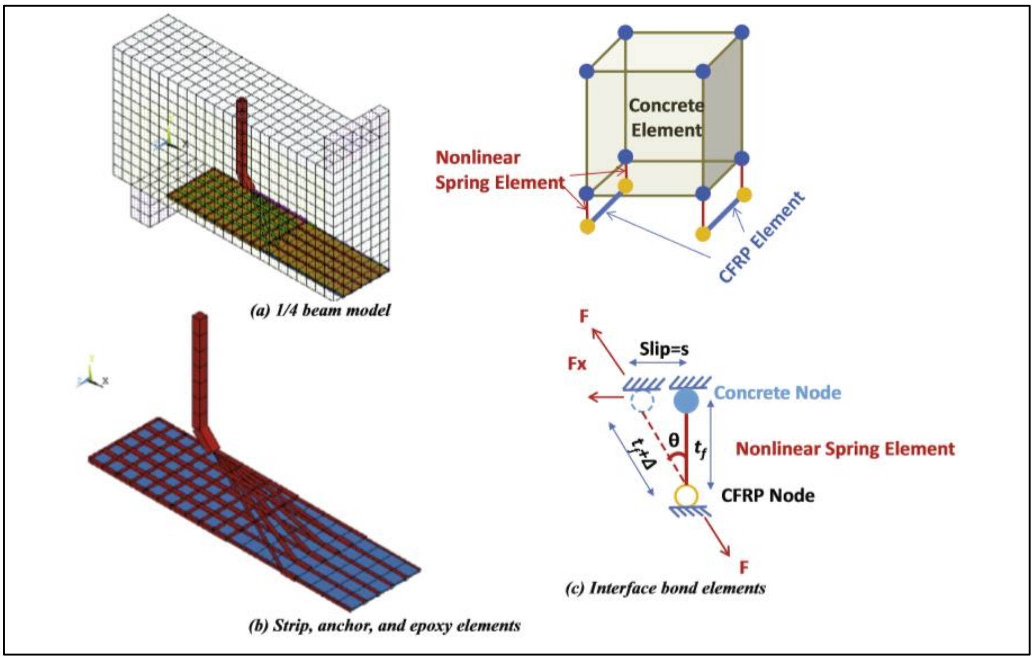

Figure 2.1. Configuration and elements of proposed model (Sun and Ghannoum, 2015)

Rvendran et al. (Rvendran, Perera and Gamage, 2016) conducted a finite element analysis to predict the flexural behavior of concrete beams externally strengthened with CFRP strips and CFRP end anchors by using ANSYS 15. The study also investigated the effect of increasing the number of CFRP end anchors and CFRP end anchors position on the flexural performance of the composite. The predicted results showed that the ultimate load capacity for the concrete beams strengthened with CFRP strips and CFRP end anchors was three times the reference beams. Also, changing the CFRP end anchor position did not show a significant effect on the ultimate load capacity. Increasing the number of CFRP end anchors lead to increasing the ultimate load capacity and decrease the mid span deflection.

Yilmaz et al. (Yilmaz, Arslan and Anil, 2018) conducted a three-dimensional nonlinear finite element analysis by using ABAQUS program to study the behavior of concrete beams strengthened in flexure by CFRP strips and mechanical anchors. The FE model was calibrated by the comparison with the experimental results for 12 specimens selected from an experimental study conducted by the authors. Then after, the analytical model was used to examine the effect of CFRP bonding length, CFRP width and the number of anchors on the bonding strength. Finally, the study suggested a multiplier to include the effect of using the mechanical anchor on the ultimate load capacity of concrete beams strengthened externally with CFRP and mechanical anchor. The multiplier could be estimated by using special graphs prepared for this purpose depending on the number of anchors and the

CFRP length and width. Consequently, the ultimate load capacity could be calculated by multiplying the estimated multiplier by the ultimate load capacity calculated from the equation suggested by Lu et al.

As a result, it could be observed that the analytical studies related to the behavior of the concrete element strengthened with CFRP anchor by using finite element method are limited. Therefore, the current study was conducted to present a simple method for modeling the CFRP anchor and to study the bond- slip behavior of this strengthening system analytically.

3. FINITE ELEMENT MODEL SIMULATION AND CALIBRATION

Finite element analysis (FEA) is a numerical method used for obtaining approximate solution for various engineering problems having complicated geometries, loading, and material properties. The FE method is based on dividing of a continuum body or a structure into small elements connected to each other by nodes. The prevalence of using the FEA was accompanied by the presence of powerful software and computers. The commercial finite element software ANSYS version 15 was chosen in this study to simulate the behavior of concrete elements strengthened with anchored CFRP strips.

This chapter presents the procedure of creating FE model in ANSYS which including the definition of model geometry, selecting the element types, defining the material property, meshing the model, defining the boundary condition, and finally running the analysis and obtaining the results. Eventually, the validity and accuracy of the finite element model was checked by the comparison of the numerical model results with existent experimental results.

3.1. Specifications of The Selected Specimens

The validity and accuracy of the adopted finite element models are studied and checked by analyzing 14 test specimens with anchored CFRP strips which have been tested experimentally by Mertoğlu (Mertoğlu, Anıl and Durucan, 2016). The specimens were arranged into two groups depending on the technique used to attach the FRP sheets to the concrete blocks: Control group, consisted of the specimens in which the CFRP sheets were attached to the concrete blocks only by epoxy resin. While the second group consisted of specimens where the CFRP sheets were attached to the concrete blocks through a combination of epoxy and CFRP fan anchors. The dimensions of the concrete blocks were 250 x 300 x 600 mm. The material properties and the basic characteristics of all specimens used in experimental work are summarized in Table 3.1 and Table 3.2, respectively. The Fan type anchors and geometric arrangement of anchors used in the retrofitting procedure are illustrated in Figures 3.1 and 3.2, respectively (Mertoğlu, Anıl and Durucan, 2016).

Table 3.1. Material properties for concrete and epoxy

Concrete	
Compressive strength	25 MPa
CFRP	
Weight	220 gr/m2
Thickness	0.12 mm
Tensile strength	4100 MPa
Modulus of elasticity	231 GPa
Ultimate strain	1.7%
Epoxy Resin	
Density	1.31 KG/lt
Mixed ratio	White/ Grey compound= 4/1
Tensile strength	30 MPa
Bending modulus of elasticity	3800 MPa

Figure 3.1. Fan type anchors used in the experimental program

Table 3.2. Summary of Specimen Properties

Specimens	b_f (mm)	L (mm)	N	P_{ult} (KN)	Displacement at P_{ult} (mm)	Stiffness (KN/mm)
50W200L	50	200	0	20.19	4.65	4.34
50W280L	50	280	0	24.63	7.39	3.33
100W200L	100	200	0	12.8	6.79	1.89
100W280L	100	280	0	13.89	6.08	2.28
50W200L 1A	50	200	1	13.7	6.75	2.03
50W200L 2A	50	200	2	14.5	7.79	1.86
50W280L 1A	50	280	1	16.73	8.39	1.99
50W280L 2A	50	280	2	18.25	9.26	1.97
50W280L 3A	50	280	3	23.45	5.52	4.25
100W200L 1A	100	200	1	26.46	9.45	2.80
100W200L 2A	100	200	2	29.15	9.89	2.95
100W280L 1A	100	280	1	35.6	8.26	4.31
100W280L 2A	100	280	2	44.12	8.94	4.94
100W280L 3A	100	280	3	50.67	9.45	5.36

*The letters W, L and A indicating the CFRP width, Length, and number of anchors respectively.

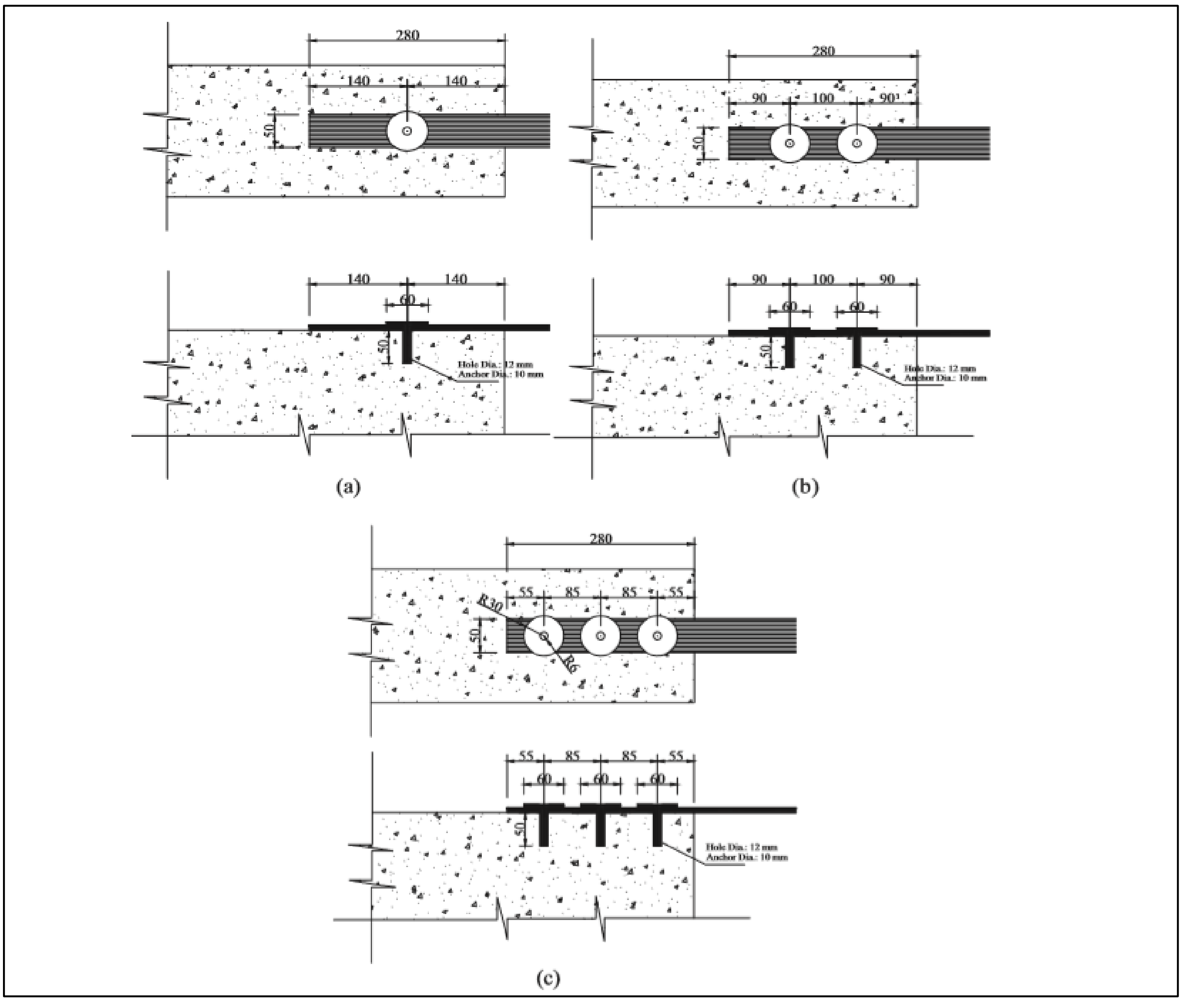

Figure 3.2. Plane and side views of test specimens (a) one anchor, (b) two anchor, (c) three anchor (Mertoğlu, Anıl and Durucan, 2016)

The specimens were tested using a specially designed machine as shown in Figure 3.3. For preventing the movement of the concrete block during the test, the specimens were fixed to a 10mm steel plate. The free end of the CFRP strips were warped twice and fixed to steel plates by using 16 bolts. The load was applied along the fiber direction until the occurrence of failure either by the rupture of the CFRP strip or by debonding. During the loading process, the strain was measured by using a uniformly distributed strain gages along the bonded length of the CFRP strip. The displacement at the loaded end were measurements by using the linear variable differential transformer (LVDT). The movement of the concrete block was prevented by adding a full height thick steel anchorage plate to the loaded face of the concrete block.

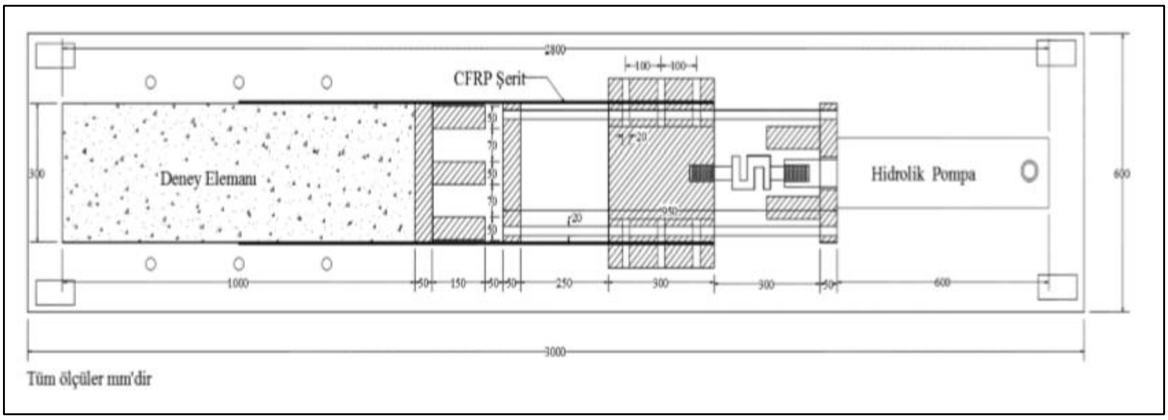

(a)

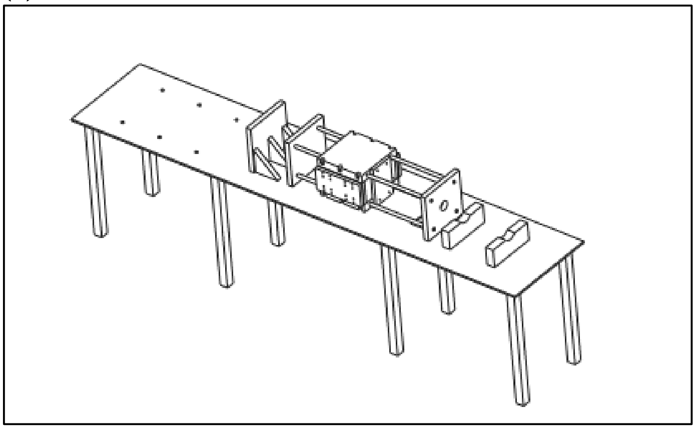

(b)

Figure 3.3. Typical test setup; (a) Plan (b) perspective views

3.2. Concrete, CFRP and Interface Finite Element Idealizations

The 8-node brick elements solid65 and solid185 were used for modeling the concrete and CFRP strips, respectively (Figure 3.4). Both elements are defined by eight nodes with three degrees of freedom in each node (translations x, y, and z directions). The element Solid65 has the ability of cracking in tension, crushing in compression and it can also undergo plastic deformation and creep. The non-linear concrete model uses the von Mises failure criterion along with the Willam and Warnke model to define the failure criteria. Solid185 is available in homogeneous and layered forms. The solid form was selected in the present study. The element has plasticity, stress stiffening, large deflection, and large strain. The contact pair, Target 170 and Contact 174 elements with the capability of debonding in tangential direction (sliding or shear) were used for modelling the epoxy. To activate the debonding for the contact pair, the Cohesion Zone Material Model (CZM) with bilinear material and critical fracture energy failure criteria was used. The CFRP anchors were represented by increasing the bonding strength at the interface over specific area where CFRP anchors penetrate the concrete.

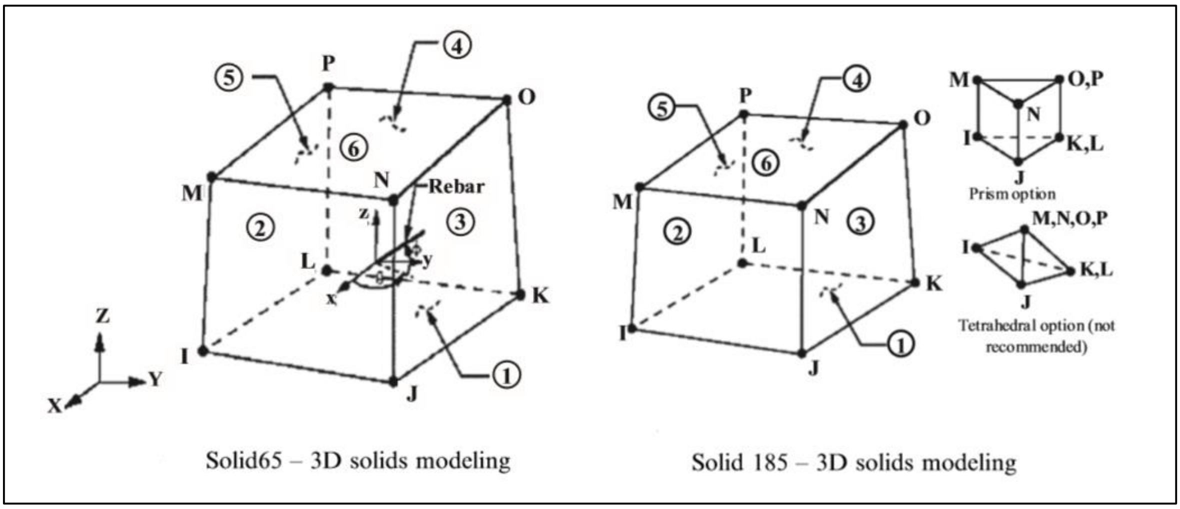

Figure 3.4. The schematic of Solid65 and Solid 185 elements

3.3. Material Properties

The response of any loaded structural member depends on the nature and the properties of the material from which it is made. Therefore, the representation of this structure using the finite element method requires the accurate modeling of the behavior and the properties of its components.

3.3.1. Concrete

Concrete is a composite material with a very low tensile strength in comparison to its high compressive strength. Also, it has different behavior in tension and compression. The presence of microcracks at the interface between coarse aggregates and mortar, even before subjected to any load, has a great effect on the mechanical behavior of concrete, where their propagation during loading contributes to the nonlinear behavior at low stress levels and causes volume expansion near failure (Propvics, 1976).

In compression, The concrete exhibit a linear elastic behavior up to $0.3f_c'$. After that, microcracks start to initiate and the stress- strain curve shows a gradual increase in curvature up to maximum compressive strength thereafter the stress-strain curve descends until the failure occurs at the ultimate strain due to the crushing of concrete (Saenz, 1964). While, in tension the stress–strain curve shows a linear elastic relationship until the maximum tensile strength. Beyond the failure stress, the concrete cracks and the strength decreases gradually to zero as shown in Figure 3.5.

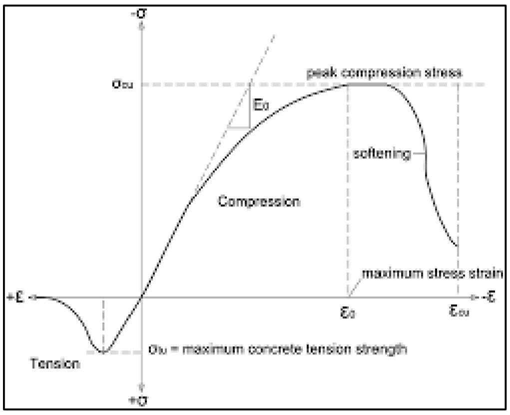

Figure 3.5. Typical stress-strain curve for normal weight concrete

The element used to represent concrete in ANSYS required both the linear and multilinear isotropic material property. For the linear isotropic material, the modulus of elasticity was calculated by using equation 3.1 (ACI committee 318, 2011) and the poisons ratio was assumed to be 0.2. The concrete cracking stress was calculated by using equation 3.2 (ACI committee 318, 2011)

$$E_c = 4700\sqrt{f_c'} \tag{3.1}$$

$$f_r = 0.62\sqrt{f_c'} \tag{3.2}$$

for the Multilinear isotropic, the stress-strain curve for concrete was constructed by using numerical expressions proposed by the Desayi and Krishnan (Desayi and Krishnan, 1964). The simplified stress-strain curve is constructed from six points connected by straight lines as shown in Figure 3.6. The curve starts at zero. Point number 1, at 0.3 f_c', is calculated for the stress-strain relationship of the concrete in the linear range (equations 3.5 and 3.1). Point numbers 2, 3, and 4 are obtained from equation 3.3, in which ε_o is calculated from equation 3.4. Point number 5 is at ε_o and f_c'. In this study, an assumption was made of perfectly plastic behavior after point number 5.

$$f_c = \frac{\varepsilon E_c}{1+\left(\frac{\varepsilon}{\varepsilon_o}\right)^2} \tag{3.3}$$

$$\varepsilon_o = \frac{2f_c'}{E_c} \tag{3.4}$$

$$E_c = \frac{\sigma}{\epsilon} \tag{3.5}$$

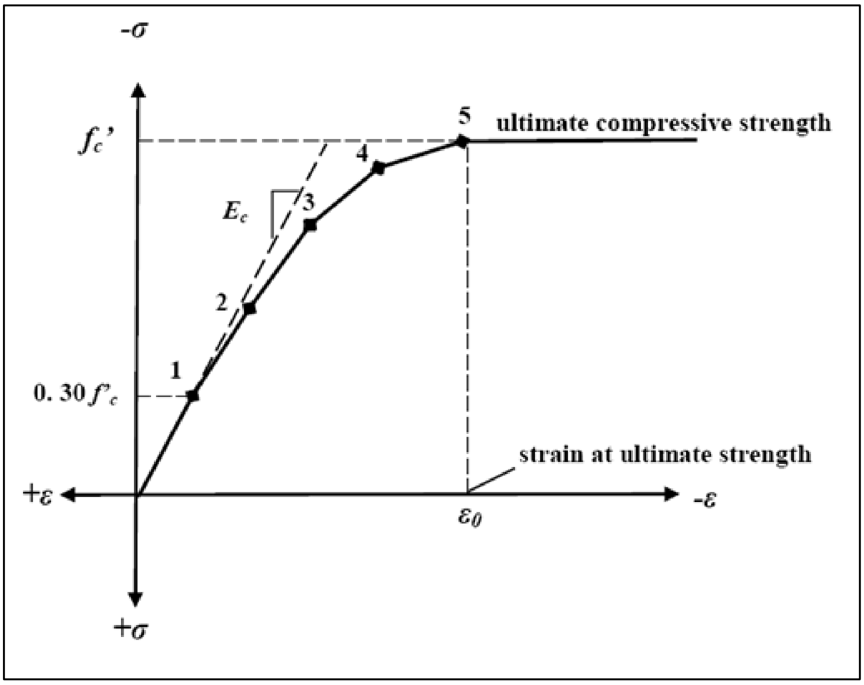

Figure 3.6. Simplified compressive uniaxial stress-strain curve for concrete

ANSYS program uses William and Warnke model to define failure criteria for the non-linear concrete model. In concrete element, once the principal stress in all direction exceeds the ultimate compressive strength of concrete, the concrete will be crushed while one of the principal stress in any direction exceeding the ultimate tensile strength of concrete, the concrete will crack. In both cases, Ansys will set the modulus of elasticity of concrete to zero in all directions for the crashed element and in the direction parallel to the principal tensile stress direction for the cracked elements. Thereafter, these elements are deactivated for further analysis. A three-dimensional failure surface for concrete is shown in Figure 3.7.

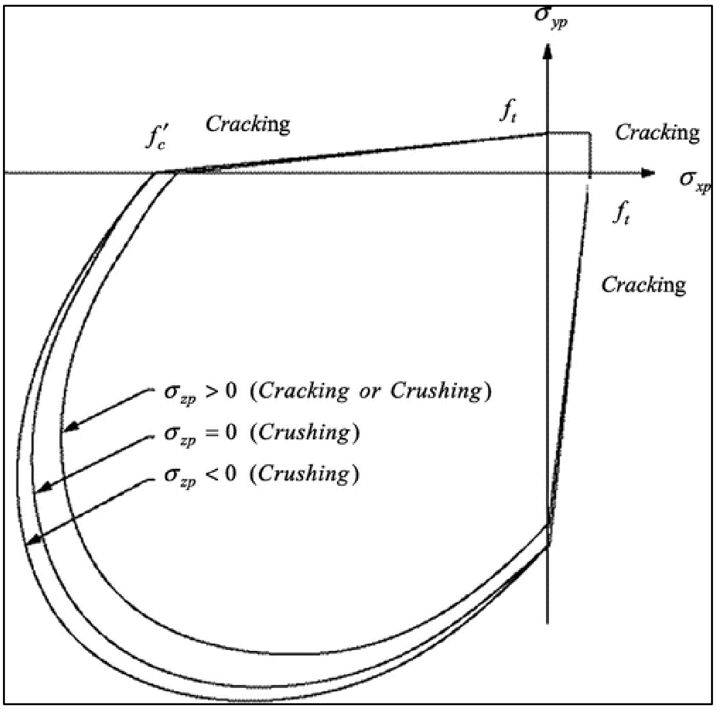

Figure 3.7. Three-dimensional failure surface for concrete

3.3.2. CFRP composites

The mechanical properties of the CFRP depend on the fiber properties, matrix properties, fiber amount and orientation (Obaidat, 2011). Since all fibers in the matrix are in one direction, the CFRP composites will provides stiffness and strength along the fiber direction in tension. Thereby, the linear elastic model was used to represent the material property of CFRP strips (Figure 3.8). The thickness of the CFRP strips used in the experimental work was 0.12 mm. In the analytical model, this value was replaced by 1.2 mm and for this the modulus of elasticity was decreased by the same percent of the thickness increment (Kachlakev, Miller, Yim, Chansawat and Potisuk, 2001).

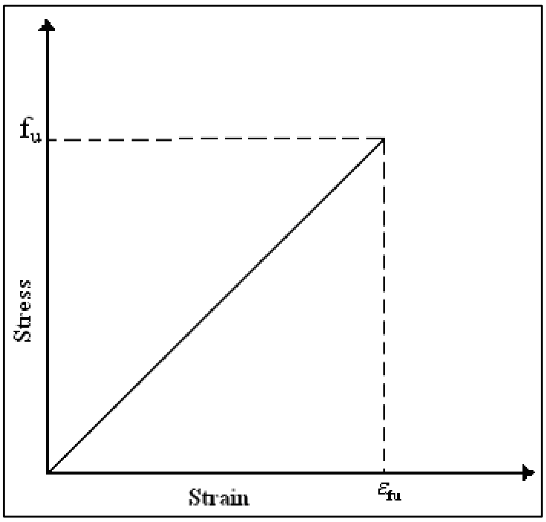

Figure 3.8. stress–strain curve for CFRP along the fiber direction

3.3.3. CFRP- concrete interface

The bond behavior between CFRP and concrete plays a major role in stress transfer mechanism and the overall behavior and capacity of the composite system. Some of the analytical studies assumed a perfect bond between CFRP and concrete and neglected the softening effect of CFRP debonding. Thereby, the analytical results show stiffer response and higher load capacity (Sun and Ghannoum, 2015). In the current study, the contact elements with cohesive zone model (CZM) were used to activate the debonding effect. The CZM based on the assumption that, the interface does not separate completely at damage onset but rather it is starts losing its stiffness gradually (Barbero, 2014). In ANSYS the CZM model is available with two failure criteria: bilinear material behavior with traction and separation distance CBDD, and bilinear material behavior with tractions and critical fracture energies CBDE. In current study, the CBDE failure criteria was selected to model CZM and implemented via the following commands:

TB,CZM,,,CBDE

TBDATA,1,σmax,Gcn,τmax,Gct,η,β

Where σmax represents the maximum normal contact stress, Gcn critical fracture energy for normal separation, Tmax maximum equivalent tangential contact stress, Gct critical fracture energy for tangential slip, η artificial damping coefficient and β flag for tangential slip under compressive normal contact stress as shown in Figure 3.9.

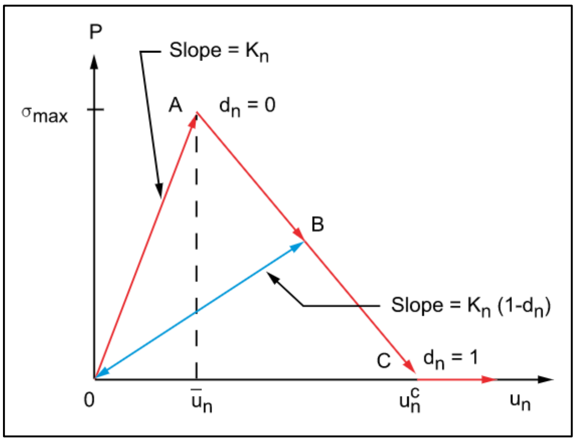

Figure 3.9. The bilinear cohesive zone material model in ANSYS

Since the debonding occurs due to shear failure, the tensile stress was neglected, and shear failure stress was only considered. Thereby, the τ_{max} and G_f as well as the K_n values are only required for simulating the debonding and these values could be obtained from bond-slip models. For stabilizing the numerical solution, the η was used and assumed to be 0.1 while a β value was 1.0.

3.4. Review of The Available Bond-Slip Models

The bond -slip model is a mathematical model that describes the relationship between the shear stress and slip at a certain point belongs to the FRP- concrete interface in concrete elements strengthened externally by using FRP. The performance of the strengthened system depends largely on the behavior of the interface between concrete and FRP. Therefore, most of the researchers' efforts were concentrated on defining an accurate bond-slip model which takes into account the effect of the all interfacial materials such as concrete, FRP, and adhesive materials.

The existence bond-slip models have been developed based on the strain distribution or Load-slip curve obtained from a pullout test, or by making use of numerical simulation. At the first method, the strain distribution in the FRP could be obtained from a closely placed strain gages mounted on the FRP strip. Based on the equilibrium between the bond stress and the axial stress in FRP strip, the shear stress of a specific point that belongs to the

FRP- concrete interface could be obtained by differentiating the axial stress in FRP. Since the modulus of elasticity of FRP is known, the shear stress could be estimated as follows:

$$\tau(x) = \frac{t_f \, d\sigma(x)}{dx} = \frac{t_f E_f d\varepsilon_f(x)}{d(x)} \tag{3.6}$$

The corresponding slip could be calculated by integrating the strain along the FRP length up to that point. The main defect of this method is that strain value suffering from large variation due to the discrete nature of the concrete substrate and the existence of cracks which in role affecting the calculated shear stress and lead to having different bond-slip models (Lu, Teng, Ye and Jiang, 2005; Obaidat, Heyden and Dahlblom, 2013; Ko, Matthys, Palmieri and Sato, 2014). The load-displacement was also used to determine the bond- slip curve indirectly by deriving a relationship between local strain at the FRP and the displacement at the loaded end without the need to measure the strain distribution at the FRP as follows (Dai, Ueda and Sato, 2005):

$$\varepsilon = f(s) \tag{3.7}$$

$$\frac{d\varepsilon}{dx} = \frac{df(s)}{ds}.\frac{ds}{dx} = \frac{df(s)}{ds}.\varepsilon = \frac{df(s)}{ds}.f(s) \tag{3.8}$$

By substituting equation 3.8 in 3.6 the bonding shear stress can be expressed as:

$$\tau(x) = \frac{t_f \, d\sigma(x)}{dx} = t_f E_f.\frac{df(s)}{ds}.f(s) \tag{3.9}$$

The numerical simulation is another method used for determining the bond-slip model. This method is based on proposing a bond-slip model with few parameters. Then after these parameters could be determined by fitting the FE analysis results to experimental results (Lu, Teng, Ye and Jiang, 2005; Obaidat, Heyden and Dahlblom, 2013).

In literature, the bond- slip curves for the unanchored CFRP-concrete joint were proposed in different shapes such as cutoff, elastoplastic and the bilinear (Figure 3.10). Among these models, the bilinear model considered to be the most realistic and represents the closest approximation to the real behavior as was proven by the experimental and theoretical studies. In this model, the shear stress increases linearly up to the maximum shear stress

τ_{max} at s_0 then after the curve descending gradually to zero at s_f. Where, s_0 and s_f represent the local slip at maximum shear stress and local slip at the completion of debonding, respectively.

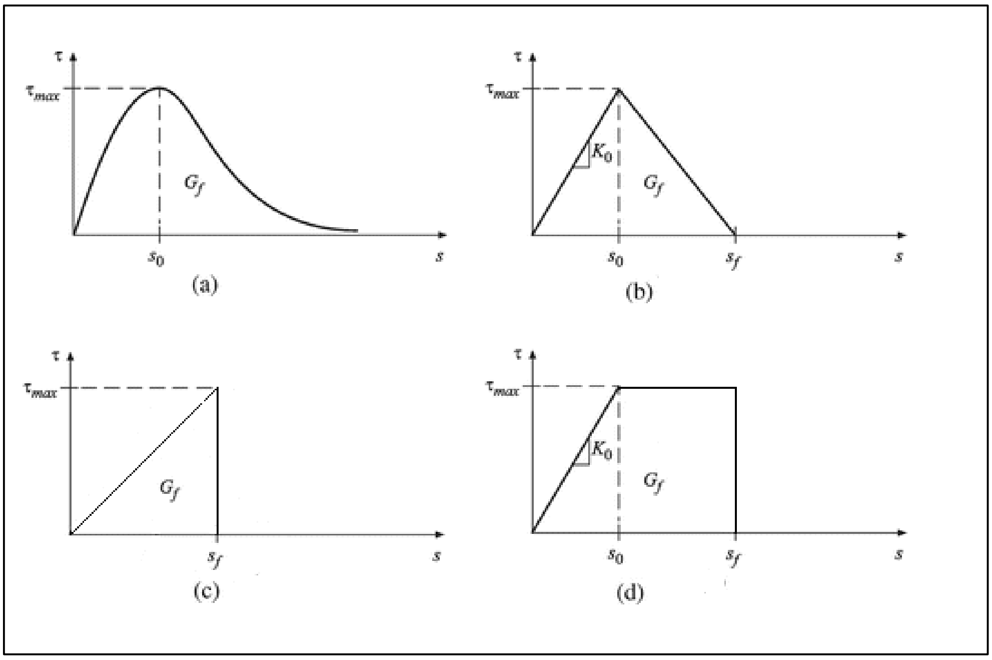

Figure 3.10. Bond-slip curves: (a) typical; (b) bilinear; (c) cutoff; (d) elasto plastic

One of the most important studies was conducted by Lu et al. (Lu, Teng, Ye and Jiang, 2005) in which a local bond slip model with few key parameters was proposed as shown in Figure 3.11. These parameters were determined by fitting the FEA results to experimental results of 235 pull test on simple FRP- concrete joint. τ_{max}, G_f, s_0 and s_f can be calculated from the following equations:

$$\tau_{max} = 1.5\beta_w f_t \quad (3.10)$$

$$G_f = 0.308\beta_w^2\sqrt{f_{ct}} \quad (3.11)$$

$$s_0 = 0.0195\beta_w f_{ct} \quad (3.12)$$

$$s_f = 2\, G_f/\tau_{max} \quad (3.13)$$

$$\beta_w = \sqrt{\frac{(2.25-b_f/b_c)}{(1.25+b_f/b_c)}} \quad (3.14)$$

Where $\beta_{w,}$ b_f and b_c represent the correction factor, the CFRP strip width and the concrete width respectively. While f_t represents the concrete tensile strength which could be calculated from equation 3.15 (ACI committee 318, 2011).

$$f_t = 0.33\sqrt{f_c'} \tag{3.15}$$

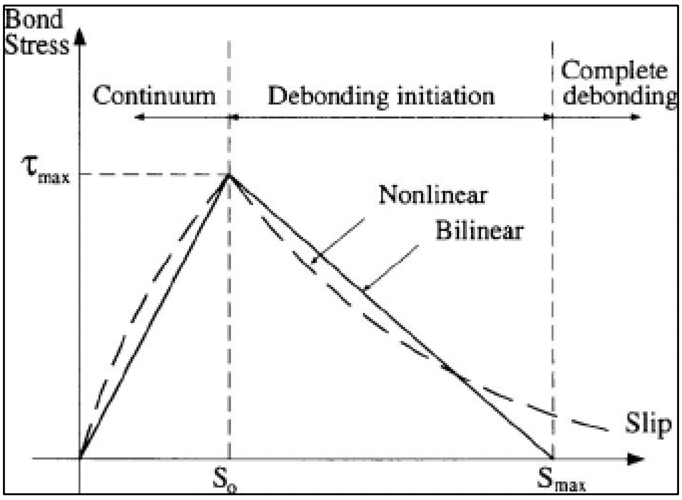

Figure 3.11. The bond- slip model proposed by Lu et al

Dai et al (Dai, Ueda and Sato, 2005) produced a new bond stress- slip model based on deriving a relationship between the loaded end displacement and the local strain on the FRP. The model parameters were determined by using the experimental results of 26 single-lap pullout test specimens with different adhesive types and FRP.

$$\tau_{max} = 0.5BG_f \tag{3.16}$$

$$S_{max} = \frac{0.693}{B} \tag{3.17}$$

$$B = 6.846\left(E_f t_f\right)^{0.108}\left(\frac{G_a}{t_a}\right)^{0.833} \tag{3.18}$$

$$G_f = 0.446\left(\frac{G_a}{t_a}\right)^{-0.352} f_c^{0.236}\left(E_f t_f\right)^{0.023} \tag{3.19}$$

Where τ_{max} represents the maximum bond stress, S_{max} maximum slip corresponding the maximum bond stress, B regression parameter, G_f fracture energy, $G_a$shear modulus of adhesive, t_a thickness of adhesive layer, E_f elastic modulus of FRP and t_f is the thickness of FRP.

Obaidat et al. (Obaidat, Heyden and Dahlblom, 2013) suggested a bilinear bond- slip model for describing the bond action between FRP and concrete. The parameters of this model were related to the adhesive shear stiffness and concrete tensile strength without introducing any geometrical correction coefficient as in the model proposed by Lu et al. The model's parameters where obtained by the fitting of the maximum load and strain distribution obtained from the FEA results to the experimental results of 18 test specimens. The K_0, τ_{max} and G_f can be estimated by using the following equations:

$$K_0 = 0.16\frac{G_a}{t_a} + 0.47 \quad (3.20)$$

$$G_f = 0.52 f_{ct}^{0.26} G_a^{-0.23} \quad (3.21)$$

$$\tau_{max} = 1.46 f_{ct}^{1.033} G_a^{0.165} \quad (3.22)$$

Where G_a represents the adhesive shear modulus in GPa, $t_a$is the adhesive thickness in mm and $f_{ct}$is the concrete tensile strength calculated by using equation (3.11)

On the other hand, Mertoğlu et al. (Mertoğlu, Anıl and Durucan, 2016) proposed a bond slip model for the multiple anchored CFRP-concrete joint as shown in Figure 3.12. The model was developed based on the load-slip curve for 14 specimens tested experimentally. It could be seen that the descending part of the bond-slip curve does not drop to zero, but it is followed by a residual constant bond stress. The parameters of the bond- slip's model are given as follows:

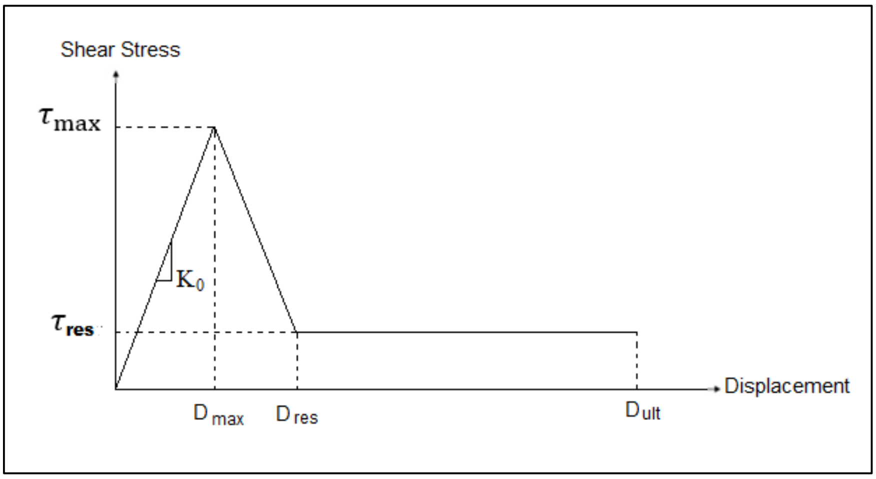

Figure 3.12. Bond slip model for the multiple anchored CFRP-concrete joint.

$$\tau_{\max\_anchor} = \tau_{max} e^{0.17N} \tag{3.23}$$

$$k_0 = calculated\ from\ any\ model\ proposed\ for\ element\ without\ anchor$$

$$\tau_{res} = 0.2\ \tau_{\max\_anchor} \tag{3.24}$$

$$D_{max} = \tau_{\max\_anchor}/K_0 \tag{3.25}$$

$$D_{res} = 1.2\ D_{\max} \tag{3.26}$$

$$D_{ult} = D_{max}(0.15N + 1.68) \tag{3.27}$$

Where $\tau_{\max\_anchor}$ represents the ultimate shear capacity of the system with anchorage τ_{max} is the maximum shear stress calculated from any model proposed for element without anchor and N is the number of anchors.

3.5. Finite Element Idealization

For unanchored specimens, the full specimen was modeled as shown in Figure 3.13. Where the elements solid65, solid185 and the contact pair Target 170 and Contact 174 elements were used for modeling the concrete, CFRP strips and CFRP-concrete interface respectively. The bond – slip model proposed by Lu et al. was selected to estimate the parameters required for implementing the CZM model for representing the CFRP-concrete interface. Where it was aproven that this model was effective for simulating the concrete-FRP interface behavior in several applications (Abdel Baky, Ebead and Neale, 2012; Zidani, Belakhdar, Tounsi and Bedia, 2015; Ko, Matthys, Palmieri and Sato, 2014). The mesh density (number of elements) was selected based on a trial solution so that the changing of the element numbers did not affect the results and in the same time did not produce convergence problem. The supports were set as fixed support. A horizontal load in the form of displacement was applied at the free end of FRP sheet. Then after, the nonlinear solution was carried out in which the applied load was automatically divided into smaller load steps and at each load step the model stiffness matrix was updated to reflect the nonlinear response of the structure. The Newton-Raphson equilibrium iterations models with displacement convergence criterion and a tolerance of (5%) were used to avoid the divergence problem. The finite element mesh, boundary conditions and loading system in ANSYS are shown in Figure 3.13.

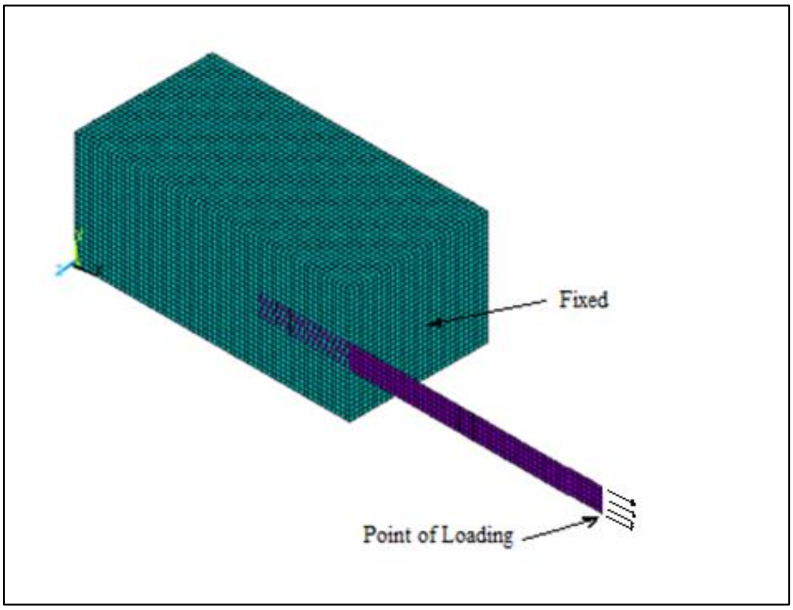

Figure 3.13. The finite element mesh, boundary conditions and loading system in ANSYS for specimen 50W200L

The finite element numerical analysis results obtained for all the tested specimens were compared with the corresponding experimental results. The comparison was made based on the ultimate load and the displacement at ultimate load. The analytical results reveal that the behavior of the numerical models agrees well with the reported experimental observations throughout the whole loading process as shown in Figure 3.14. The ultimate load and the displacement at ultimate load were reasonably predicted in comparison with the experimental results as shown in Table 3.3. Where the average difference in the ultimate load and the displacement at ultimate load were 1.75% and 6.7% respectively. As result, it could be concluded that the simulation method is appropriate for predicting the load carrying capacity of unanchored CFRP strips on a concrete surface.

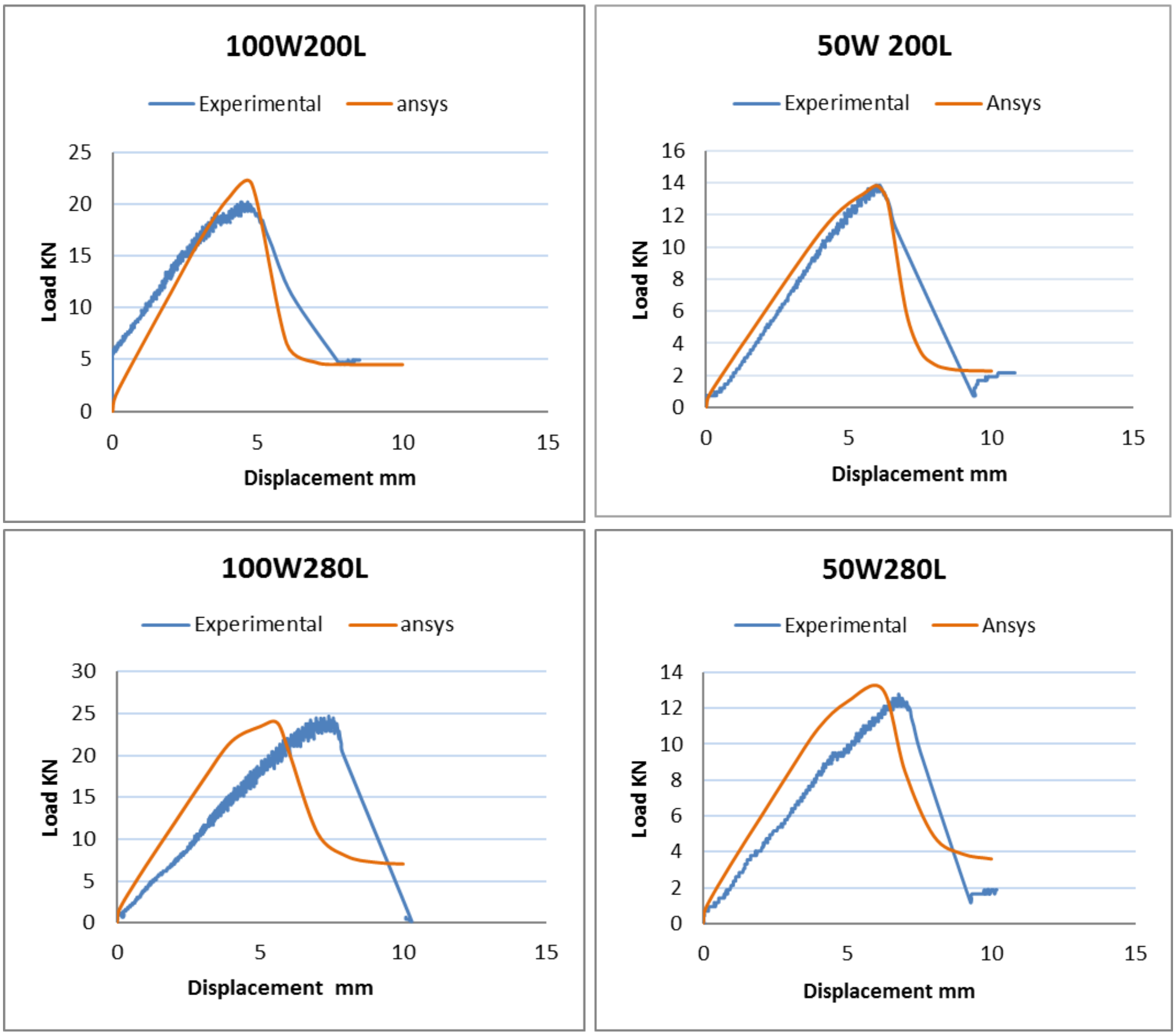

Figure 3.14. Comparison of load -displacement curves of unanchored specimens obtained from FE analysis and experiment

The same method was used for modeling the anchored specimens. The only difference was in representing the concrete- CFRP interface. Where the Lu model was used to represent the entire interface except for a specific area where the CFRP anchors penetrate the concrete. In this area, the bonding strength was increased to represent the effect of CFRP anchor. To simplify the simulation, the circular CFRP fan anchors are transformed to equivalent square area as shown in Figure 3.15 in which the bond-slip model proposed by Mertoğlu et al. (Mertoğlu, Anıl and Durucan, 2016) along with the bond- slip model proposed by Lu et al. were used to estimate the CZM parameters to represent the CFRP anchor effect. But, the value of the fracture energy of the anchored system G_{f_anchor} which is represented by the area under the bond-slip curve and estimated by using Mertoğlu model was smaller than the fracture energy of the unanchored system which estimated by using Lu model (equation 3.6) as shown in Figure 3.16, and that contrast to the fact that the existence of the anchors causes an increase in the bonding strength and fracture enrgy in comparison to the unanchored system (Ozbakkaloglu, Fang and Gholampour, 2017; Mertoğlu, Anıl and Durucan, 2016).

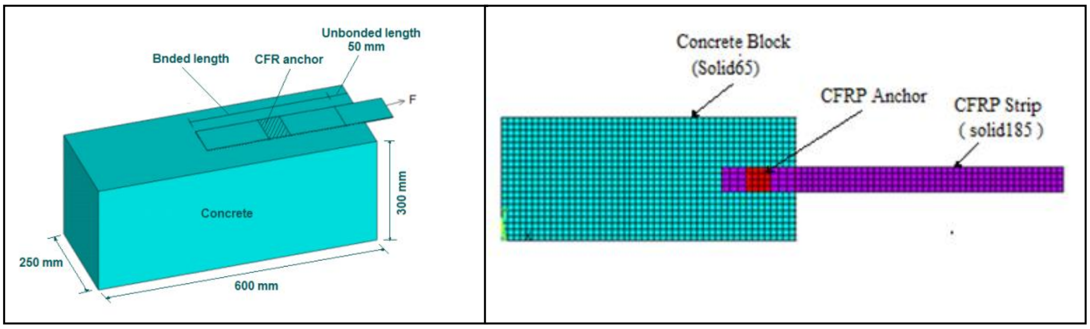

Figure 3.15. 3D FEA models of anchored FRP-concrete block

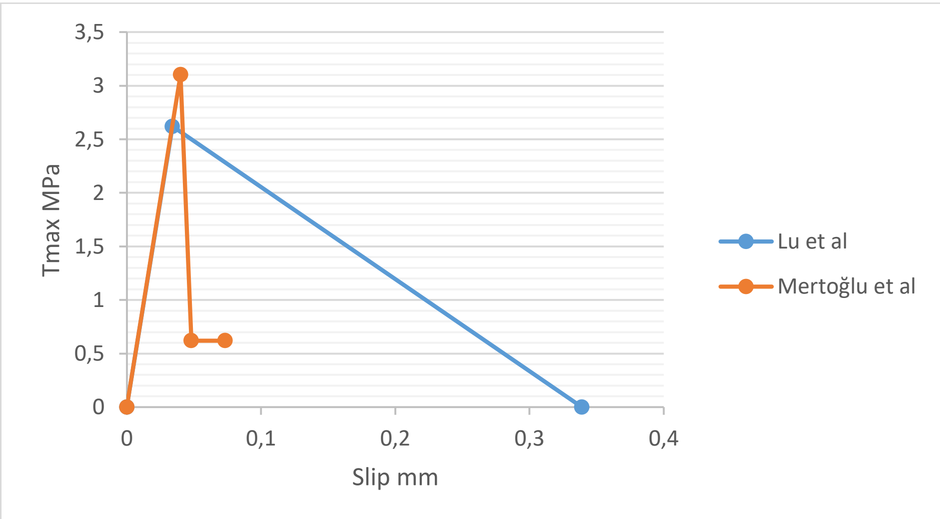

Figure 3.16. The comparison between the bond-slip model proposed by Lu et al . and Mertoğlu et al

In order to provide a simple approach to represent the CFRP anchor effect in FEA, a new bond-slip model for the interface where the CFRP anchor penetrates the concrete was proposed. The proposed model is an enhancement of bond- slip model originally proposed by Mertoğlu et al. The modification was implemented depending on the fitting of the nonlinear finite element results to experimental results from the literature as will be explained below.

3.6. Proposing New Bond-Slip Model

In the current study, the bilinear model shown in Figure 3.16 was proposed to represent the bond- slip model that will be used for modeling the CFRP anchor effect. The reason behind this selection is that the bilinear model considered being the most realistic and represents the closest approximation to the real behavior in comparesion to other models as mentioned earlier. The $\tau_{\max\_anchor}$ represents the ultimate shear capacity of the anchored system which could be calculated from equation 3.23. While S_{0_anchor} , S_{f_anchor}, K_{0_anchor} and G_{f_anchor} represents the local slip at maximum shear stress, local slip at the completion of debonding, initial stiffness and the fracture energy of the anchored system respectively.

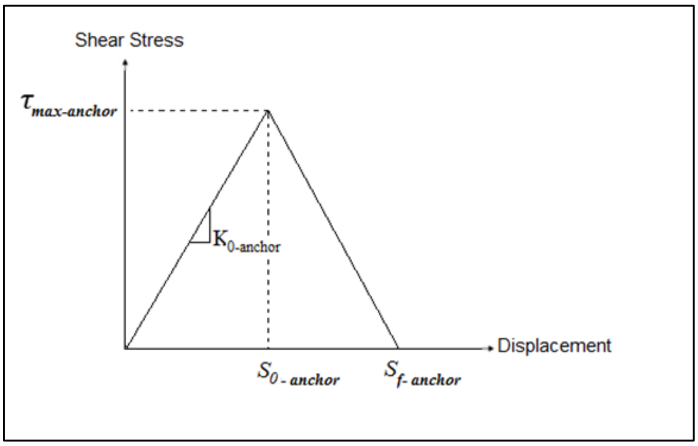

Figure 3.17. The new suggested anchored bond-slip model

For specifying the values of $S_{0-anchor}$ and $k_{0-anchor}$,the experimental results for the 14 selected specimens showed in Table 3.2 were reviewed, and the displacement at peak load and the stiffness were normalized and plotted against the number of anchors to clarify the effect of using anchors on the displacement at peak load and the stiffness. A simple linear regression was implemented as shown in the Figure 3.18.

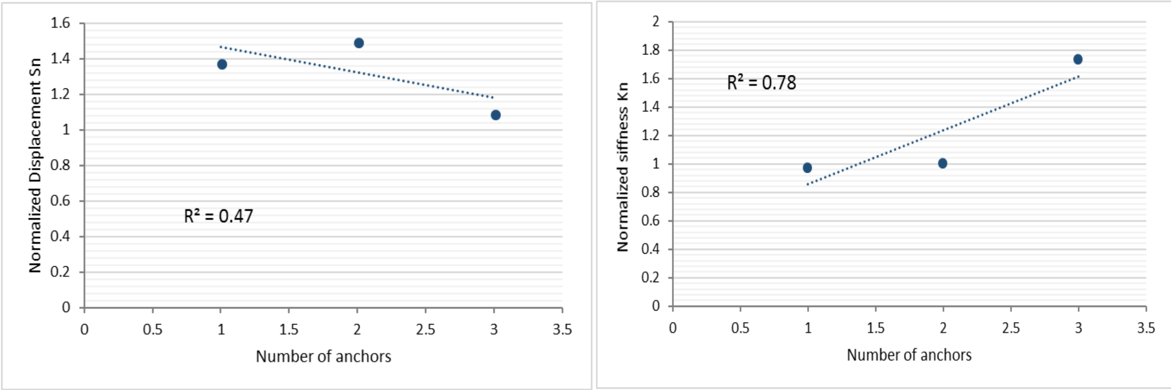

(a) (b)

Figure 3.18. The relationship between the number of anchors and: a) normalized displacement S_n b) normalized stiffness K_n

The linear regression reveals that increasing the number of anchors decreases the displacement at ultimate load, in contrast, the stiffness was increases by increasing the number of anchors. This finding is consistent with the result of a study conducted by Ko et al. (Ko, Matthys, Palmieri and Sato, 2014). Where In that study, a regression analysis for the results of 107 test taken from different studies showed that increasing the bond stress decreasing the corresponding displacement. Or in other words, increasing the bond strength increasing the stiffness of the bond- slip model and that contrast with the assumption originally made by Mertoğlu et al., where they assumed that the stiffness of the anchored bond-slip model has the same stiffness of the unanchored bond-slip model. Besides that, the regression analysis shown in Figure 3.18 also clarify that the displacement at ultimate load is less affected by the changing of the anchors' numbers in comparison to the stiffness. Therefore, it was assumed that the displacement at maximum load for the element without any anchor S_0 which obtained from Lu model (equation 3.7) could be used for the currently proposed bond-slip model. Consequently, the value of $k_{0-anchor}$ could be estimated as follow:

$$k_{0-anchor} = \frac{\tau_{max-anchor}}{s_0} \tag{3.28}$$

The next step is to estimate the $G_{f-anchor}$ value which represents an important factor to calculate $s_{f-anchor}$. The $G_{f-anchor}$ value was related to G_f as shown in equation 3.29.

$$G_{f-anchor} = \alpha\, G_f \tag{3.29}$$

In order to estimate the value of α, several 3D FE simulations were performed for different values of $G_{f-anchor}$. The results of the 3D FEA were fitted to experimental results. The value of $G_{f-anchor}$ which gives the closest Load-displacement behavior and ultimate load capacity P_{ult} to the experimental results was chosen as shown in the Figure 3.19. Then after, the selected $G_{f-anchor}$ were normalized by dividing over the G_f obtained from equation 3.6 which was used in the implementation of CZM model of the adjacent CFRP strip. The relationship between the number of anchors and the normalized anchored fracture energy G_{fn} was plotted as shown in Figure 3.20.

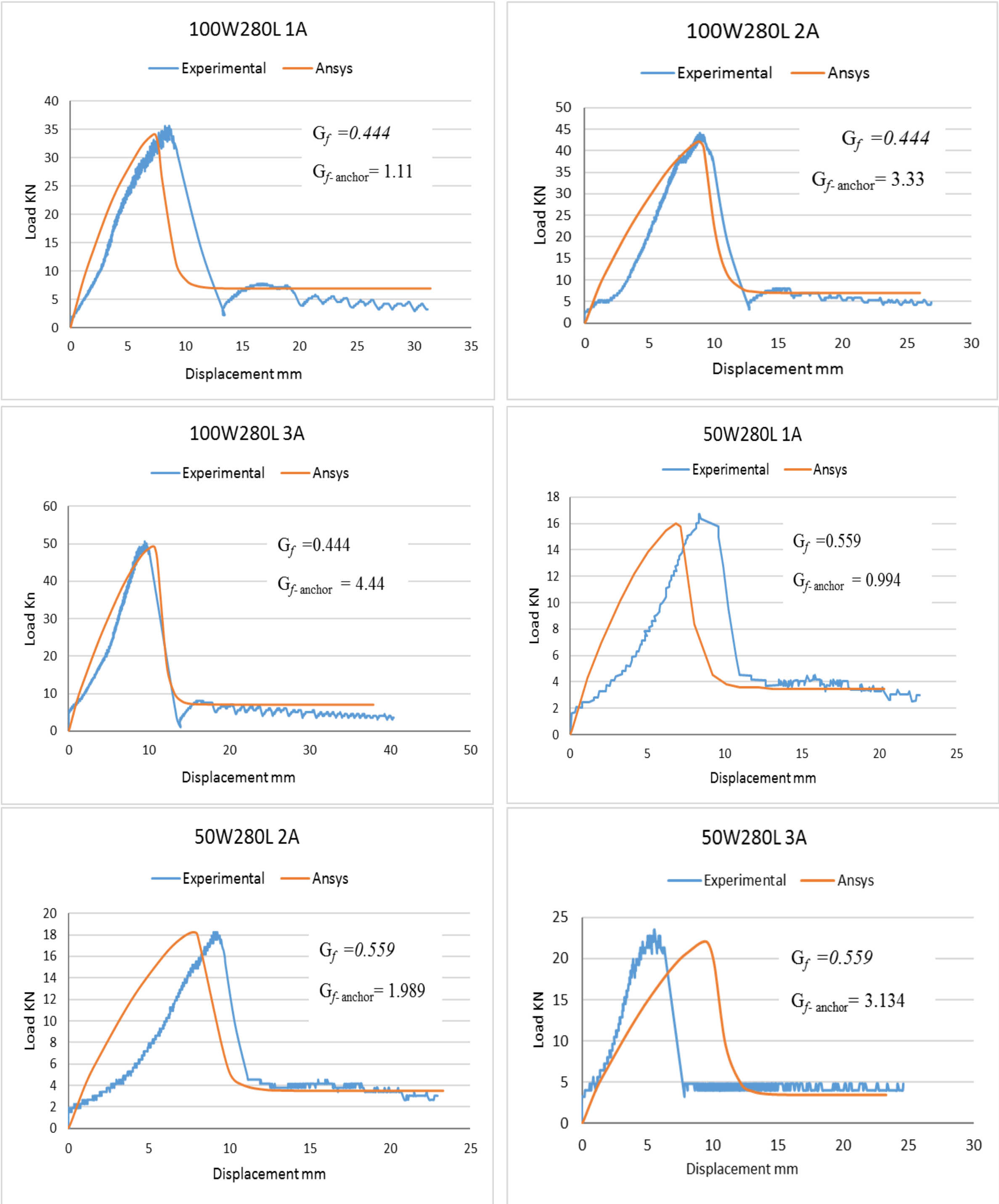

Figure 3.19. Comparison of load-displacement curves of anchored specimens obtained from FE analysis and experiment

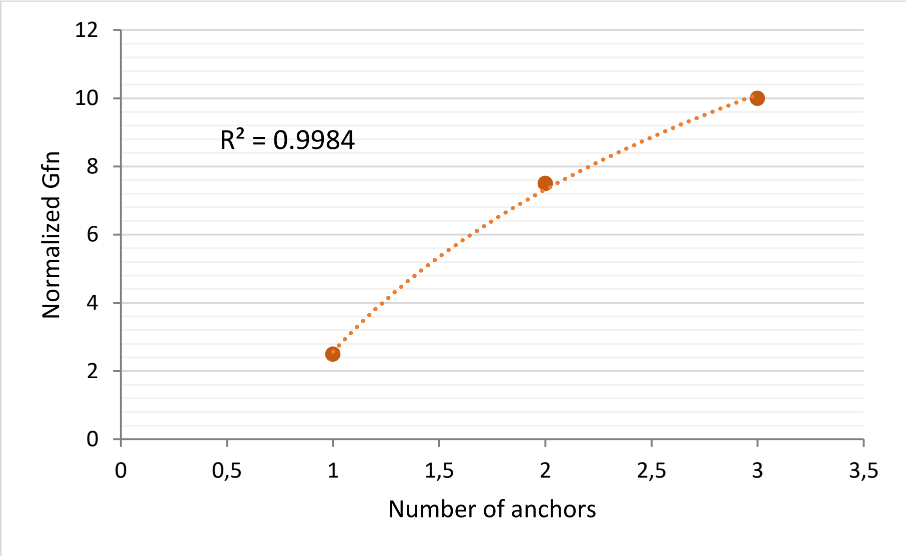

Figure 3.20. The relationship between the normalized anchored fracture energy and the number of anchors

It's obvious that the G_{fn} increasing with the increasing the number of anchors. Several functions were fitted to the data plotted in the Figure above by using Excel program and the function with the highest R^2 value was selected. The selected function has an R^2 value of 99.8% which indicate that 99.8% of the normalized anchored fracture energy G_{fn} could be evaluated reasonably by using the following equation:

$$\alpha = (\frac{b_f}{100})(6.868\ln(N) + 2.5645) \tag{3.30}$$

Finally, the value of $s_{f-anchor}$ could be estimated by using the following equation:

$$S_{f-anchor} = \frac{2G_{f-anchor}}{\tau_{max-anchor}} \tag{3.31}$$

For verifying the accuracy of the proposed equation, further analysis was implemented for four anchored specimens and the results obtained from the FE analysis were compared to the experimental results. The comparison results showed that there is a good agreement between the FE analysis and the experimental results as shown in Figure 3.21.

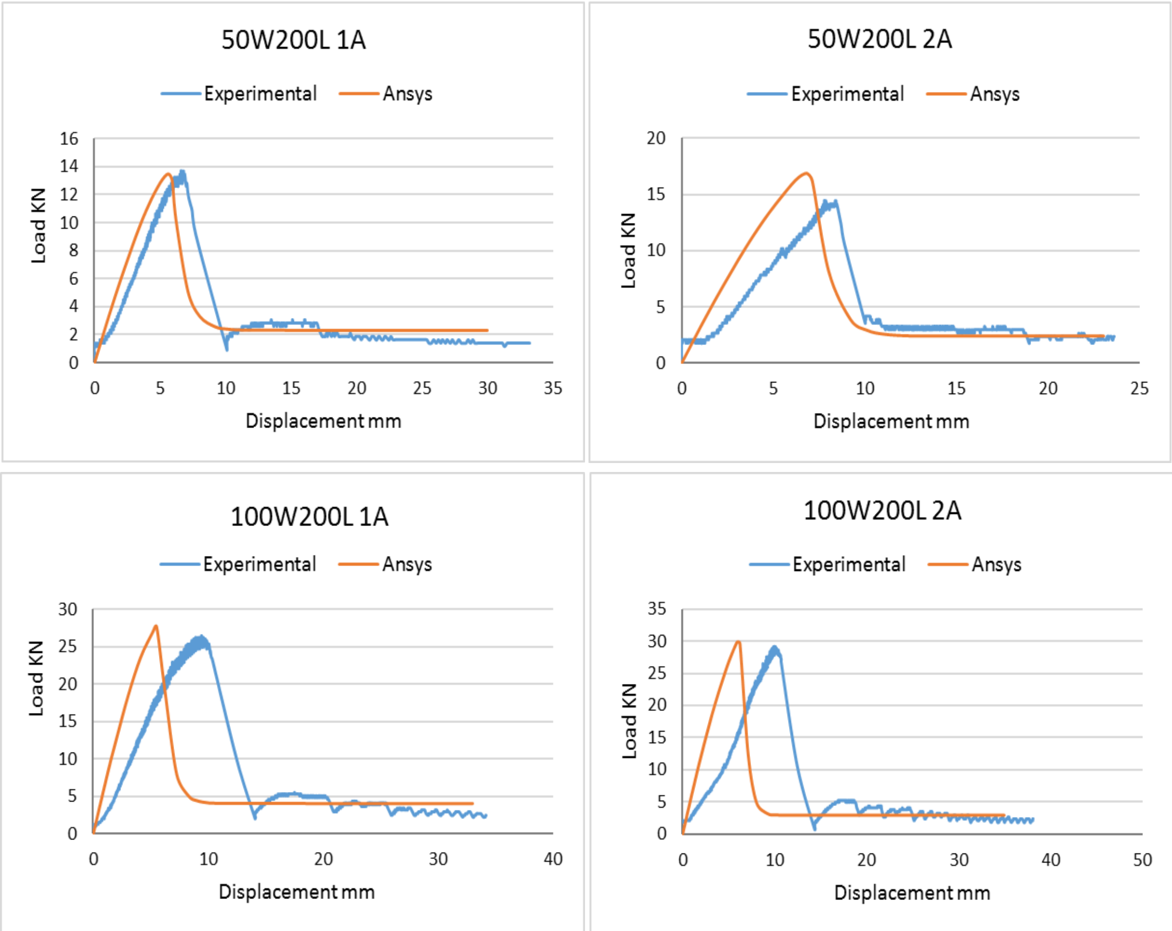

Figure 3.21. The comparison of the FE results for the specimens strengthened with CFRP have 200 mm bonding length and different width and anchor number and the experimental results.

A comparison between the experimental results for the selected 14 specimens and the analytical results obtained by using the new proposed model for simulating the CFRP anchor effect is shown in Figure 3.22. The results obtained from the proposed equations reveal that there is a good agreement with those obtained from experiments with R^2 equal to 0.99. Table 3.3 compares the P_{ult} obtained from experiments and FE study for all specimens.

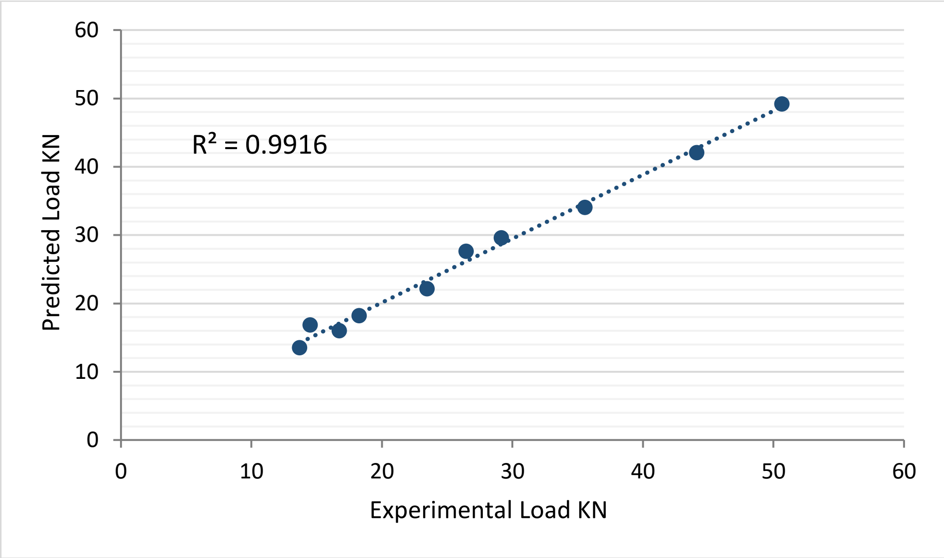

Figure 3.22. A comparison between the experimental P_{ult} and the analytical P_{ult} obtained by using the new proposed model

Table 3.3. The experimental and the analytical shear load and displacements for all specimens

No.	Specimens	Experimental Results		ANSYS Results		Load Ratio (ANSYS/ Exp.)	Displacement Ratio (ANSYS/ Exp.)	Residual Load		Residual Displacement	
		MAK. Load	MAK. Dis.	MAK. Load	MAK. Dis.			Exp.	ANSYS	Exp.	ANSYS
1	100W200L	20.19	4.45	21.91	4.8	1.08	1.07	-	-	-	-
2	100W280L	24.63	7.39	23.87	5.6	0.97	0.76	-	-	-	-
3	50W200L	12.8	6.79	13.85	6	1.08	0.88	-	-	-	-
4	50W280L	13.89	6.08	13.06	6.22	0.94	1.02	-	-	-	-
5	50W200L 1A	13.7	6.75	13.5	6.25	0.99	0.93	3.1	3.15	13.5	12.01
6	50W200L 2A	14.5	7.79	16.87	6.49	1.16	0.83	3.9	3.15	10.3	13
7	50W280L 1A	16.73	8.39	15.99	6.83	0.96	0.82	3.75	3.87	13.5	12
8	50W280L 2A	18.25	9.02	18.21	9.01	1	1	3.76	3.64	12.7	13
9	100W200L 1A	26.46	9.45	27.64	5.513	1.04	0.58	4.53	4.6	15.3	9.2
10	100W200L 2A	29.15	9.89	29.61	6.23	1.02	0.63	4	4.5	15.7	11
11	100W280L 1A	35.57	8.62	34.03	7.43	0.96	0.86	7.15	7.04	15.3	14
12	100W280L 2A	44.12	8.94	42.08	8.93	0.95	1	7.5	7.1	14.1	15
13	100W280L 3A	50.67	9.45	49.19	10.43	0.97	1.1	7.1	7.3	15.3	16
14	50W280L 3A	23.45	5.52	22.13	9.52	0.94	1.7	4.83	3.97	7.9	14

3.7 The Interface behavior for anchored Specimen

In the current study, a single anchored specimen was selected to examine the interface behavior at different loading values. For this purpose, path (A) was generated by selecting different nodes that belong to the middle of the CFRP strip along the bonding length of the specified specimen as shown in Figure 3.23. Then, the stress values were obtained from the FE analysis for all nodes that belong to path (A) and plotted against the distance from the loaded end at different loading values as shown below in Figure 3.24. Figure 3.25 shows the loading values at which the stress distribution along the bonded length was examined.

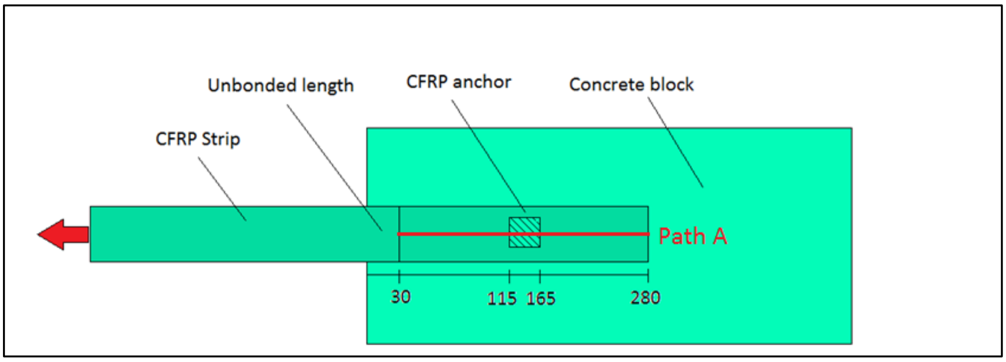

Figure 3.23. The position of path A

The comparison illustrated that the anchored specimen before loading has undeformed bonded area and stresses equal to zero. After applying the load, the stresses are initiated at the bonded area near the loaded end and then start to increase by increasing the applied load, whereas they decrease exponentially toward the unloaded end until the applied load reached 23.5 KN. At that value, the stress distribution takes a different shape and the bonded area is divided to three zones: The first zone is a constant stress zone which represents the debonded zone, the second zone represents the stress transfer zone which has the S shape and the third zone is the fully bonded zone in which the stresses are near or equal to zero. It could be observed that increasing the applied load gradually lead to extend the debonded zone toward the unloaded end till reaching the anchor position. Then after, the further increasing of the applied load causes a jump in the stresses due to the activation of the CFRP anchor till it reach its maximum value at ultimate load (34.4 KN). At the same time, the stresses in the CFRP strip behind the CFRP anchor are increased which refer to the mobilization of the bonded area. The more increase in the applied load produces a decrease in stresses, which indicates initiation of debonding in the bonded area behind the

CFRP anchor, However, stresses do not drop to zero as in the unanchored specimen because of the CFRP anchor clamping pressure which is responsible for activating frictional resistance between CFRP plate and roughened concrete substrate as stated by Zang et. al (Zhang and Smith, 2012).

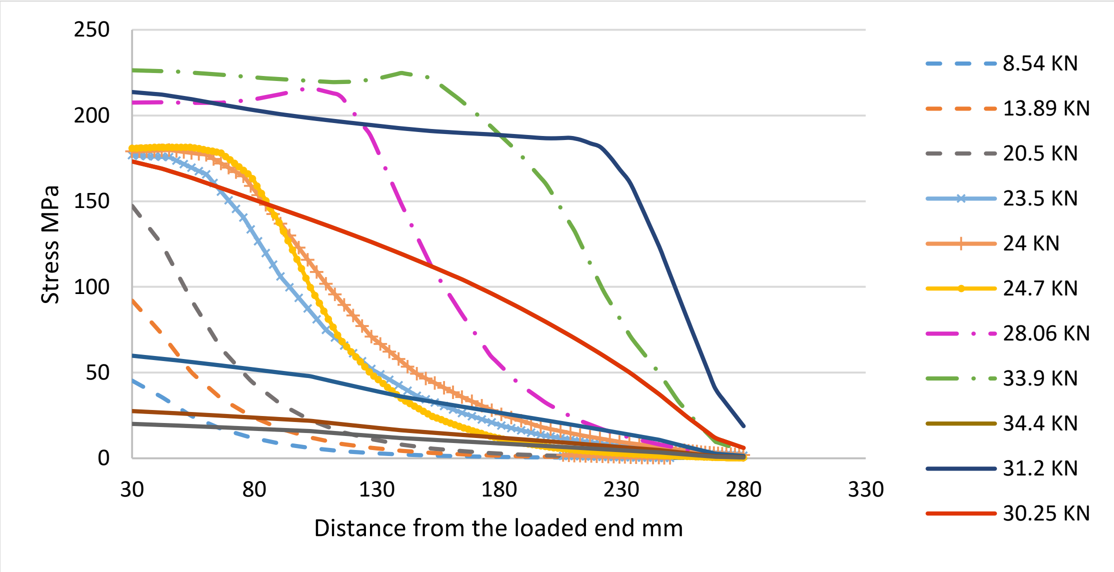

Figure 3.24. The comparison of the longitudinal stress distribution in CFRP strip for a single anchored specimen at different loading values

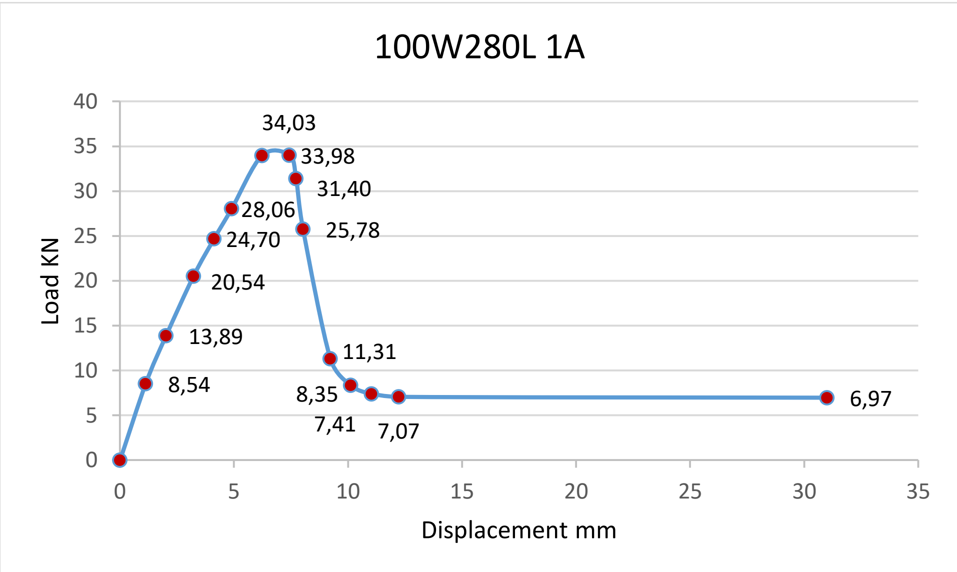

Figure 3.25. The loading values at which the stress distribution along the bonded length was examined

Also, from the comparison of the stress distribution in an unanchored specimen with the anchored specimen at ultimate load, it could be observed that the existence of anchors increases the amount of the stress transmitted from the CFRP to the concrete substrate as shown in Figure 3.26 below.

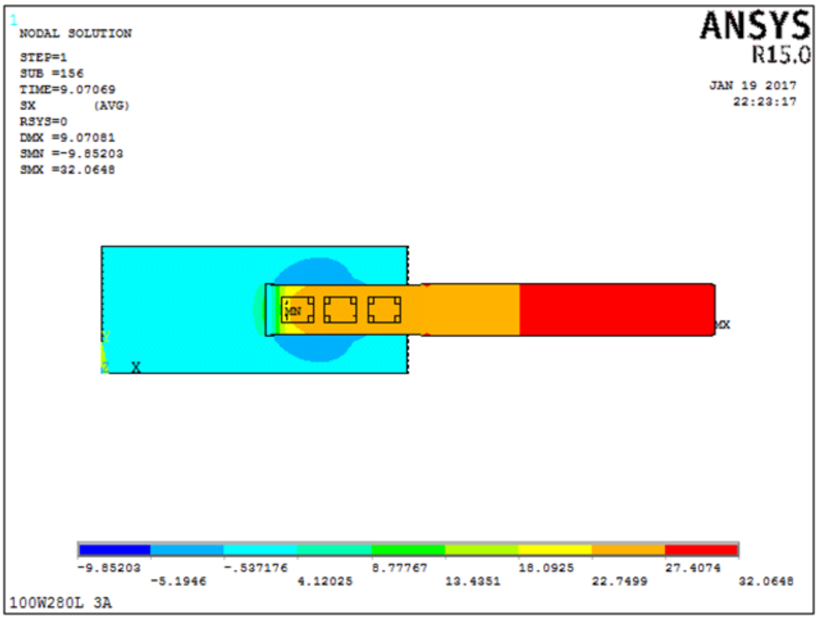

(a)

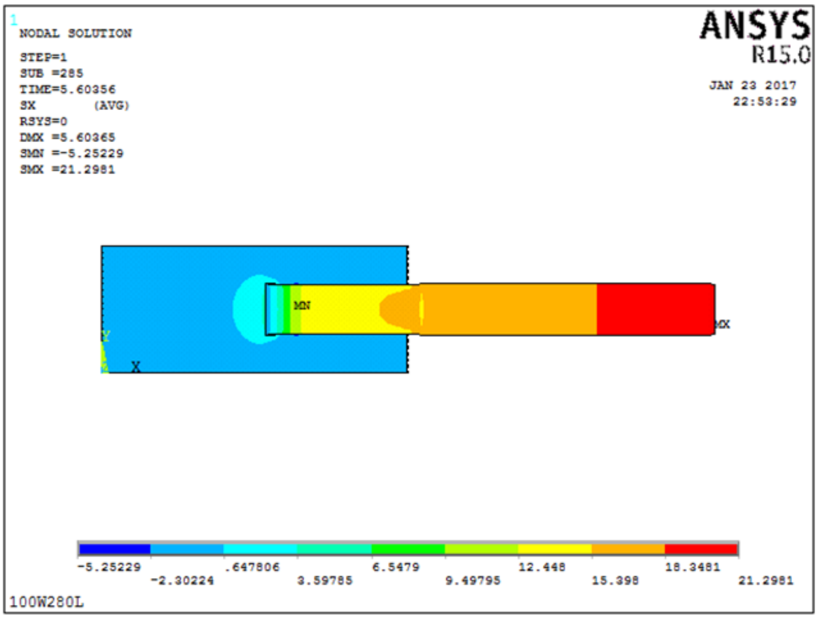

(b)

Figure 3.26. The stress distribution in (a) anchored specimen; (b) unanchored specimens

4. A PARAMETRIC STUDY OF THE FACTORS AFFECTING THE BOND-SLIP BEHAVIOR

In the previous chapter, an analytical model was developed for simulating the load transfer mechanism from CFRP strips to concrete in the existence of CFRP anchors. A new bond-slip model for representing the interface between CFR anchor and concrete was representing also the validity and the accuracy of the proposed model was checked by the comparison of the analytical results with the experimental results. In this chapter study, A parametric study was performed to investigate the influence of changing the concrete compressive strength, the CFRP strips width and length in additional to the number of CFRP anchors on the bonding strength of concrete specimens strengthened with anchored CFRP strips.

4.1. The Effect of The CFRP Width (Bf)

The effect of the CFRP width was examined through many experimental studies for unanchored CFRP strip. These studies showed that increasing the CFRP width had a significant effect on the ultimate load except when the CFRP to concrete width ratio is small which is leading to increase the stress concentration near the loaded end Thereby, reducing the ultimate load P_u.

In current study, it was observed that:

1. Increasing the CFRP width in the specimens with the same compressive strength, CFRP strip length and number of anchors increasing the ultimate load Pu; that the relation has a linear trend with a good correlation coefficient (R^2 value exceeding 0.96) as shown in Figure 4.1.a and b
2. For specimens with f_c= 25 MPa, the existence of the CFRP anchors increase the effect of the CFRP width specially when the CFRP strip width b_f is greater than 25 mm. For instance, in specimen with f_c= 25 MPa and L= 280 mm, increasing the bf from 50 mm to 100 mm, increases the P_u by 70% in reference element while increase P_u by 116% in the existence of three anchors.
3. For any b_f, changing the number of CFRP anchor from 1 to 2 or 3 has no significant effect on P_u value when the concrete compressive strength is 10 MPa as shown in Figure 4.1.b

4. For any concrete compressive strength (fc=10 or 25 MPa), the existence of CFRP anchors had no effect on the P_u value when bf=25 mm.

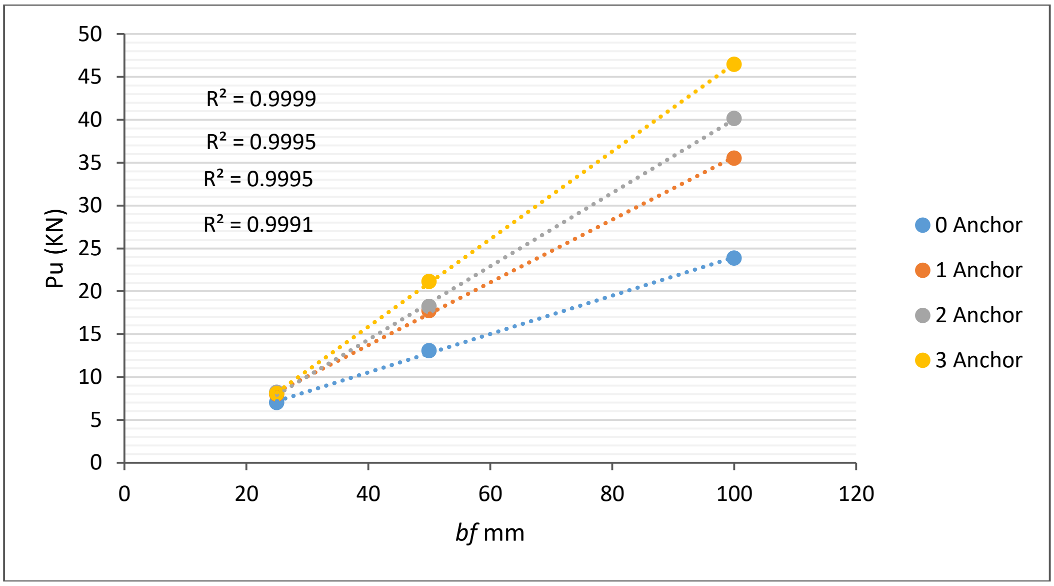

(a)

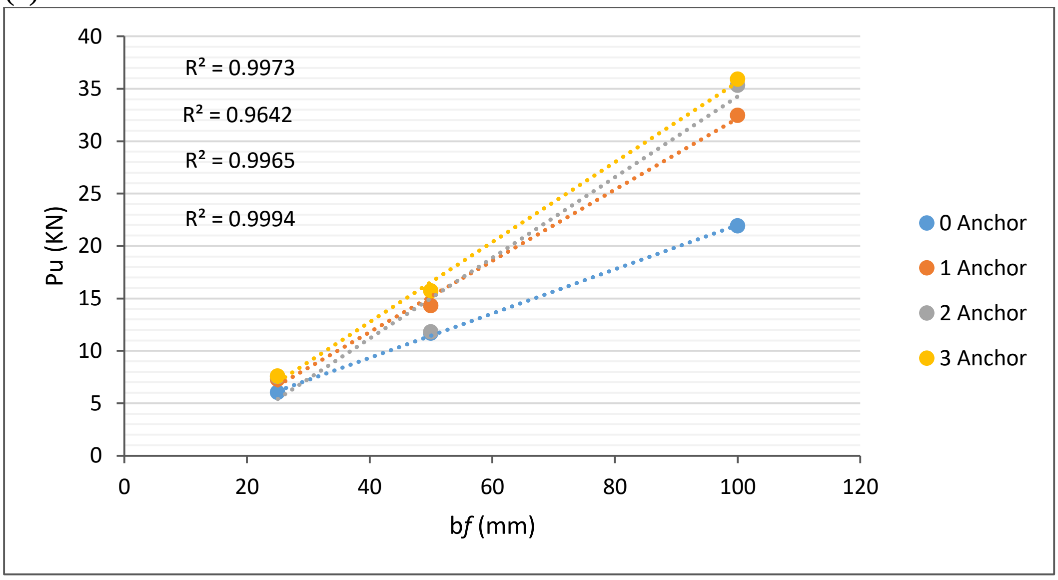

(b)

Figure 4.1. The effect of b_f and anchors number on the ultimate load capacity a) when L=280 mm, f_c= 25 MPa. b) when L=280 mm, f_c=10 MPa

4.2. The Effect of Compressive Strength

Most of the concrete members strengthened with CFRP fail in the concrete substrate at few millimeters beneath the concrete surface, that makes the concrete strength an important factor that effecting the bond strength. Based on the results obtained from the numerical analysis, the changing of concrete compressive strength from 10 MPa to 25 MPa for the unanchored specimens (reference) with same bonding length increases the ultimate load P_{ult} by an average of 13.4% regardless of the CFRP strips width as shown in Figure 4.2 (a). The specimens with CFRP anchors showed different behavior; It could be noticed from the comparison of Figures 4.2 (b), (c), and (d) that the effect of the compressive strength in specimens with the same CFRP length is related to the CFRP width and the number of anchors. The effect of the compressive strength increases by increasing the CFRP strips width and the number of anchors except for the specimens with b_f=25 mm, for any anchors number, changing the compressive strength did not show significant effect on the ultimate load. The maximum increment in the ultimate load was 29.3% when b_f=100 mm, L=280 mm, and A=3. The effect of changing the compressive strength is shown in Table 4.1

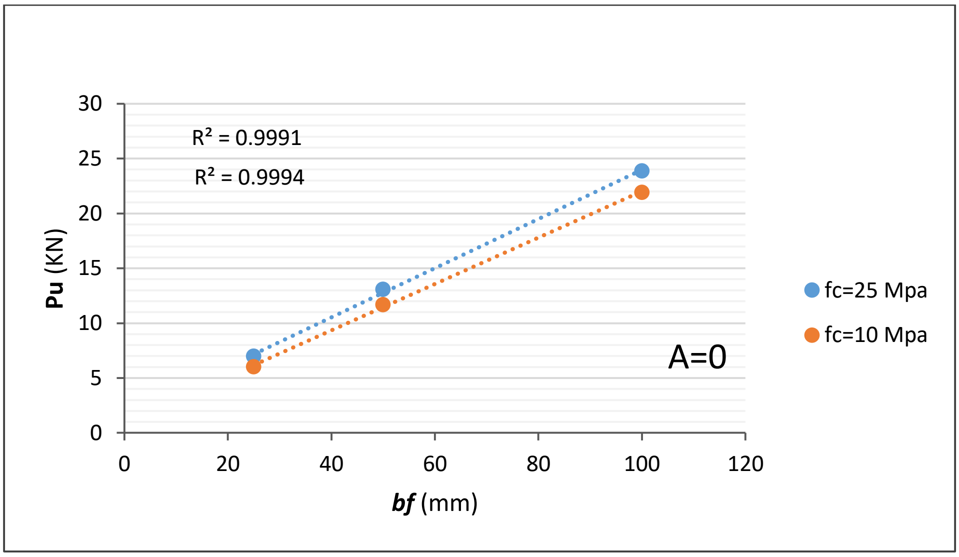

(a)

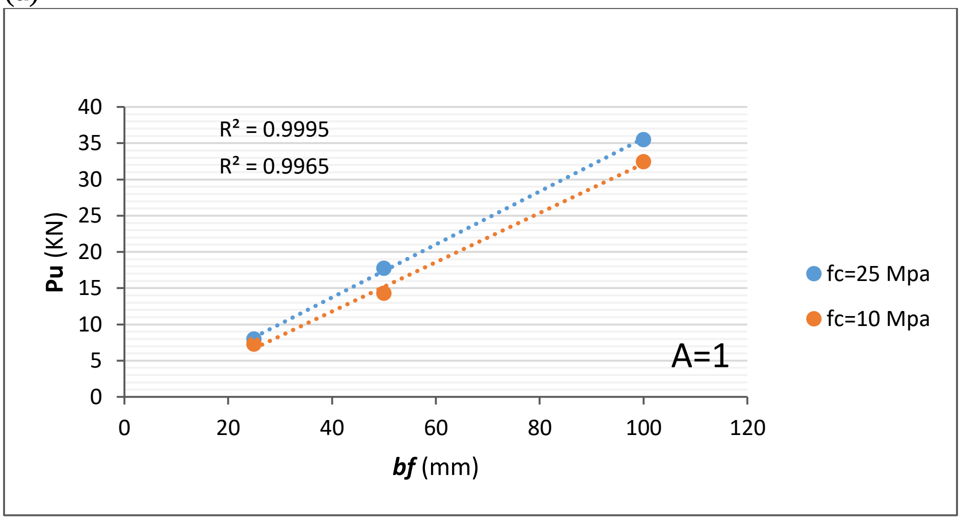

(b)

Figure 4.2. The Effect of CFRP width (*bf*) and concrete compressive strength (*f 'c)* on the ultimate load (P_u) when L= 180 mm

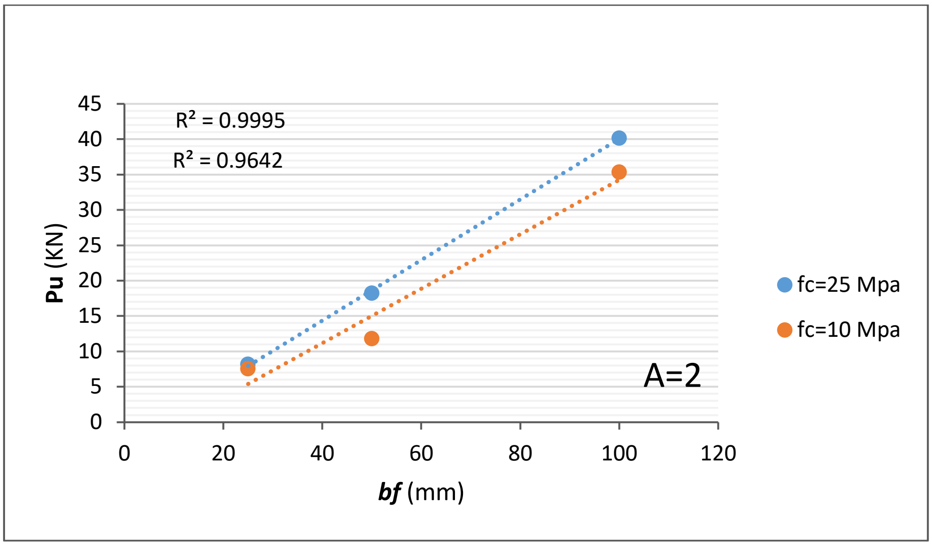

(c)

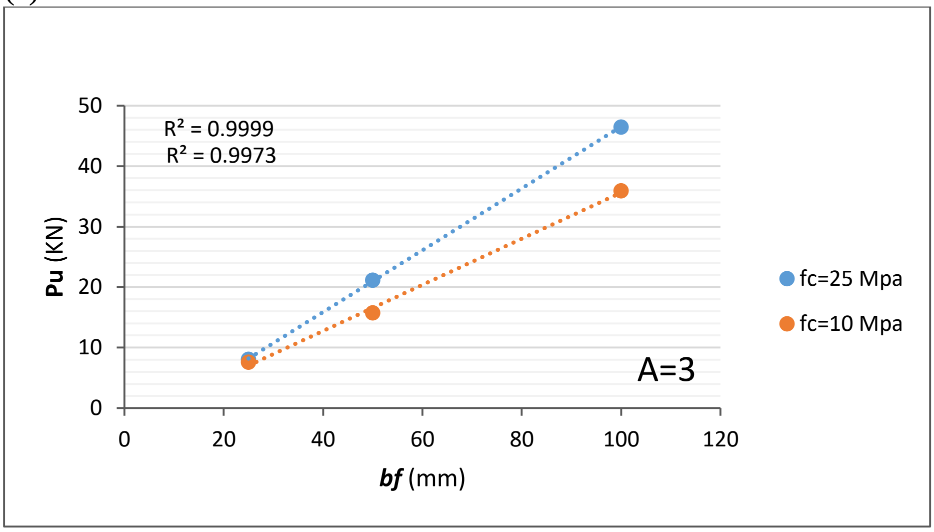

(d)

Figure 4.2. (continued) The Effect of CFRP width (*bf*) and concrete compressive strength (*f 'c*) on the ultimate load (P_u) when L= 180 mm

Table 4.1. The effect of the concrete compressive strength on the ultimate bonding strength

Specimen Definition	Compressive strength				The increment in P_{ult} %
	25 MPa		10 MPa		
	P_{ult} (kN)	Displacement at P_{ult} (mm)	P_{ult} (kN)	Displacement at P_{ult} (mm)	
25W150L	6.467	5.3236	5.503	4.4436	17.5
25W150L 1A	7.545	6.184	7.014	5.738	7.6
25W150L 2A	7.638	6.3636	7.079	5.943	7.9
50W150L	11.843	4.957	11.085	5	6.8
50W150L 1A	13.816	5.724	13336	5.438	3.6
50W150L 2A	14.162	5.9236	13.055	5.0236	8.5
100W150L	21.645	4.484	18.167	3.67	19.1
100W150L 1A	23.971	5.0236	21.374	4.4236	12.2
100W150L 2A	24.616	5.2036	21.75	4.527	13.2
25W200L	6.737	5.9036	5.774	4.963	16.7
25W200L 1A	7.7	6.8436	7.172	6.356	7.4
25W200L 2A	8.04	7.1	7.458	6.602	7.8
50W200L	13.854	6.0034	12.797	5.6436	8.3
50W200L 1A	14.242	6.25	12.088	5.177	17.8
50W200L 2A	14.601	6.4907	12.362	5.3957	18.1
100W200L	21.905	4.803	18.925	4.803	15.7
100W200L 1A	27.625	6.5507	22.045	4.8276	25.3
100W200L 2A	28.73	6.5507	22.707	5.0507	26.5
25W280L	6.996	6.7636	6.03	5.7236	16.0
25W280L 1A	7.999	7.5353	7.29	6.8084	9.7
25W280L 2A	8.191	7.925	7.547	7.249	8.5
25W280L 3A	8.041	7.865	7.596	7.4735	5.9
50W280L	13.065	6.22	11.678	5.77	11.9
50W280L 1A	17.738	8.7707	14.319	6.7307	23.9
50W280L 2A	18.219	9.0107	11.818	4.929	54.2
50W280L 3A	21.148	10.571	15.709	7.7507	34.6
100W280L	23.871	5.6036	21.928	5.306	8.9
100W280L 1A	35.526	8.8907	32.469	8.0508	9.4
100W280L 2A	40.159	10.031	35.33	8.8307	13.7
100W280L 3A	46.447	11.951	35.917	9.0707	29.3

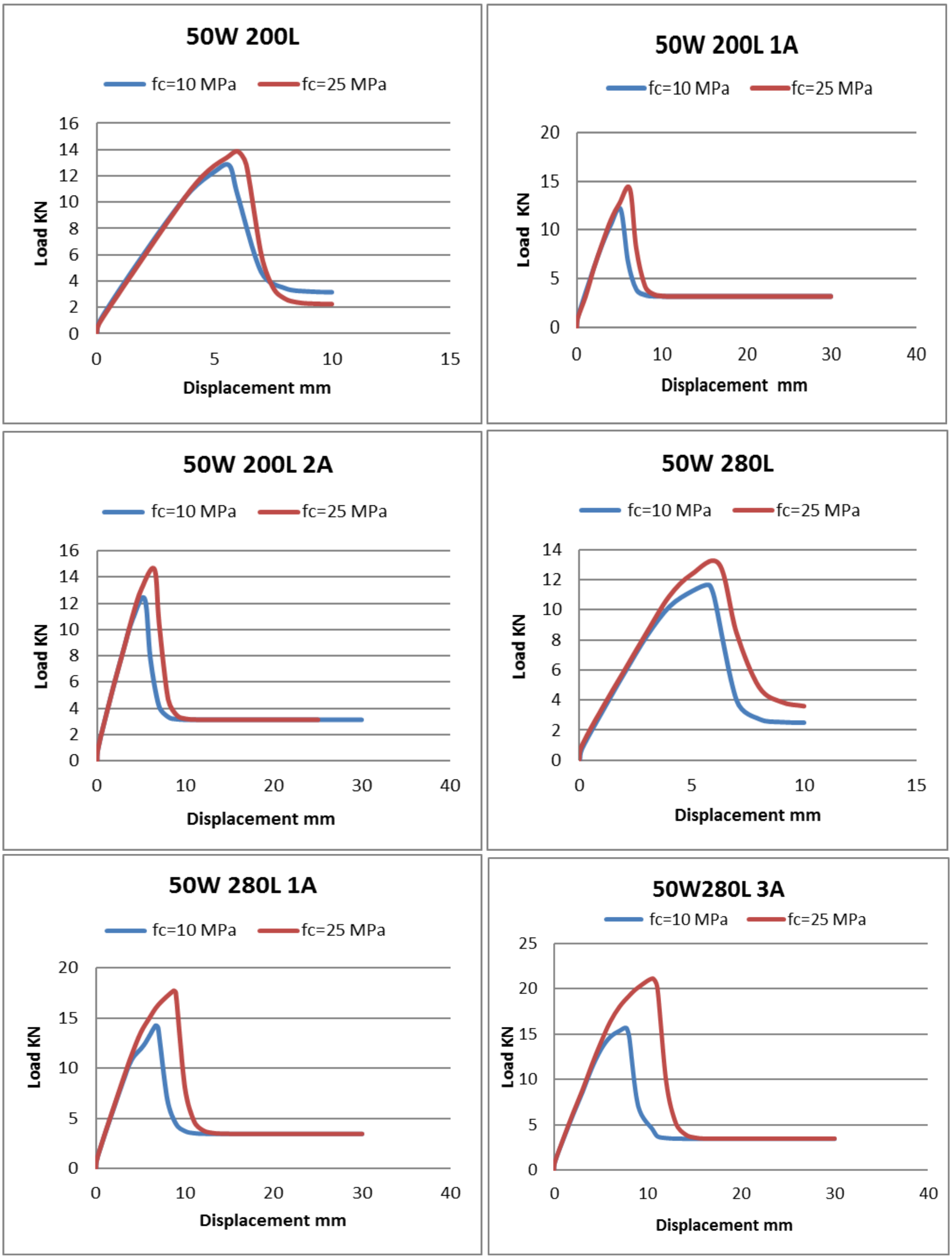

Figure 4.3. The effect of changing the compressive strength

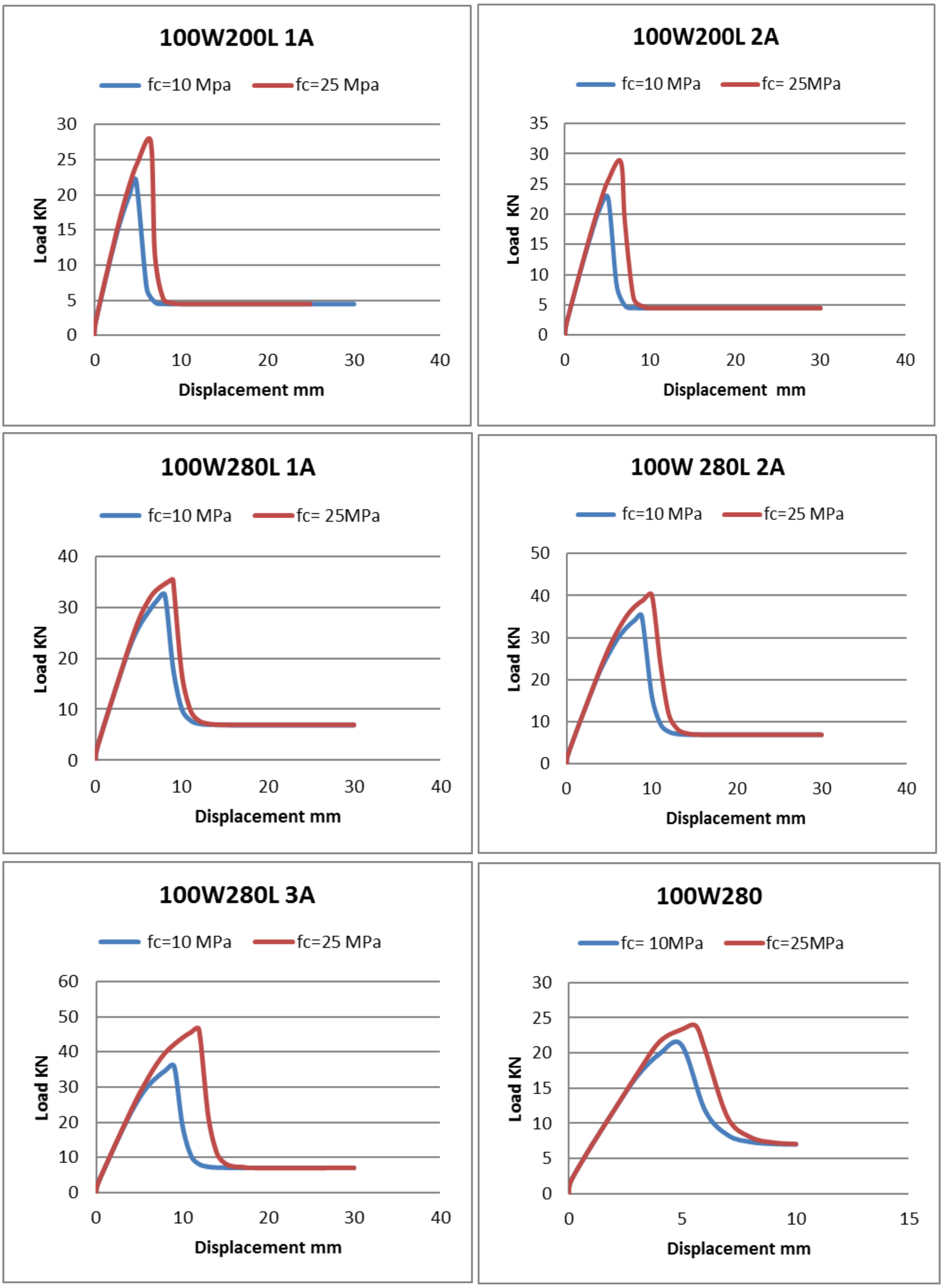

Figure 4.3. (continued) The effect of changing the compressive strength

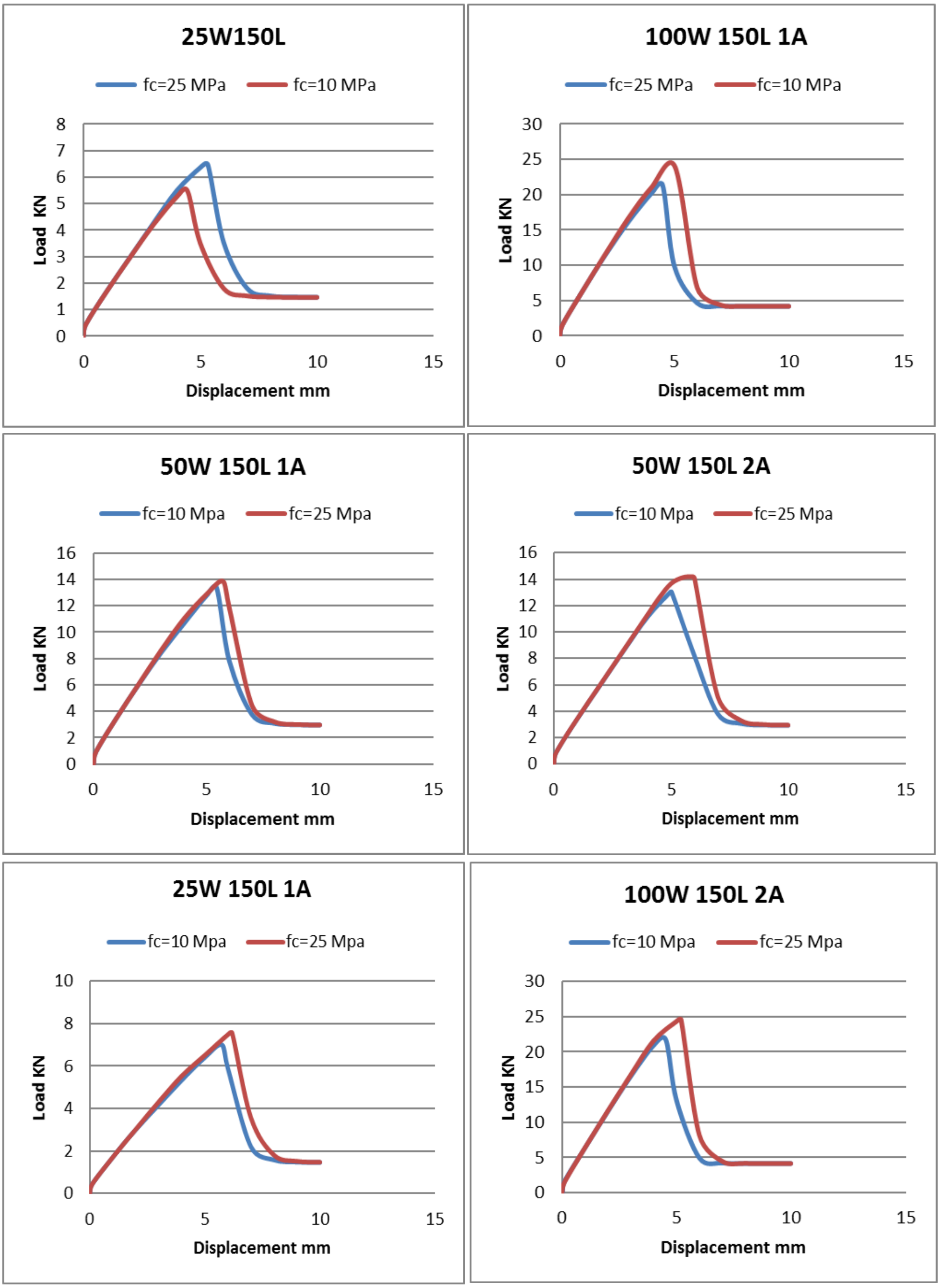

Figure 4.3. (continued) The effect of changing the compressive strength

4.3. The Effect of the CFRP Length

The effect of changing the CFRP length on the ultimate load is shown in Figure 4.4. From Figure 4.4 (a) it could be notice that, for reference specimens which have the same compressive strength and the same b_f, increasing the “L” has slightly effect on the ultimate load value. For instance, in reference element with a compressive strength of 25 MPa and b_f of 100 mm, increasing “L” value from 200 mm to 280 mm increases the P_u by 9%. Also, it could be notice that, the existence of the CFRP anchors increases the effect of the CFRP length. For instance, the specimen with a compressive strength of 25 MPa and b_f of 100 mm, increasing “L” value from 200 mm to 280 mm in the existence of 2 anchors increases the Pu by 39% in compression to the reference elements. The same effect could also be seen for specimens with a compressive strength of 10 MPa as shown in Figure 4.4 (b). For any compressive strength values changing the length of the CFRP strip has no significant effect on the P_u when the b_f is 25 mm.

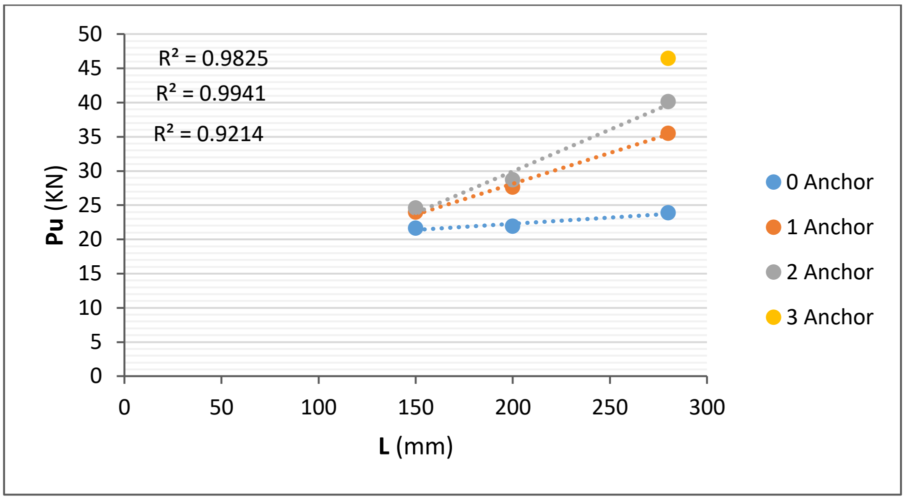

(a)

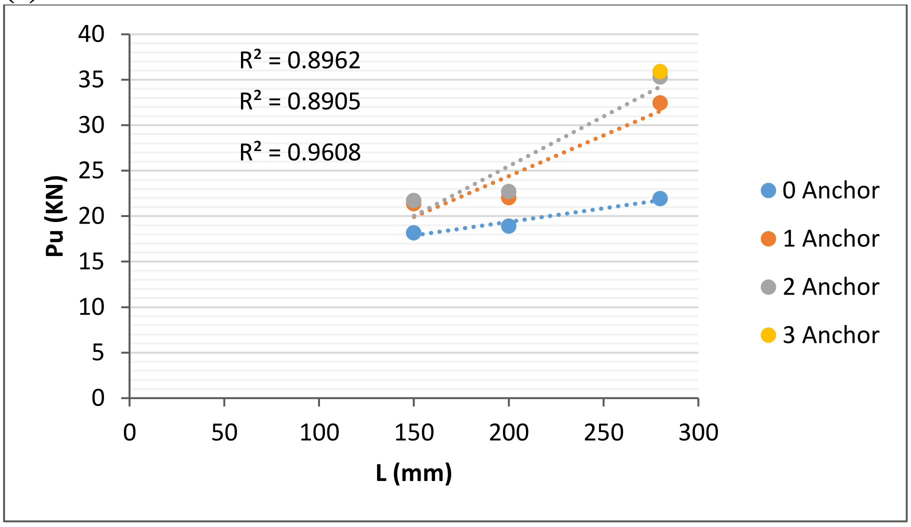

(b)

Figure 4.4. The effect of L and anchors number on the ultimate load capacity a) for specimen with b_f=100 mm, f_c= 25 MPa. b) for specimen with b_f=100 mm, f_c=10 MPa

5. ANALYTICAL STUDY

5.1. Review for The Available Bond Strength Models

There are many computational models had been proposed to estimate the ultimate load capacity Pu for concrete strengthened with unanchored CFRP strips. Whereas, limited models were submitted to estimate Pu for concrete strengthened with anchored CFRP strips. This section includes a review for the most conveniently used models.

Maeda et al. (Maeda, Asano, Sato, Ueda and Kakuta, 1997) investigated the effect of CFRP thickness (t_f) and modulus of elasticity (E_f) on the bonding strength by conducting a simple tension test. The study showed that increasing the bonding length beyond a certain value which is named as effective length (L_e) has no effect on the bonding strength. In another word, the bonding strength is not depending on the bonding length. The results also showed that there is an exponential relationship between L_e and the CFRP stiffness and that, the bonding stress τ_u varies linearly with CFRP sheet stiffness as shown in equations below:

$$L_e = e^{6.134-0.58ln(E_f t_f)} \tag{5.1}$$

$$\tau_u = 110.2 \times 10^{-6} E_f t_f \tag{5.2}$$

Finally, the ultimate load of CFRP sheet (P_u) could be estimated by multiplying the active bond area by the bonding stress as shown in equation 5.3:

$$P_u = \tau_u L_e b_f \tag{5.3}$$

Khalifa et al. (Khalifa, Gold, Nanni, and Abdel Aziz, 1998) suggested to modify equation 5.3 by adding the effect of concrete compressive strength to become as flows:

$$P_u = 110.2 \times 10^{-6} E_f t_f L_e b_f \left(\frac{f_c'}{42}\right)^{2/3} \tag{5.4}$$

Chen and Teng (Chen and Teng, 2001) reviewed and assisted the available strength models for FRP-to-concrete and steel plate-to-concrete bonded joints and proposed a new design model which could predict the effective length (L_e) and the bonding strength based on existing experimental observations as flows:

$$P_u = 0.427\beta_p\beta_L\sqrt{f_c' L_e} \tag{5.5}$$

$$L_e = \sqrt{\frac{E_f t_f}{\sqrt{f_c'}}} \tag{5.6}$$

$$\beta_p = \sqrt{\frac{2-(b_f/b_c)}{1+(b_f/b_c)}} \tag{5.7}$$

$$\beta_L = \begin{cases} 1 & L \geq L_e \\ sin\left(\frac{\pi L}{2L_e}\right) & L < L_e \end{cases} \tag{5.8}$$

Where β_P, β_L represents the geometric width coefficient and the geometric bond length coefficient respectively.

Based on the interfacial fracture energy, Lu et al. (Lu, Teng, Ye and Jiang, 2005) proposed a new model to estimate the bonding strength for CFRP-concrete joint as given in equation 5.9:

$$P_u = b_f\beta_L\sqrt{2E_f t_f G_f} \tag{5.9}$$

Where;

$$G_f = 0.308\beta_w^2\sqrt{f_t} \tag{5.10}$$

$$\beta_w = \sqrt{\frac{2.25-(b_f/b_c)}{1.25+(b_f/b_c)}} \tag{5.11}$$

$$f_t = 0.33\sqrt{f_c'} \tag{5.12}$$

The bond strength model proposed by Tanaka and Sato are given by the following equations as mentioned in (Ahmed, Bakay and Shrive , 2009):

$$P_u = \tau_u L b_f \tag{5.13}$$

$$\tau_u = 6.13 - \ln(L) \tag{5.14}$$

While, Iso bond strength model mentioned in (Ahmed, Bakay and Shrive , 2009) and (Lu, Teng, Ye and Jiang, 2005) is given by:

$$P_u = \tau_u L_e b_f \tag{5.15}$$

$$\tau_u = 0.93(f_c')^{0.44} \tag{5.16}$$

$$L_e = 0.125(E_f t_f)^{0.57} \tag{5.17}$$

Hiroyuki and Wu mentioned in (Ahmed, Bakay and Shrive , 2009) proposed the fowling bond strength model:

$$P_u = \tau_u L b_f \tag{5.18}$$

$$\tau_u = 0.27(L)^{-0.669} \tag{5.19}$$

The Sato bond strength model mentioned in (Ahmed, Bakay and Shrive , 2009) and (Lu, Teng, Ye and Jiang, 2005) is given by:

$$P_u = \tau_u L_e (b_f + 7.4) \tag{5.20}$$

$$\tau_u = 2.68 \times 10^{-5} (f_c')^{0.2} E_f t_f \tag{5.21}$$

$$L_e = 1.89(E_f t_f)^{0.4} \qquad \text{When, } L > L_e; L = L_e \tag{5.22}$$

İssa et al. (Issa, Rahma and Alrousan, 2016) conducted an experimental study to investigate the effect of CFRP bond width (b_f), and concrete ultimate compressive strength (f_c') on the bond strength of CFRP-concrete interface and suggested a modification for the ultimate load prediction model originally proposed by Chen and Teng. The proposed equations for calculating P_u shown in equation 5.23:

$$P_u = \tau_{max} b_f L \qquad \text{When, } L > L_e; L = L_e \tag{5.23}$$

Where, τ_{max} represents the maximum shear stress and could be calculated from the equation below

$$\tau_{max} = 0.385\ \beta_{\omega,\xi} \beta_L \sqrt{f_c'} \tag{5.24}$$

While, L_e, $\beta_{\omega,\xi}$, and β_L could be calculated from equations 5.6, 5.25 and 5.26 respectively

$$\beta_{\omega,\xi} = \sqrt{\frac{2.25-(b_f/b_c)}{1.25-(b_f/b_c)}} \tag{5.25}$$

$$\beta_L = \sqrt{\frac{2.25-(L/L_e)}{1.25+(L/L_e)}} \tag{5.26}$$

Zang and smith (Zhang and Smith, 2012) proposed a numerical model to estimate the ultimate load capacity for a single and multiple anchored CFRP strengthening system. In which it was showed that the ultimate load capacity is effected by the distance between the anchor and the unloaded end of the CFRP plate. For single anchored CFRP strengthening system:

$$P_{u,saj} = K_{saj} P_u \tag{5.27}$$

$$K_{saj} = A\left(\frac{L_{end}}{Le}\right) + B \tag{5.28}$$

While, for multiple strengthening system:

$$P_{u,maj} = K_{saj} P_u \tag{5.29}$$

$$K_{maj} = \sum_{i=1}^{n} \left[A\left(\frac{L_{end}}{Le}\right) + B - 1\right] + 1 \tag{5.30}$$

Where, $P_{u,saj}$ and $P_{u,maj}$ represents the ultimate load carrying capacity for a single and multiple anchored joint respectively, P_u is the ultimate load carrying capacity for unanchored joint, L_{end} is the distance between the anchor and the unloaded end of the

CFRP plate, and L_e is the effective length calculated based on Chen and Teng's model (equation 5.6). Finally, A and B represents constants equal to 0.7 and 1 respectively. The proposed model is applicable within the range $0.22 < L_{end}/L_e < 1.76$.

5.2. Comparison of The FEA Results with Some of The Bond Strength Models

By the comparison of the bonding strength P_u obtained from the analytical study with P_u estimated from bond strength models mentioned in the previous section, it could be notice that, for unanchored specimens the P_u estimated by using the models proposed by Khalifa, Tanaka, Hiroyuki, and Iso were under estimated while the results obtained by using Sato, Chen and Tang, and Lu et al. models were more accurate. Although, P_u obtained by using Maeda et al. model was close to the FEA results, but their model did not take in account the effect of very important factor that effecting the bonding strength which is the concrete compressive strength. For the anchored specimen, the results were compared with Pu estimated from the model proposed by Zang and Smith. It could be seen that, most of the results were overestimated beside some of the results were questionable since Lend/Le for some specimens lying out of the range mentioned above as illustrated in Table 5.1 and Figure 5.1 respectively.

Table 5.1. A compression of Pu obtained from the analytical study with Pu estimated from some of the most conveniently used models

No.		Sample	Ultimate Load KN	Maeda	Ratio	Khalifa	Ratio	Tanaka and Sato	Ratio	Hiroyuki and Wu	Ratio	Iso	Ratio
1	Experimental	100W200L	20.19	20.30	0.99	14.37	1.41	16.63	1.21	15.85	1.27	16.33	1.24
2		100W280L	23.63	20.30	1.16	14.37	1.64	13.87	1.70	17.72	1.33	16.33	1.45
3		50W200L	12.8	10.15	1.26	7.18	1.78	8.32	1.54	7.92	1.62	8.16	1.57
4		50W280L	13.89	10.15	1.37	7.18	1.93	6.93	2.00	8.86	1.57	8.16	1.70
5		50W200L 1A	13.7	10.15	1.35	7.18	1.91	8.32	1.65	7.92	1.73	8.16	1.68
6		50W200L 2A	14.5	10.15	1.43	7.18	2.02	8.32	1.74	7.92	1.83	8.16	1.78
7		50W280L 1A	16.73	10.15	1.65	7.18	2.33	6.93	2.41	8.86	1.89	8.16	2.05
8		50W280L 2A	18.25	10.15	1.80	7.18	2.54	6.93	2.63	8.86	2.06	8.16	2.24
9		100W200L 1A	26.46	20.30	1.30	14.37	1.84	16.63	1.59	15.85	1.67	16.33	1.62
10		100W200L 2A	29.15	20.30	1.44	14.37	2.03	16.63	1.75	15.85	1.84	16.33	1.79
11		100W280L 1A	35.57	20.30	1.75	14.37	2.48	13.87	2.57	17.72	2.01	16.33	2.18
12		100W280L 2A	44.12	20.30	2.17	14.37	3.07	13.87	3.18	17.72	2.49	16.33	2.70
13		100W280L 3A	50.67	20.30	2.50	14.37	3.53	13.87	3.65	17.72	2.86	16.33	3.10

Table 5.1. (continued) A compression of Pu obtained from the analytical study with Pu estimated from some of the most conveniently used models

14		50W280L 3A	23.45	10.15	2.31	7.18	3.26	6.93	3.38	8.86	2.65	8.16	2.87
15	ANSYS f'_c= 25 Mpa	25W150L	6.467	5.08	1.27	3.59	1.80	4.20	1.54	3.60	1.80	4.08	1.58
16		25W150L 1A	7.545	5.08	1.49	3.59	2.10	4.20	1.80	3.60	2.09	4.08	1.85
17		25W150L 2A	7.638	5.08	1.50	3.59	2.13	4.20	1.82	3.60	2.12	4.08	1.87
18		50W150L	11.843	10.15	1.17	7.18	1.65	8.40	1.41	7.20	1.64	8.16	1.45
19		50W150L 1A	13.816	10.15	1.36	7.18	1.92	8.40	1.65	7.20	1.92	8.16	1.69
20		50W150L 2A	14.162	10.15	1.40	7.18	1.97	8.40	1.69	7.20	1.97	8.16	1.73
21		100W150L	21.645	20.30	1.07	14.37	1.51	16.79	1.29	14.41	1.50	16.33	1.33
22		100W150L 1A	23.971	20.30	1.18	14.37	1.67	16.79	1.43	14.41	1.66	16.33	1.47
23	ANSYS f'_c= 25 Mpa	100W150L 2A	24.616	20.30	1.21	14.37	1.71	16.79	1.47	14.41	1.71	16.33	1.51
24		25W200L	6.737	5.08	1.33	3.59	1.88	4.16	1.62	3.96	1.70	4.08	1.65
25		25W200L 1A	7.7	5.08	1.52	3.59	2.14	4.16	1.85	3.96	1.94	4.08	1.89
26		25W200L 2A	8.04	5.08	1.58	3.59	2.24	4.16	1.93	3.96	2.03	4.08	1.97
27		50W200L	13.854	10.15	1.36	7.18	1.93	8.32	1.67	7.92	1.75	8.16	1.70
28		50W200L 1A	14.242	10.15	1.40	7.18	1.98	8.32	1.71	7.92	1.80	8.16	1.74
29		50W200L 2A	14.601	10.15	1.44	7.18	2.03	8.32	1.76	7.92	1.84	8.16	1.79

Table 5.1. (continued) A compression of Pu obtained from the analytical study with Pu estimated from some of the most conveniently used models

30		100W200L	21.905	20.30	1.08	14.37	1.52	16.63	1.32	15.85	1.38	16.33	1.34
31		100W200L 1A	27.625	20.30	1.36	14.37	1.92	16.63	1.66	15.85	1.74	16.33	1.69
32		100W200L 2A	28.73	20.30	1.42	14.37	2.00	16.63	1.73	15.85	1.81	16.33	1.76
33		25W280L	6.996	5.08	1.38	3.59	1.95	3.47	2.02	4.43	1.58	4.08	1.71
34		25W280L 1A	7.999	5.08	1.58	3.59	2.23	3.47	2.31	4.43	1.81	4.08	1.96
35		25W280L 2A	8.191	5.08	1.61	3.59	2.28	3.47	2.36	4.43	1.85	4.08	2.01
36		25W280L 3A	8.041	5.08	1.58	3.59	2.24	3.47	2.32	4.43	1.82	4.08	1.97
37		50W280L	13.065	10.15	1.29	7.18	1.82	6.93	1.88	8.86	1.47	8.16	1.60
38		50W280L 1A	17.738	10.15	1.75	7.18	2.47	6.93	2.56	8.86	2.00	8.16	2.17
39		50W280L 2A	18.219	10.15	1.79	7.18	2.54	6.93	2.63	8.86	2.06	8.16	2.23
40		50W280L 3A	21.148	10.15	2.08	7.18	2.94	6.93	3.05	8.86	2.39	8.16	2.59
41		100W280L	23.871	20.30	1.18	14.37	1.66	13.87	1.72	17.72	1.35	16.33	1.46
42		100W280L 1A	35.526	20.30	1.75	14.37	2.47	13.87	2.56	17.72	2.01	16.33	2.18
43		100W280L 2A	40.159	20.30	1.98	14.37	2.80	13.87	2.90	17.72	2.27	16.33	2.46
44		100W280L 3A	46.447	20.30	2.29	14.37	3.23	13.87	3.35	17.72	2.62	16.33	2.84

Table 5.1. (continued) A compression of Pu obtained from the analytical study with Pu estimated from some of the most conveniently used models

45	ANSYS f_c'= 10 Mpa	25W150L	5.503	5.08	1.08	1.95	2.82	4.20	1.31	3.60	1.53	2.73	2.02
46		25W150L 1A	7.014	5.08	1.38	1.95	3.60	4.20	1.67	3.60	1.95	2.73	2.57
47		25W150L 2A	7.079	5.08	1.39	1.95	3.63	4.20	1.69	3.60	1.97	2.73	2.60
48		50W150L	11.085	10.15	1.09	3.90	2.84	8.40	1.32	7.20	1.54	5.45	2.03
49		50W150L 1A	13.336	10.15	1.31	3.90	3.42	8.40	1.59	7.20	1.85	5.45	2.44
50		50W150L 2A	13.055	10.15	1.29	3.90	3.35	8.40	1.56	7.20	1.81	5.45	2.39
51		100W150L	18.167	20.30	0.89	7.80	2.33	16.79	1.08	14.41	1.26	10.91	1.67
52		100W150L 1A	21.374	20.30	1.05	7.80	2.74	16.79	1.27	14.41	1.48	10.91	1.96
53		100W150L 2A	21.75	20.30	1.07	7.80	2.79	16.79	1.30	14.41	1.51	10.91	1.99
54		25W200L	5.774	5.08	1.14	1.95	2.96	4.16	1.39	3.96	1.46	2.73	2.12
55		25W200L 1A	7.172	5.08	1.41	1.95	3.68	4.16	1.72	3.96	1.81	2.73	2.63
56		25W200L 2A	7.458	5.08	1.47	1.95	3.82	4.16	1.79	3.96	1.88	2.73	2.73
57		50W200L	12.797	10.15	1.26	3.90	3.28	8.32	1.54	7.92	1.61	5.45	2.35
58		50W200L 1A	12.088	10.15	1.19	3.90	3.10	8.32	1.45	7.92	1.53	5.45	2.22
59		50W200L 2A	12.362	10.15	1.22	3.90	3.17	8.32	1.49	7.92	1.56	5.45	2.27
60		100W200L	18.925	20.30	0.93	7.80	2.43	16.63	1.14	15.85	1.19	10.91	1.73

Table 5.1. (continued) A compression of Pu obtained from the analytical study with Pu estimated from some of the most conveniently used models

61		100W200L 1A	22.045	20.30	1.09	7.80	2.83	16.63	1.33	15.85	1.39	10.91	2.02
62		100W200L 2A	22.707	20.30	1.12	7.80	2.91	16.63	1.37	15.85	1.43	10.91	2.08
63		25W280L	6.03	5.08	1.19	1.95	3.09	3.47	1.74	4.43	1.36	2.73	2.21
64		25W280L 1A	7.29	5.08	1.44	1.95	3.74	3.47	2.10	4.43	1.65	2.73	2.67
65		25W280L 2A	7.547	5.08	1.49	1.95	3.87	3.47	2.18	4.43	1.70	2.73	2.77
66		25W280L 3A	7.596	5.08	1.50	1.95	3.90	3.47	2.19	4.43	1.71	2.73	2.79
67	ANSYS f'_c= 10 Mpa	50W280L	11.678	10.15	1.15	3.90	2.99	6.93	1.68	8.86	1.32	5.45	2.14
68		50W280L 1A	14.319	10.15	1.41	3.90	3.67	6.93	2.07	8.86	1.62	5.45	2.63
69		50W280L 2A	11.818	10.15	1.16	3.90	3.03	6.93	1.70	8.86	1.33	5.45	2.17
70		50W280L 3A	15.709	10.15	1.55	3.90	4.03	6.93	2.27	8.86	1.77	5.45	2.88
71		100W280L	21.928	20.30	1.08	7.80	2.81	13.87	1.58	17.72	1.24	10.91	2.01
72		100W280L 1A	32.469	20.30	1.60	7.80	4.16	13.87	2.34	17.72	1.83	10.91	2.98
73		100W280L 2A	35.33	20.30	1.74	7.80	4.53	13.87	2.55	17.72	1.99	10.91	3.24
74		100W280L 3A	35.917	20.30	1.77	7.80	4.61	13.87	2.59	17.72	2.03	10.91	3.29

Table 5.1. (continued) A compression of Pu obtained from the analytical study with Pu estimated from some of the most conveniently used models

No.		Sample	Ultimate Load KN	Sato	Ratio	Cheng and Teng	Ratio	Zang and Smith	Ratio	Lu	Ratio
1	Experimental	100W200L	20.19	17.18	1.17	16.99	1.19	16.99	1.19	17.67	1.14
2		100W280L	23.63	17.18	1.38	16.99	1.39	16.99	1.39	17.67	1.34
3		50W200L	12.8	9.18	1.39	9.73	1.31	9.73	1.31	9.92	1.29
4		50W280L	13.89	9.18	1.51	9.73	1.43	9.73	1.43	9.92	1.40
5		50W200L 1A	13.7	9.18	1.49	9.73	1.41	18.89	0.73	9.92	1.38
6		50W200L 2A	14.5	9.18	1.58	9.73	1.49	27.58*	0.53	9.92	1.46
7		50W280L 1A	16.73	9.18	1.82	9.73	1.72	22.58*	0.74	9.92	1.69
8		50W280L 2A	18.25	9.18	1.99	9.73	1.87	35.36*	0.52	9.92	1.84
9		100W200L 1A	26.46	17.18	1.54	16.99	1.56	32.97	0.80	17.67	1.50
10		100W200L 2A	29.15	17.18	1.70	16.99	1.72	48.15*	0.61	17.67	1.65
11		100W280L 1A	35.57	17.18	2.07	16.99	2.09	39.43*	0.90	17.67	2.01
12		100W280L 2A	44.12	17.18	2.57	16.99	2.60	61.72*	0.71	17.67	2.50
13		100W280L 3A	50.67	17.18	2.95	16.99	2.98	84.12*	0.60	17.67	2.87
14		50W280L 3A	23.45	9.18	2.55	9.73	2.41	48.19*	0.49	9.92	2.36
15	ANSYS	25W150L	6.467	5.18	1.25	5.22	1.24	5.22	1.24	5.26	1.23
16		25W150L 1A	7.545	5.18	1.46	5.22	1.44	8.93	0.84	5.26	1.43
17		25W150L 2A	7.638	5.18	1.47	5.22	1.46	12.59*	0.61	5.26	1.45

Table 5.1. (continued) A compression of Pu obtained from the analytical study with Pu estimated from some of the most conveniently used models

18		50W150L	11.843	9.18	1.29	9.73	1.22	9.73	1.22	9.92	1.19
19		50W150L 1A	13.816	9.18	1.50	9.73	1.42	16.65	0.83	9.92	1.39
20		50W150L 2A	14.162	9.18	1.54	9.73	1.45	23.46*	0.60	9.92	1.43
21		100W150L	21.645	17.18	1.26	16.99	1.27	16.99	1.27	17.67	1.22
22		100W150L 1A	23.971	17.18	1.40	16.99	1.41	29.06	0.82	17.67	1.36
23	ANSYS f_c'= 25 Mpa	100W150L 2A	24.616	17.18	1.43	16.99	1.45	40.96*	0.60	17.67	1.39
24		25W200L	6.737	5.18	1.30	5.22	1.29	5.22	1.29	5.26	1.28
25		25W200L 1A	7.7	5.18	1.49	5.22	1.47	10.13	0.76	5.26	1.46
26		25W200L 2A	8.04	5.18	1.55	5.22	1.54	14.78*	0.54	5.26	1.53
27		50W200L	13.854	9.18	1.51	9.73	1.42	9.73	1.42	9.92	1.40
28		50W200L 1A	14.242	9.18	1.55	9.73	1.46	18.89	0.75	9.92	1.44
29		50W200L 2A	14.601	9.18	1.59	9.73	1.50	27.55*	0.53	9.92	1.47
30		100W200L	21.905	17.18	1.27	16.99	1.29	16.99	1.29	17.67	1.24
31		100W200L 1A	27.625	17.18	1.61	16.99	1.63	32.97	0.84	17.67	1.56
32		100W200L 2A	28.73	17.18	1.67	16.99	1.69	48.09*	0.60	17.67	1.63
33		25W280L	6.996	5.18	1.35	5.22	1.34	5.22	1.34	5.26	1.33
34		25W280L 1A	7.999	5.18	1.54	5.22	1.53	12.12*	0.66	5.26	1.52
35		25W280L 2A	8.191	5.18	1.58	5.22	1.57	18.97*	0.43	5.26	1.56
36		25W280L 3A	8.041	5.18	1.55	5.22	1.54	25.85*	0.31	5.26	1.53

Table 5.1. (continued) A compression of Pu obtained from the analytical study with Pu estimated from some of the most conveniently used models

37		50W280L	13.065	9.18	1.42	9.73	1.34	9.73	1.34	9.92	1.32
38		50W280L 1A	17.738	9.18	1.93	9.73	1.82	22.58*	0.79	9.92	1.79
39		50W280L 2A	18.219	9.18	1.98	9.73	1.87	35.34*	0.52	9.92	1.84
40		50W280L 3A	21.148	9.18	2.30	9.73	2.17	48.19*	0.44	9.92	2.13
41		100W280L	23.871	17.18	1.39	16.99	1.40	16.99	1.40	17.67	1.35
42		100W280L 1A	35.526	17.18	2.07	16.99	2.09	39.43*	0.90	17.67	2.01
43		100W280L 2A	40.159	17.18	2.34	16.99	2.36	61.69*	0.65	17.67	2.27
44		100W280L 3A	46.447	17.18	2.70	16.99	2.73	84.12*	0.55	17.67	2.63
45	ANSYS f'_c= 10 Mpa	25W150L	5.503	4.32	1.28	4.15	1.32	4.15	1.32	4.64	1.19
46		25W150L 1A	7.014	4.32	1.63	4.15	1.69	7.10	0.99	4.64	1.51
47		25W150L 2A	7.079	4.32	1.64	4.15	1.70	10.01*	0.71	4.64	1.53
48		50W150L	11.085	7.65	1.45	7.74	1.43	7.74	1.43	8.75	1.27
49		50W150L 1A	13.336	7.65	1.74	7.74	1.72	13.24	1.01	8.75	1.52
50		50W150L 2A	13.055	7.65	1.71	7.74	1.69	18.66*	0.70	8.75	1.49
51		100W150L	18.167	14.31	1.27	13.52	1.34	13.52	1.34	15.58	1.17
52		100W150L 1A	21.374	14.31	1.49	13.52	1.58	23.11	0.92	15.58	1.37
53		100W150L 2A	21.75	14.31	1.52	13.52	1.61	32.57*	0.67	15.58	1.40
54		25W200L	5.774	4.32	1.34	4.15	1.39	4.15	1.39	4.64	1.24
55		25W200L 1A	7.172	4.32	1.66	4.15	1.73	8.06	0.89	4.64	1.55

Table 5.1. (continued) A compression of Pu obtained from the analytical study with Pu estimated from some of the most conveniently used models

56		25W200L 2A	7.458	4.32	1.73	4.15	1.80	11.76*	0.63	4.64	1.61
57		50W200L	12.797	7.65	1.67	7.74	1.65	7.74	1.65	8.75	1.46
58		50W200L 1A	12.088	7.65	1.58	7.74	1.56	15.02	0.80	8.75	1.38
59		50W200L 2A	12.362	7.65	1.62	7.74	1.60	21.91*	0.56	8.75	1.41
60		100W200L	18.925	14.31	1.32	13.52	1.40	13.52	1.40	15.58	1.21
61		100W200L 1A	22.045	14.31	1.54	13.52	1.63	26.22	0.84	15.58	1.42
62		100W200L 2A	22.707	14.31	1.59	13.52	1.68	38.25*	0.59	15.58	1.46
63		25W280L	6.03	4.32	1.40	4.15	1.45	4.15	1.45	4.64	1.30
64		25W280L 1A	7.29	4.32	1.69	4.15	1.76	9.64*	0.76	4.64	1.57
65		25W280L 2A	7.547	4.32	1.75	4.15	1.82	15.09*	0.50	4.64	1.63
66		25W280L 3A	7.596	4.32	1.76	4.15	1.83	20.56*	0.37	4.64	1.64
67	ANSYS f'_c= 10 Mpa	50W280L	11.678	7.65	1.53	7.74	1.51	7.74	1.51	8.75	1.34
68		50W280L 1A	14.319	7.65	1.87	7.74	1.85	17.96*	0.80	8.75	1.64
69		50W280L 2A	11.818	7.65	1.55	7.74	1.53	28.10*	0.42	8.75	1.35
70		50W280L 3A	15.709	7.65	2.05	7.74	2.03	38.32*	0.41	8.75	1.80
71		100W280L	21.928	14.31	1.53	13.52	1.62	13.52	1.62	15.58	1.41
72		100W280L1A1	32.469	14.31	2.27	13.52	2.40	31.36*	1.04	15.58	2.08
73		100W280L 2A	35.33	14.31	2.47	13.52	2.61	49.06*	0.72	15.58	2.27
74		100W280L 3A	35.917	14.31	2.51	13.52	2.66	66.90*	0.54	15.58	2.31

* the validity of this model is questionable for the specimens with L_{end}/L_e values lying out of the interval $0.22< L_{end}/L_e < 1.76$.

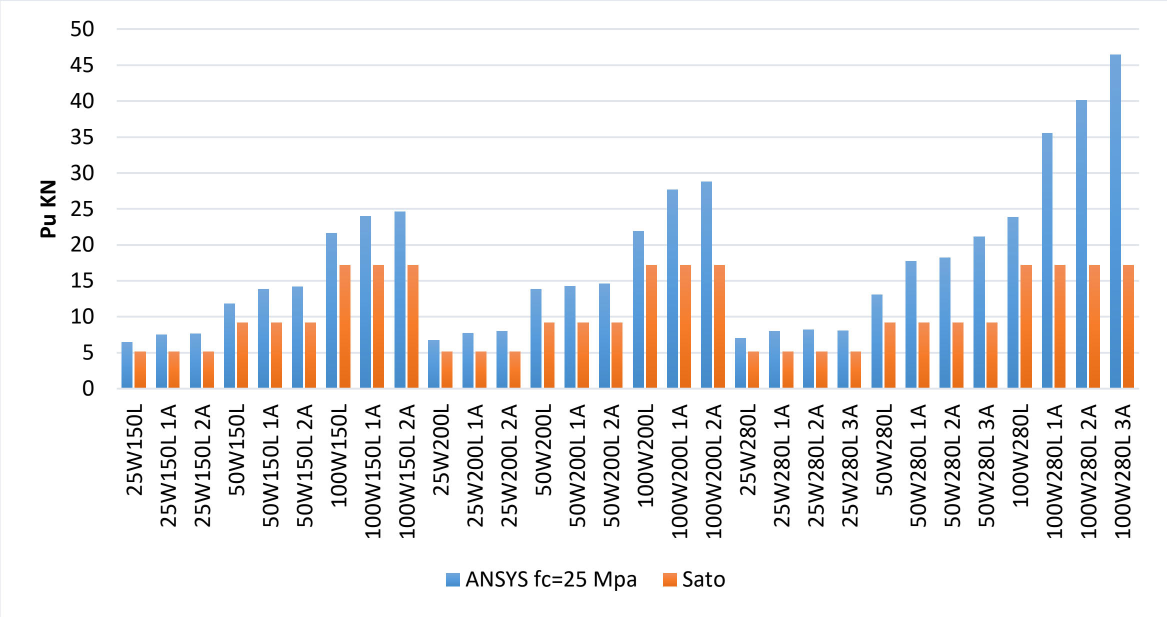

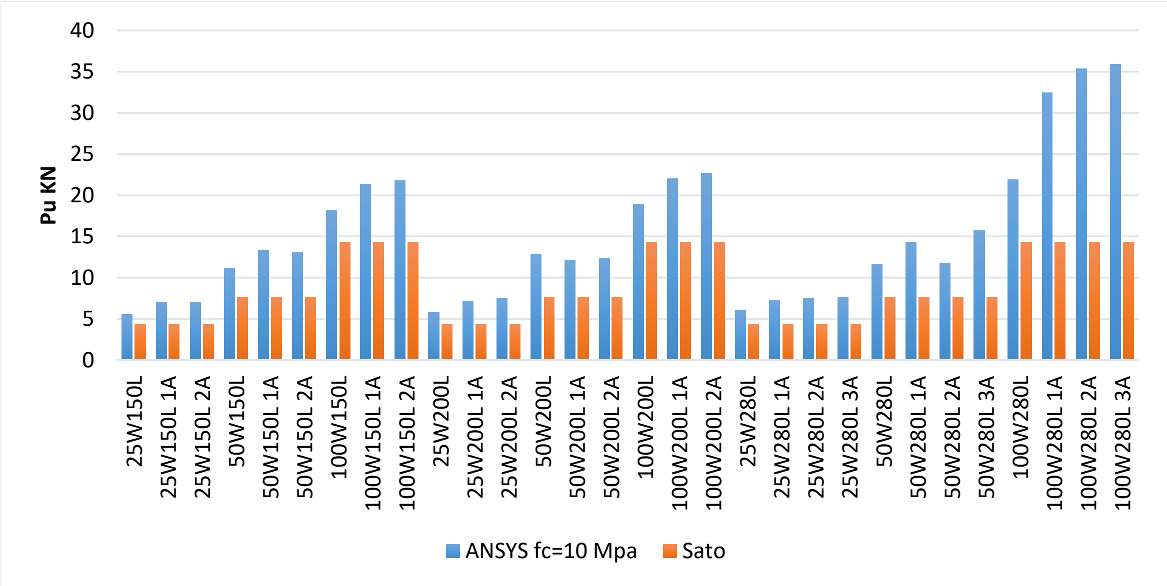

a) Sato model

Figure 5.1. Comparison of P_u obtained from most conveniently used models and FEA results; a) Sato model, b) Tanaka and Sato model, c) Maeda model, d) Khalifa model, e) Hiroyuki and Wu model, f) M. Iso model, g) Chen and Teng model, h) Zang and Smith model

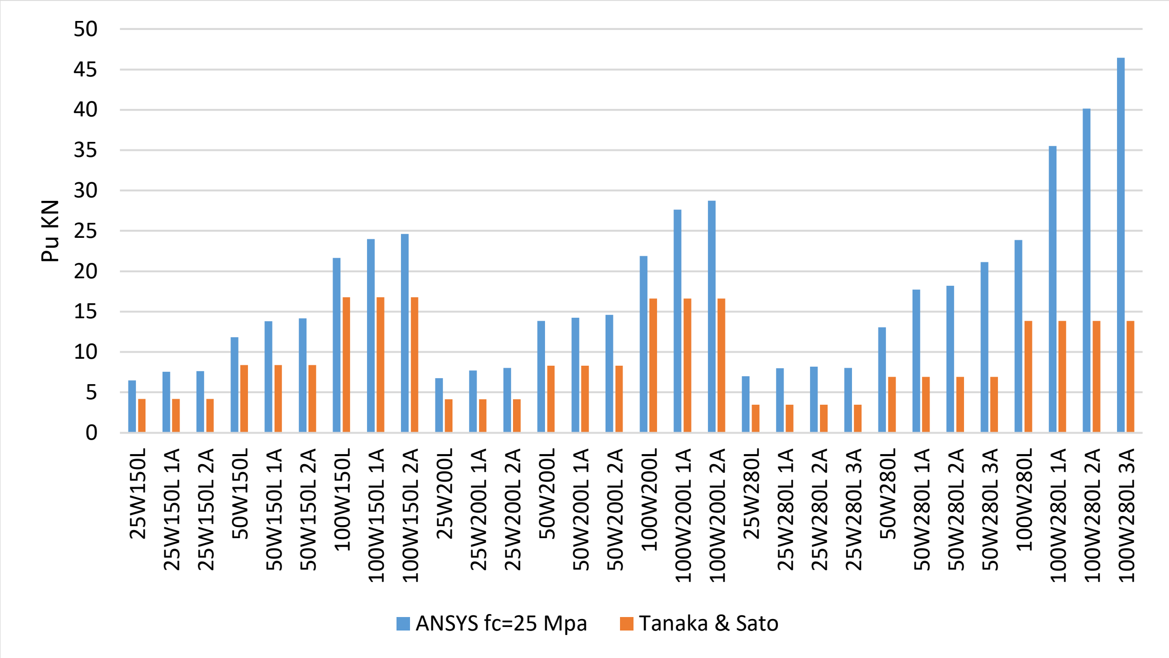

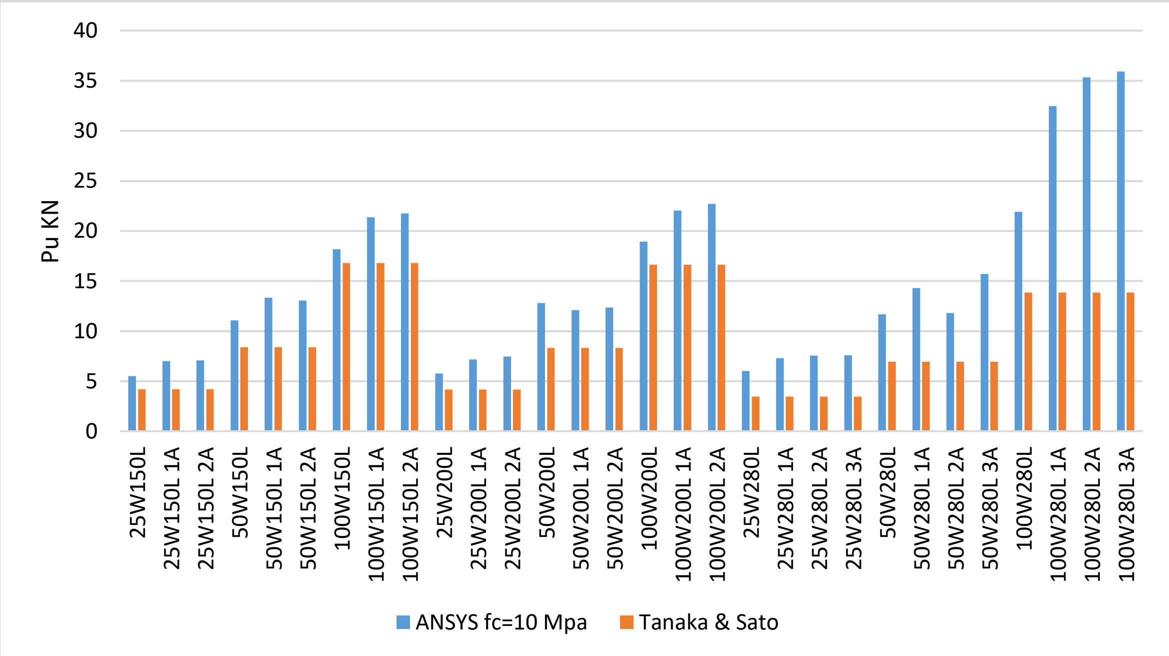

b) Tanaka and Sato model

Figure 5.1. (continued) Comparison of P_u obtained from most conveniently used models and FEA results; a) Sato model, b) Tanaka and Sato model, c) Maeda model, d) Khalifa model, e) Hiroyuki and Wu model, f) M. Iso model, g) Chen and Teng model, h) Zang and Smith model

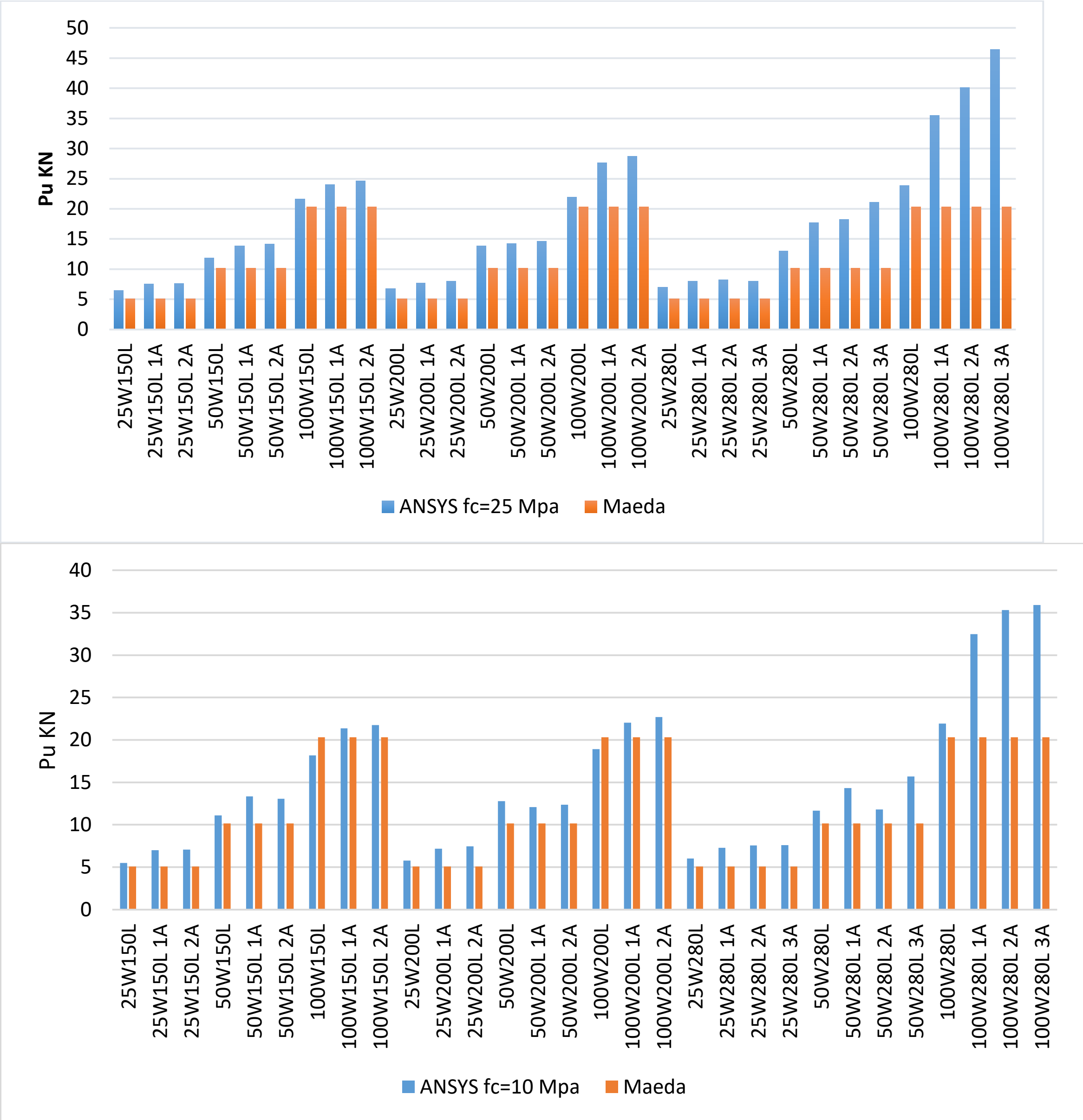

c) Maeda model

Figure 5.1. (continued) Comparison of P_u obtained from most conveniently used models and FEA results; a) Sato model, b) Tanaka and Sato model, c) Maeda model, d) Khalifa model, e) Hiroyuki and Wu model, f) M. Iso model, g) Chen and Teng model, h) Zang and Smith model

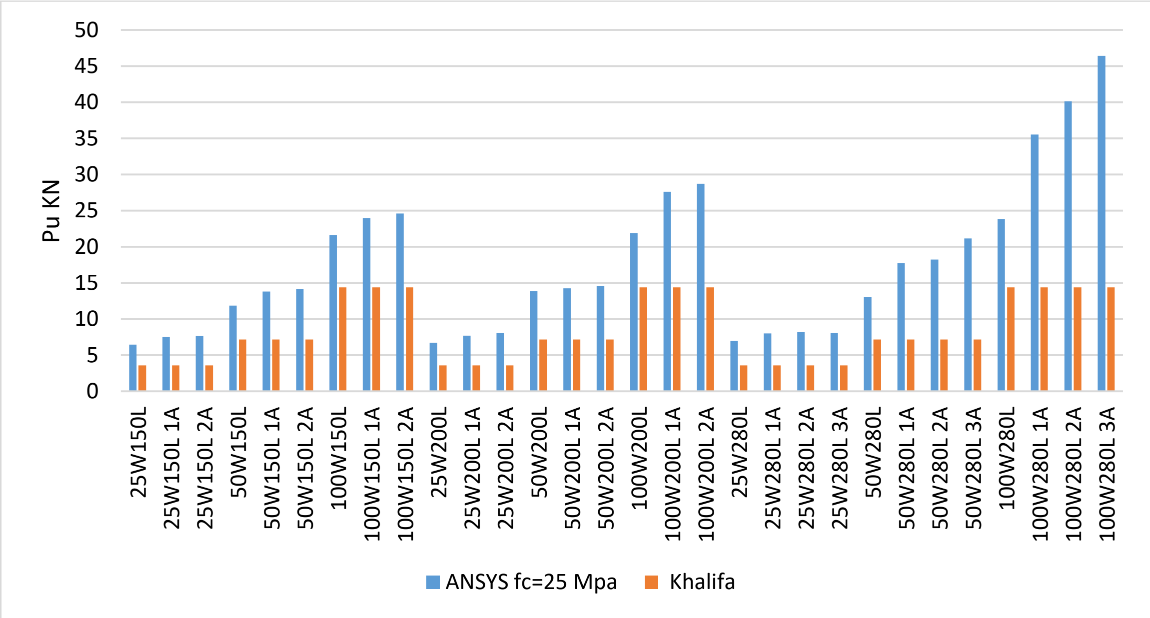

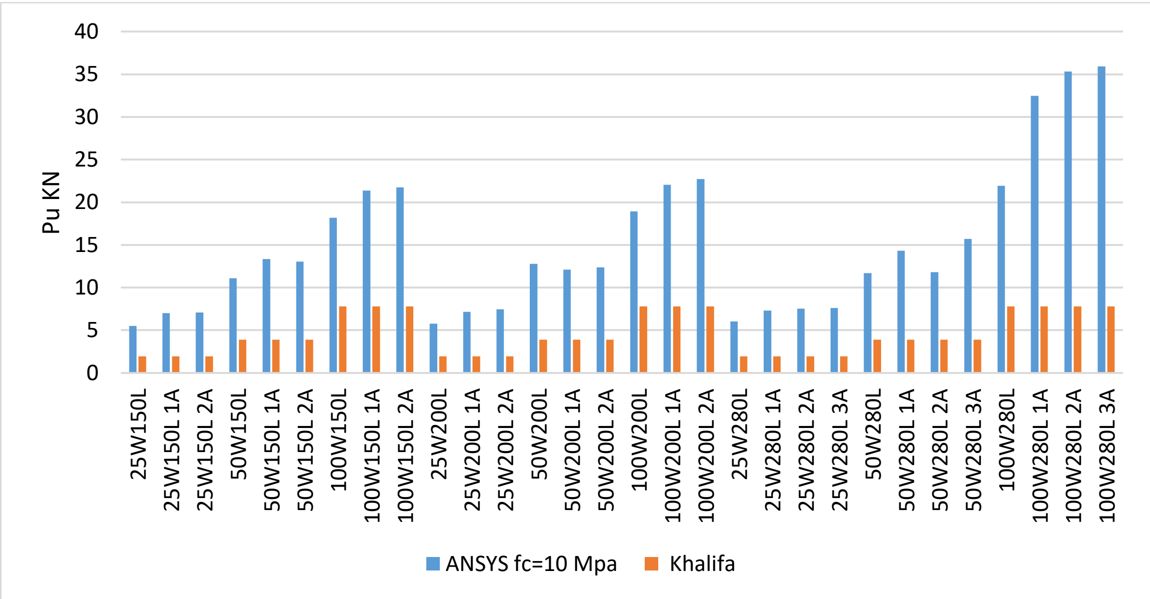

d) Khalifa model

Figure 5.1. (continued) Comparison of P_u obtained from most conveniently used models and FEA results; a) Sato model, b) Tanaka and Sato model, c) Maeda model, d) Khalifa model, e) Hiroyuki and Wu model, f) M. Iso model, g) Chen and Teng model, h) Zang and Smith model

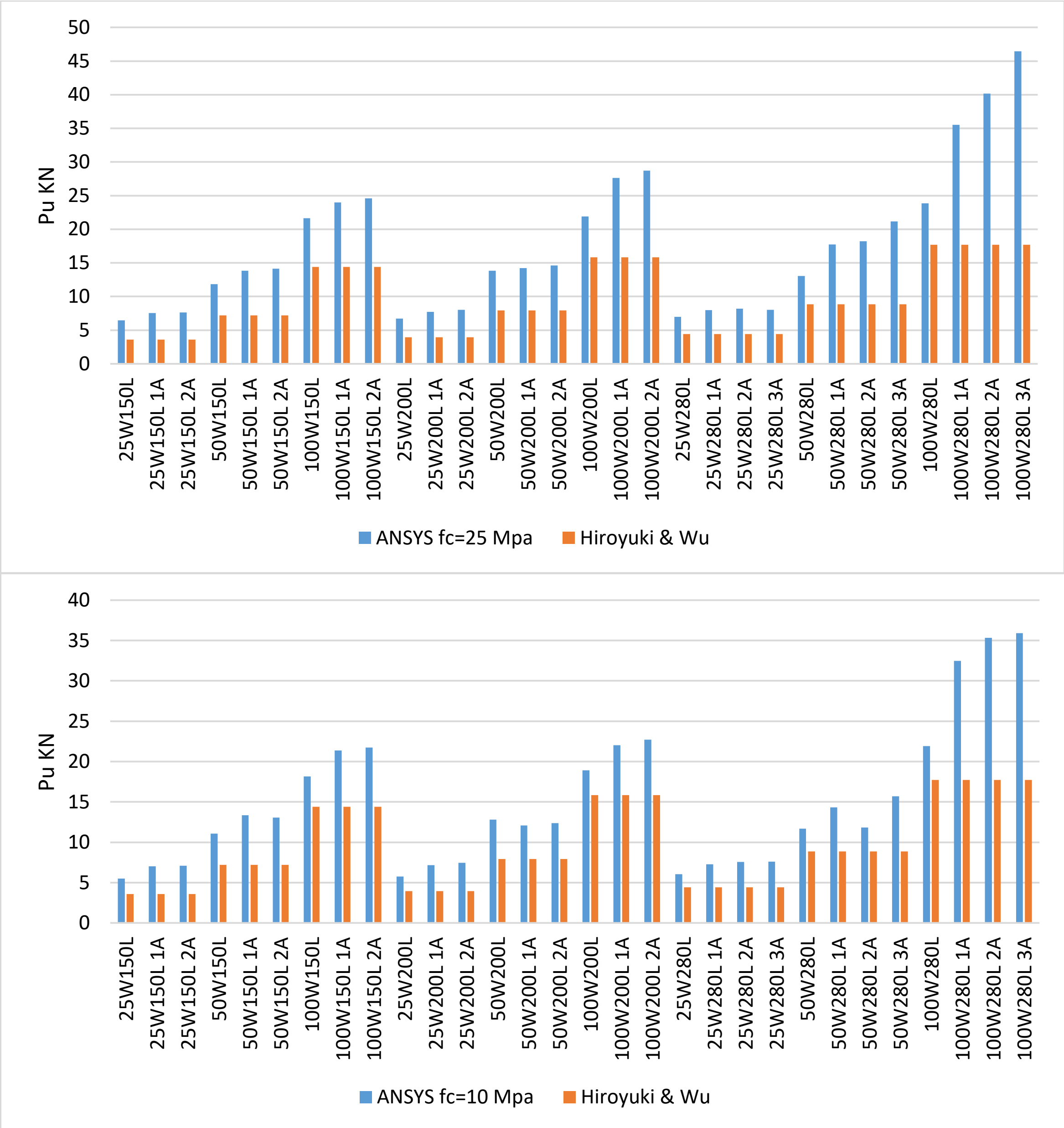

e) Hiroyuki and Wu model

Figure 5.1. (continued) Comparison of P_u obtained from most conveniently used models and FEA results; a) Sato model, b) Tanaka and Sato model, c) Maeda model, d) Khalifa model, e) Hiroyuki and Wu model, f) M. Iso model, g) Chen and Teng model, h) Zang and Smith model

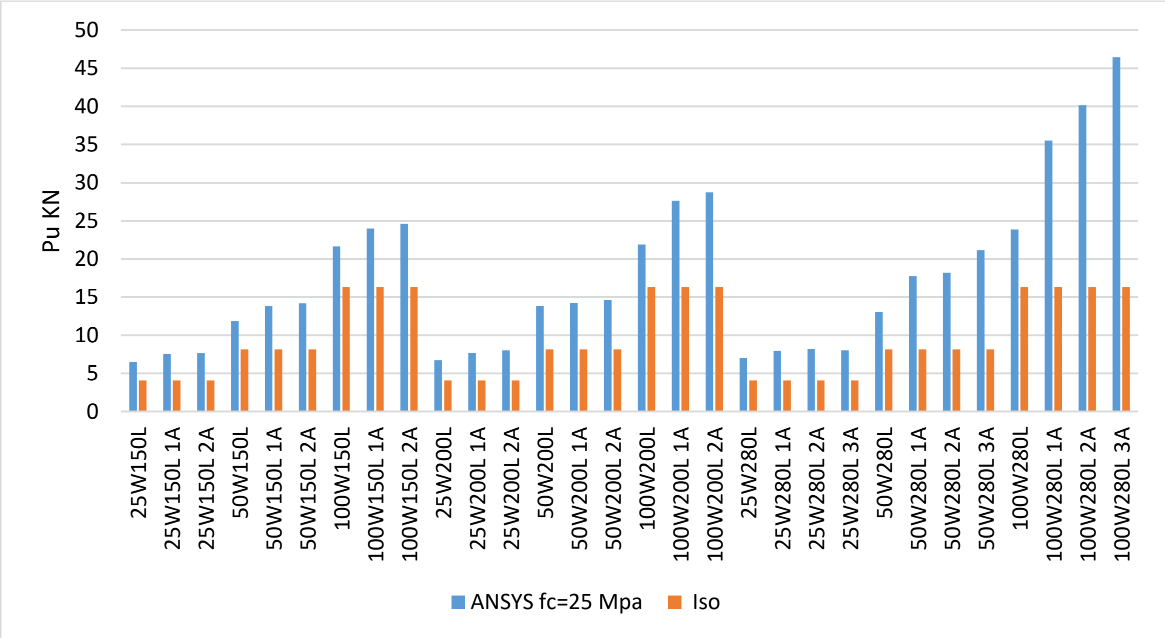

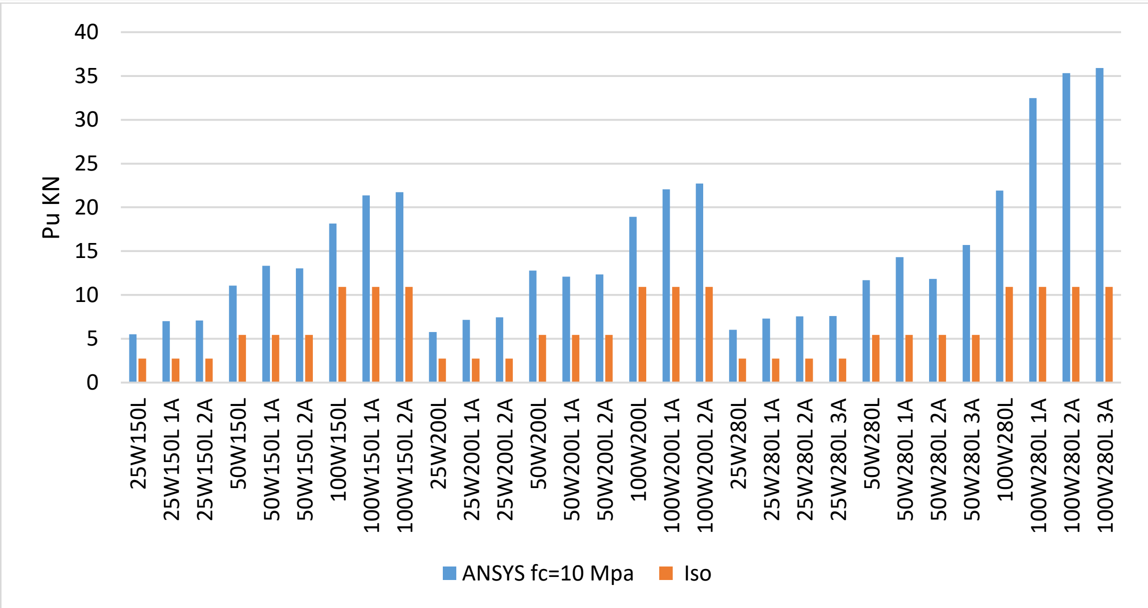

f) M. Iso model

Figure 5.1. (continued) Comparison of P_u obtained from most conveniently used models and FEA results; a) Sato model, b) Tanaka and Sato model, c) Maeda model, d) Khalifa model, e) Hiroyuki and Wu model, f) M. Iso model, g) Chen and Teng model, h) Zang and Smith model

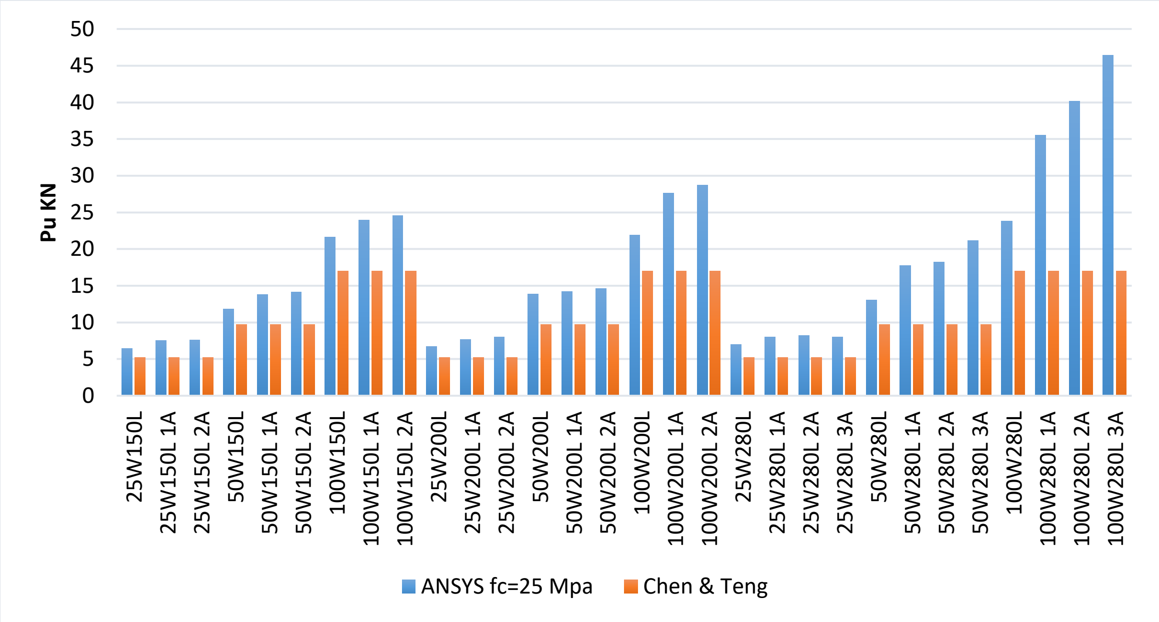

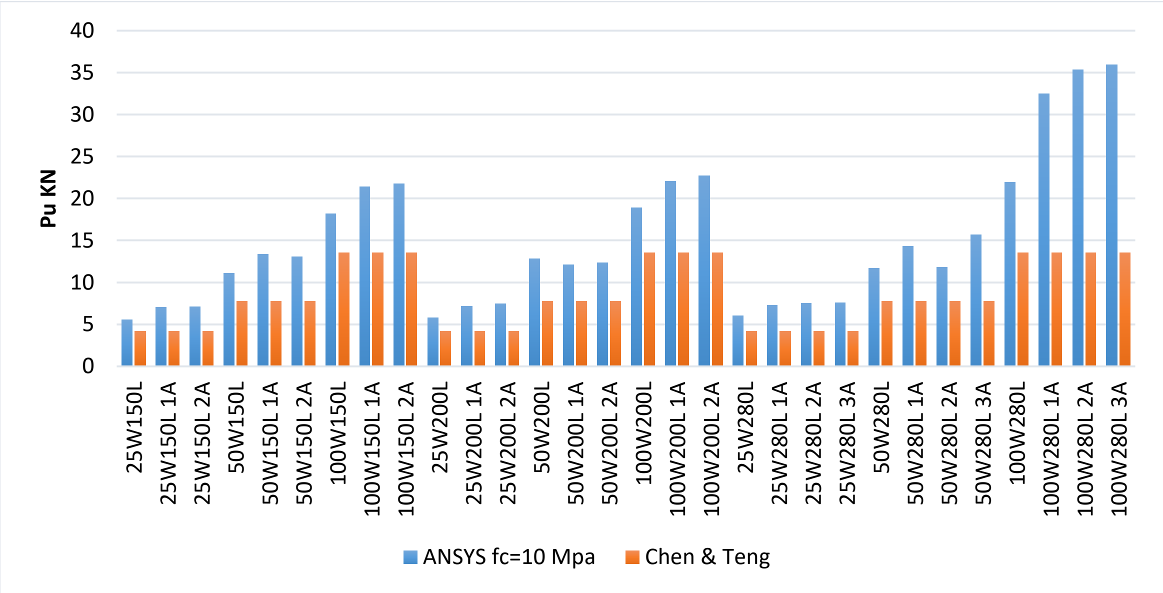

g) Chen and Teng model

Figure 5.1. (continued) Comparison of P_u obtained from most conveniently used models and FEA results; a) Sato model, b) Tanaka and Sato model, c) Maeda model, d) Khalifa model, e) Hiroyuki and Wu model, f) M. Iso model, g) Chen and Teng model, h) Zang and Smith model

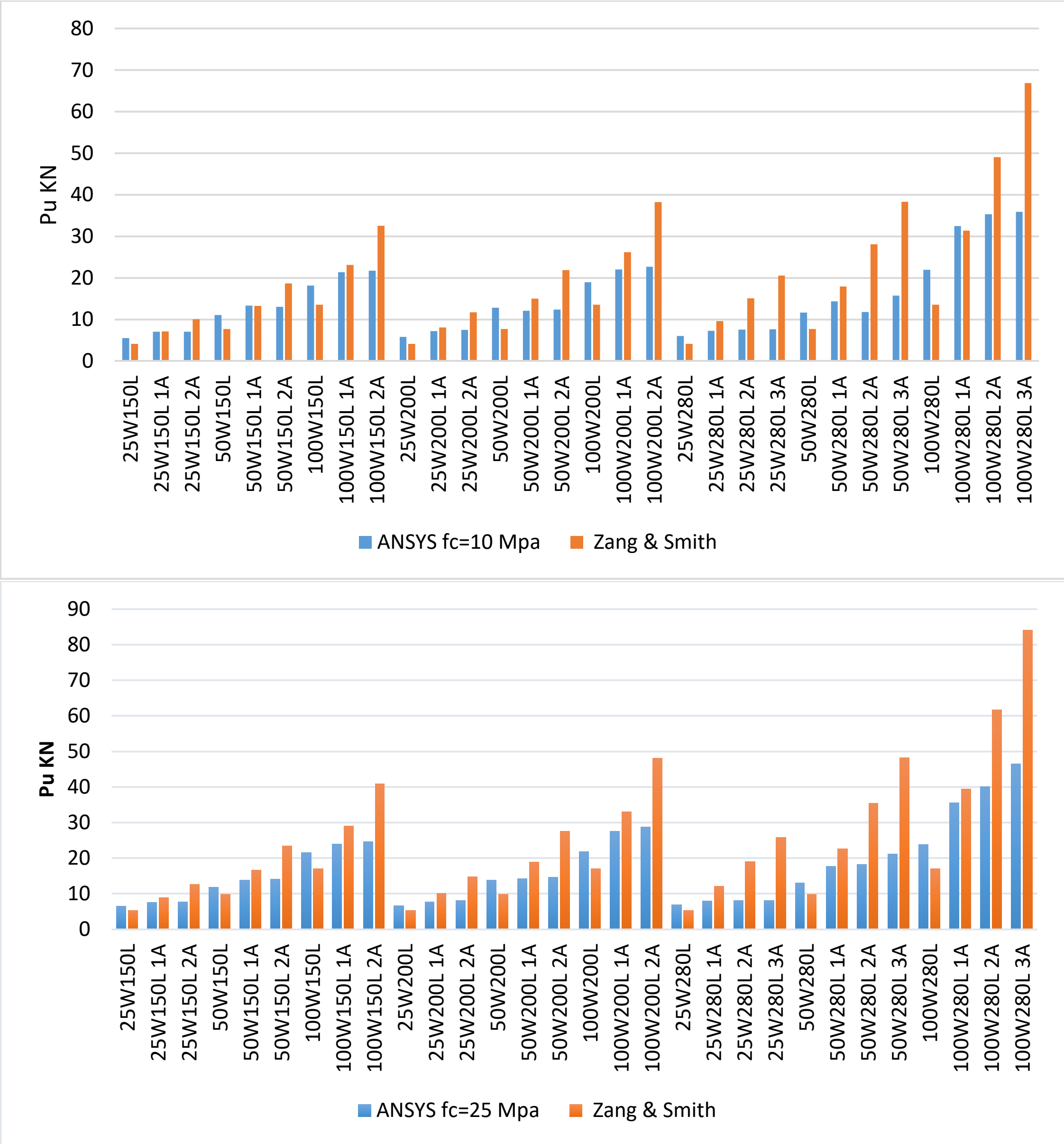

h) Zang and Smith model

Figure 5.1. (continued) Comparison of P_u obtained from most conveniently used models and FEA results; a) Sato model, b) Tanaka and Sato model, c) Maeda model, d) Khalifa model, e) Hiroyuki and Wu model, f) M. Iso model, g) Chen and Teng model, h) Zang and Smith model

5.3. Analytical Model

In the current study, the empirical model to calculate P_u was proposed based on the regression analysis of the results obtained from the analytical study. The proposed model was an enhancement of the ultimate load prediction model given by equation 9 which was originally proposed by Yuan et al. mentioned in (Lu, Teng, Ye and Jiang, 2005).

$$Pu = \beta_l b_f \sqrt{2E_f t_f G_f} \tag{5.31}$$

Most of the available models for example (Maeda, Asano, Sato, Ueda and Kakuta, 1997; Chen and Teng, 2001) for obtaining Pu did not include the length effect when L is greater than Le. Although the increment in the CFRP length has a minor effect on Pu it showed a different effect in the existence of anchors as mentioned earlier. Therefore, the current study included the modification of the bond length factor β_l when the bond length L is greater than L_e. β_l will be calculated by using equation 5.32 instead of $\beta_l = 1$ originally adopted in Yuan et al. Figure 5.2 shows the effect of bond length factor effect.

$$\beta_l = 2.178 \times 10^{-3} L + 0.742 \qquad \text{for } L > Le \tag{5.32}$$

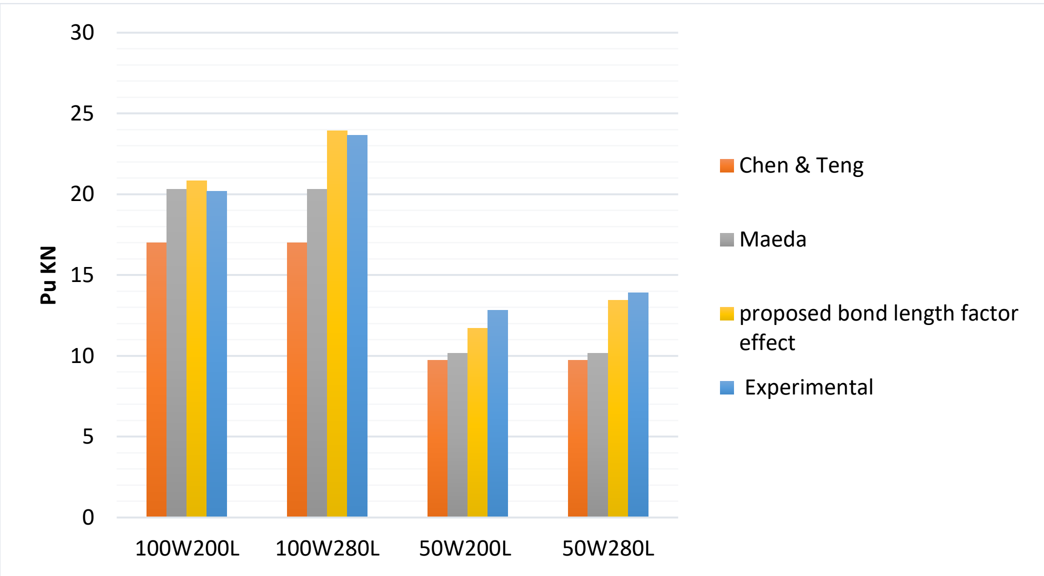

Figure 5.2. The effect of changing the bond length factor

The modification also includes the anchors effect. To specify the effect of anchors on the ultimate bonding strength, the ultimate bonding strength obtained from the analytical study were normalized by dividing the ultimate bonding strength of the anchored specimens by the ultimate bonding strength for the specimen without anchors. After that the average normalized bonding strength P_n was plotted against the number of anchors as shown in Figure 5.3 and the fitted function form was selected depending on the highest R^2 value. Figure 5.3 revealed that, there is an exponential correlation between P_n and the number of anchors with R^2=0.94.

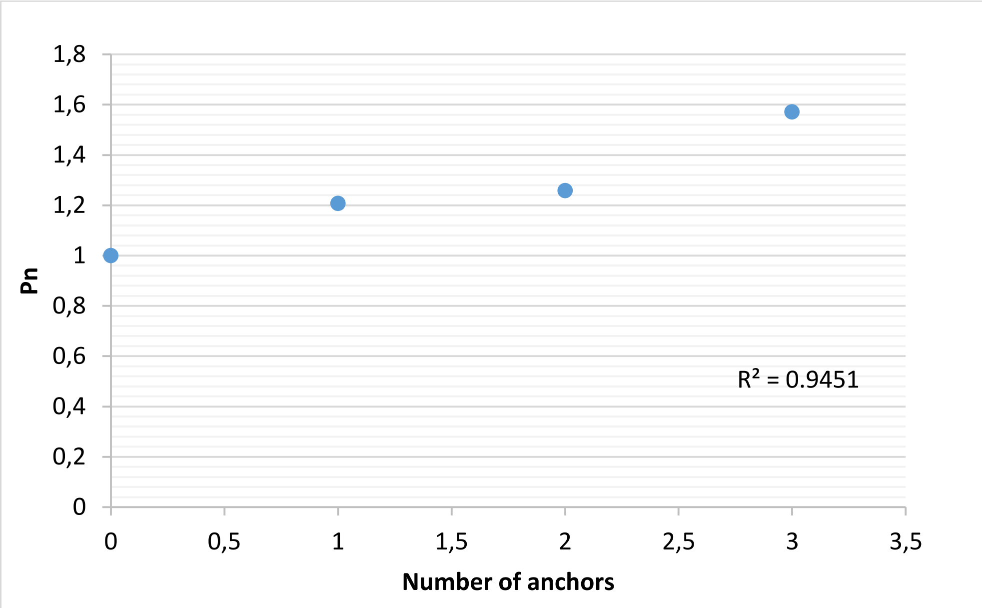

Figure 5.3. The relationship between averages normalized bonding strength and number of anchors

As a result, the ultimate bonding Capacity can be found from equation (5.33):

$$Pu = \beta_l b_f e^{0.18N}\sqrt{2E_f t_f G_f} \tag{5.33}$$

Where N represent the number of anchors. From the comparison of the P_u estimated by using the modified equation with the analytical results, it can be found that, the ultimate bond strengths predicted using the proposed model give results in close agreement with the analytical results (R^2=0.94) and perform better than the results estimated by using Zang and Smith model (R^2= 0.76) as shown in Figure 5.4(a) and (b), respectively. Figure 5.5 shows the comparison of P_u obtained from FEA results with Zang and Smith model and the proposed model.

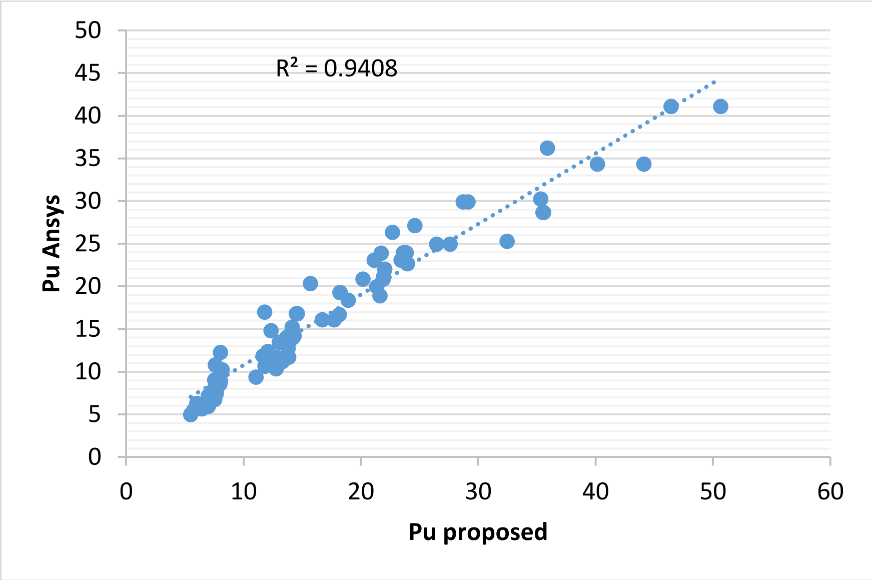

(a)

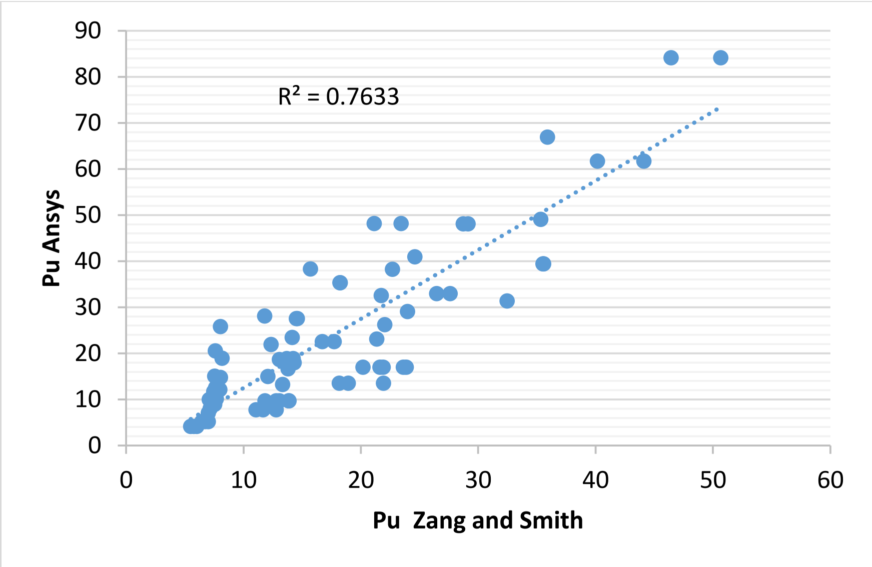

(b)

Figure 5.4. A comparison of the analytical Pu obtained by using ANSYS with the estimated Pu by using: a) proposed model b) Zang and Smith model

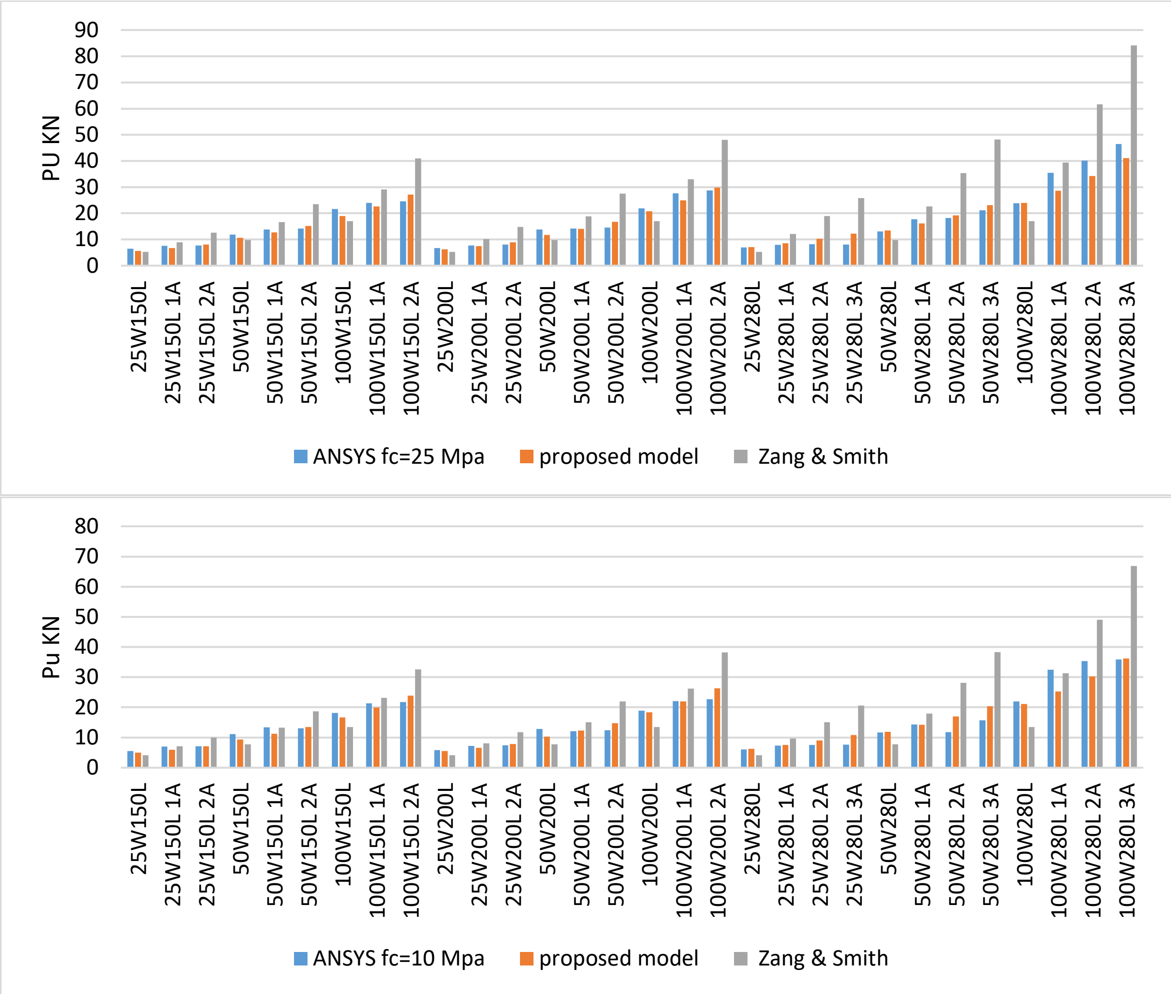

Figure 5.5. Comparison of P_u obtained from FEA results with Zang and Smith model and the proposed model

6. SUMMARY AND CONCLUSION

In the current study, a three-dimensional nonlinear finite element analysis for concrete specimens strengthened with anchored CFRP strips was conducted by using ANSYS (v.15) to evaluate the bond- slip behavior in the strengthening system. The efficiency of the strengthened system depends mainly on the behavior of the interface between concrete and CFRP. Therefore, an accurate simulation is required for the CFRP- concrete interface and the used anchor. The contact elements with a cohesive zone model (CZM) used to represent the CFRP- concrete interface. The bond-slip model proposed by Lu et al was used to calculate the required parameters for implementing the CZM model for the entire interface except for a specific area where the CFRP anchors penetrate the concrete. In this area, the bonding strength was increased to represent the effect of CFRP anchor. To simplify the simulation, the circular CFRP fan anchors are transformed to an equivalent square area in which the bond-slip model proposed by Mertoğlu et al after the modification was used for calculating the CZM parameters. The parameters of the modified bond-slip model were estimated by fitting of the finite element analysis results to the experimental results obtained from the experimental program conducted by Mertoğlu et al. The FE model was calibrated based on the experimental results and the interface behavior of a single anchored specimen was discussed. Then after, the analytical model was used for implementing additional analysis for sixty specimens to investigate the influence of several parameters which were not examined experimentally such as concrete strength, strip width, number of anchorages, bond length. Finally, the overall results were used for proposing an equation to calculate the bond strength of the anchored system. Based on the results and discussions presented in the current study, the following conclusions were obtained:

1. A simple method was produced to represent the CFRP anchor in FE analysis. This method is based on increasing the bonding strength between CFRP and concrete over a specific area where the CFRP anchor penetrates the concrete. This could be implemented by using the following proposed bilinear bond-slip model.

$$\tau_{\max\_anchor} = \tau_{max} e^{0.17N}$$

$$K_{0\_anchor} = \frac{\tau_{\max\_anchor}}{s_0}$$

$$G_{f-anchor} = \alpha G_f$$

$$\alpha = \left(\frac{b_f}{100}\right)(6.868\ln(N) + 2.5645)$$

$$S_{f-anchor} = \frac{2G_{f-anchor}}{\tau_{max-anchor}}$$

Where, s_0 represents the slip at the maximum shear stress that could be calculated by Lu et al model.

2. The analytical results obtained for the specimens that are chosen to verify the accuracy and the validity of the adopted models show that the proposed numerical simulation method is appropriate for predicting the load carrying capacity of anchored CFRP strips on a concrete surface.
3. From the parametric study it could be observed that:

- For unanchored specimens, increasing the bonding length has slightly effect on the ultimate load value. While the existence of the CFRP anchors increase the effect of the CFRP length.
- Increasing the number of anchors, increasing the ultimate bonding strength.
- Increasing the width of CFRP strip increasing the bonding strength.
- Increasing the number of anchors has no significant effect on the ultimate bonding strength when the CFRP strip width to concrete width ratio is small.
- Increasing the number of anchors has less effect on the ultimate bonding strength when decreasing the concrete compressive strength.

4. The proposed bond strength model (shown below) based on the finite element results was able to predict the bonding strength of the concrete specimens strengthened with CFRP strips and CFRP anchors more accurately than the other models.

$$Pu = B_l b_f e^{0.18N}\sqrt{2E_f t_f G_f}$$

$$B_l = 2.187 \times 10^{-3}L + 0.742 \qquad \text{for } L > L_e$$

5. The numerical study was able to predict the ultimate load more accurately in comparison to the corresponding displacement, therefore, the analytical model showed stiffer behavior. That could be attributed to the difference in concrete behavior in Ansys in comparison to concrete behavior in reality. Where the concrete behavior in Ansys is isotropic while, in reality, the aggregate distribution in concrete affecting the strain value measured by using the strain gauges mounted on the CFRP strip surface which in

role affecting the displacement value. The strain gauges Located above a crack will show higher strain value than those sits over a big aggregate.

6. In the current study, the effect of using a concrete with 25 MPa and 10 MPa on the ultimate strength was examined. Further studies could be implemented to investigate the effect of using high strength concrete on the behavior and on the ultimate strength of the anchored strengthening system. Also, further numerical studies could be conducted to investigate the effect of the distance between CFRP anchors and anchors' angle on the ultimate load and the behavior of the strengthening system. The bonding strength model suggested in the current study, including the effect of anchors' number and the effect of increasing the bonding length more than the effective length, this model could be generalized to include the effect of the distance between the anchors and the anchors' angle.

REFERENCE

Abdel Baky, H., Ebead, U. and Neale, K. (2012). Nonlinear micromechanics- based bond -slip model for FRP/concrete interfaces. *Engineering Structure,* 39, 11-23.

ACI 440.2R-08. (2008). *Guide for the design and construction of externally bonded frp systems for strengthening concrete structures.* MI: Farmington Hills.

ACI committee 318. (2011). *Building Code Requirements for Structural Concrete (318M-11).* Michigan, USA: American Concrete Institute.

Ahmed, E. S., Bakay, R. and Shrive, N. (2009). Bond strength of FRP laminates to Concrete: State-of-the-art review. *Electronic Journal of Structural Engineering*, 9, 45-61.

Al-Musawe, A., Al-Mahaidi, R. and Zaho, X. L. (2015). Effect of CFRP properties on the bond characteristics between steel and CFRP laminate under quasi-static loading. *Construction and Building Material*, 98, 489-501.

Barbero, E. J. (2014). *Finite element analysis of composite materials using ansys* (Second Edition ed.). New York: CRC Press, 273-276.

Belarba, A., Acun, B. (2013). FRP Systems in Shear Strengthening of Reinforced Concrete Structures. *11th International Conference on Modern Building Materials, Structures and Techniques, MBMST 2013,* University of Houston, Vilnius, Lithuania, 2-8.

Brena, S. F., McGuirk, G. N. (2013,). Advances on the behavior characterization of FRP-anchored carbon fiber-reinforced Polymer (CFRP) sheets used to strengthen concrete elements. *International Journal of Concrete Structures and Materials,* 7(1), 3-16.

Büyüköztürk, O., Yu, T.Y. (2006). *Understanding and Assessment of Debonding Failures in FRP-Concrete Systems.* Seventh International Congress on Advances in Civil Engineering, İstanbul.

Buyukozturk, O., Gunes, O. and Karaca, E. (2004). Progress on understanding debondng problems in reinforced concrete and steel members strengthened using FRP composites. *Construction and Building Materials*, 18(1), 9-19.

Ceroni, F., Pecce, M., Matthys, S. and Taerwe, L. (2008). Debonding strength and anchorage devices for reinforced concrete elements strengthened with FRP sheets. *Composites Part B: Engineering,* 39(3), 429-441.

Chen, J. F., Teng, J. G. (2001). Anchorage strength models for FRP and steel plates bonded to concrete. *Journal of Structural Engineerring,* 127(7), 784-791.

Dai, J., Ueda, T. and Sato, Y. (2005). Development of the nonlinear bond stress-slip model of fiber reinforced plastics sheet-concrete interfaces with simple method. *Journal of Composite for Construction,* 9(1), 52-62.

Desayi, P., Krishnan, S. (1964). Equation for the stress-strain curve of concrete. *Journal of the American Concrete Institute,* 61, 345-350.

Ferracuti, B., Mazzotti, S. and Mazzotti, C. (2007). Interface law for frp–concrete delamination. *Composite structures,* 80(4), 523-531.

Grelle, S. V., Sneed, L. H. (2013). Review of anchorage systems for externally bonded FRP laminates. *International Journal of Concrete Structures and Materials,* 7(1), 17-33.

Holmer, N. P. (2010). *Parametric study of the bond between fiber reinforced polymers and concrete using finite element analysis.* Master Thesis, Marquette University, Wisconsin, 46-48.

Hosseini, A., Mostofinejad, D. (2013). Experimental investigation into bond behavior of CFRP sheets attached to concrte using EBR and EBROG techniques. *Journal of Composites Part B,* 15, 130-139.

İnternet: Kim, N., Shin, Y. S., Choi, E. and Kim, H. S. (2015, May). Relationships Between interfacial Shear Stresses and Moment Capacities of RC Beams Strengthened with Various Types of FRP Sheets. URL: http://www.webcitation.org/query?url=http%3A%2F%2Fdx.doi.org%2F10.1016%2Fj.conbuildmatanddate=2018-05-22. Retrieved From 05.07.2015.

İnternet: Rvendran, A., Perera, D. and Gamage, J. (2016). Finite element analysis of CFRP strengthened concrete beams. URL: http://www.webcitation.org/query?url=https%3A%2F%2Fwww.researchgate.net%2Fpublication%2F311230295_Finite_Element_Analysis_of_CFRP_Strengthened_Concrete_Beamsanddate=2018-05-22. Retrieved From 10.05.2017.

Issa, M. A., Rahma, M. and Alrousan, R. (2016). Prediction of ultimate load at the CFRP-concrete interface under pure shear mode. *Journal of Composite Material,* 6(6), 183-195.

Kachlakev, D. I., Miller, T. H., Potisuk, T., Yim, S. C. and Chansawat, K. (2001). Finite element modeling of reinforced concrete structures strengthened with FRP laminates- final report. *Oregon Department of Transportation Research Group and Federal Highway Administration Report*. Washington. 21-23.

Kalfat, R., Al-Mahaidi, R. and Smith, S. (2013). Anchorage devices used to improve the performance of reinforced concrete beams retrofitted with FRP composites: State-of-the-art review. *Journal Of Composites For Construction*, 17(1), 14-33.

Khalifa, A. M. (2016). Flexural performance of RC beams strengthened with near surface mounted CFRP strips. *Alexandria Engineering Journal*, 55, 1497-1505.

Khalifa, A., Gold, W. J., Nanni, A. and M.I, A. (1998). Contribution of externally bonded FRP to shear capacity of flexural members. *Journal of Composites for Construction,* 2(4), 195-203.

Ko, H., Matthys, S., Palmieri, A. and Sato, Y. (2014). Development of a simplified bond stress-slip model for bonded FRP-concrete interfaces. *Construction and Building Materials,* 68, 142-157.

Koutas, L., Triantafillou, T. C. (2013). Use of anchors in shear strengthening of reinforced concrete T-beams with FRP. *Journal of Composites for Construction,* 17(1), 101-107.

Lu, X., Teng, J., Ye, L. and Jiang, J. (2005). Bond–slip models for FRP sheets/plates bonded to concrete. *Engineering Structures*, 27, 920–937.

Maeda, T., Asano, Y., Sato, Y., Ueda, T. and Kakuta, Y. (1997). A Study on Bond Mechanism of Carbon Fiber Sheet. *Non-Metallic (FRP) Reinforcement for Concrete Structures, Proceedings of the Third Symposium,* Japan, 1, 279-286.

Mertoğlu, Ç., Anıl, Ö. and Durucan, C. (2016). Bond slip behavior of anchored CFRP strips on concrete surfaces. *Construction and Building Material,* 123, 553-564.

Mustafa, A., Razaqpur, A. G. (2013). CFRP Anchor for Preventing Premature Debonding of Externally Bonded FRP Laminates from Concrete. *Journal of Composites for Construction*, 17(5), 641-650.

Naser, M., Hawileh, R., Abdalla, J. A. and Al-Tamimi, A. (2012). Bond behavior of CFRP cured laminates: Experimental and numerical investigation. *Journal of Engineering Materials and Technology*, 134(2), 1-9.

Niemitz, C., James, R. and Breña, S. (2010). Experimental behavior of carbon fiber-reinforced polymer (CFRP) sheets attached to concrete surfaces using CFRP anchors. *Journal of Composites for Construction*, 14(2), 185-194.

Obaidat, Y. T. (2011). *Structural retrofitting of concrete beams using debonding issues*. Ph.D. Thesis, Lund University, Sweden, 22-24.

Obaidat, Y. T., Heyden, S. and Dahlblom, O. (2013). Evaluation of parameters of bond actin between FRP and concrete. *Composite for Structure*, 17(5), 626-635.

Obaidat, Y., Heyden, S. and Dahlblom, O. (2010). The effect of CFRP and CFRP/concrete interface model when modelling retofitted RC beams with FEM. *Compos Structure*, 92(6), 1391-1398.

Orton, S. L. (2007). *Development of a CFRP system to provide continuity in existing reinforced concrete building vulnerable to progressive collapse.* Ph.D. Thesis, university of Taxas, Austin, 55-57.

Orton, S. L., Jirsa, J. O. and Bayrak, O. (2008, December). Design considerations of carbon fiber anchors. *Journal Of Composites For Construction*, 12(6), 608-616.

Ozbakkaloglu, T., Fang, C. and Gholampour, A. (2017). Influence of FRP anchor configuration on the behavior of FRP plates externally bonded on concrete members. *Engineering Sructure,* 133, 133-150.

Propvics, S. (1970). A review of stress-strain relationships of concrete. *ACI*, 67(3), 243-248.

Rasheed, H. A. (2015). *Strengthening design of reinforced concrete with FRP*. New York: Taylor and Francis Group, 41-44.

Saenz, L. (1964). Discussion equation for the stress - strain curve of concrete, *ACI*, 61, 1229–35.

Smith, S. T., Teng, J. G. (2002). FRP-strengthened RC beams. I: Review of debonding strength models. *Engineering Structure,* 24(4), 385-395.

Sun, W., Ghannoum, W. (2015). Modeling of anchored CFRP strips bonded to concrete. *Construction and Building Materials,* 85, 144-156.

Teng, J. G., Chen , J. F., Smith, S. T. and Lam, L. (2002). *FRP strengthened RC structures.* West Sussex: Wiley, 13-16.

Teng, J. G., Smith, S. T., Yao, J. and Chen, J. F. (2003). Intermediate crack-induced debonding in RC beams and slabs. *Construction and Building Materials*, 17(6-7), 447-462.

Waseem, M., Kumar, K. (2014). Finite element modeling for delamination analysis of double cantilever beam specimen. *SSRG International Journal of Mechanical Engineering,* 1(5), 27-33.

Yılmaz, T., Arslan, B. and Anıl, Ö. (2018). Nonlinear FEA of mechanical anchorages on CFRP-to-concrete bonded joint. *Magazine of Concrete Research*, in Press.

Zhang, H. W., Smith, S. T. (2012). FRP-to-concrete joint assemblages anchored with multiple FRPanchor. *Composite Structure,* 94, 403-414.

Zidani, M. B., Belakhdar, K., Tounsi, A. and Bedia, E. A. (2015). Finite element analysis of initially damaged beams repaired with FRP plates. *Composite Structures,* 134, 429-439.

CURRICULUM VITAE

Personal Information

Surname, Name:	SAKIN, Shaimaa
Nationality:	Iraqi
Birthdate:	13.06.1982, Wasit
Marital Status:	Single
Telephone No.:	00905398875511
E-MAIL	shtsakin@yahoo.com

Education

Degree	Education Unit	Date of graduation
PhD.	Gazi University/ F. B. E.	Continues
Master	University of Technology/ Structural Engineering/ Baghdad/ Iraq.	2008
Bachelor	Al-Mustansiriya University/ Civil Engineering/ Baghdad/ Iraq.	2004
High school	Al- Khoulod High school/ Baghdad/ Iraq	2000

Work Experience

Year	Place	Position
2010- present	College of Engineering/Al-Mustansiriya University, Baghdad/ Iraq	Assistant Lecturer
2009-2010	College of Pharmacy/Al-Mustansiriya University, Baghdad/ Iraq	Assistant Engineer
2006-2009	Office of Engineering /Al-Mustansiriya University, Baghdad/ Iraq	Assistant Engineer

Foreign Languages

English,

Turkish

Publications

Sakin, S. (2014). Punching Shear in Voided Slab. *Civil and Environmental Research, 6*(10).

Abbas, A. N., Muhammed, N. J., and Sakin, S. (2014). Effect of the Distance between Points Load on the Behavior of Strengthened Reinforced Concrete Beams. *Chemistry and Materials Research*, 6(8).

Kareem, S., Sakin, S., and Yousif, M. (2013). Non-linear FE modeling of tow-way Reinforced Concrete Slab of NSC, HSC and LWC under Concentrated Load. *Journal of Engineering and Development*, *17*(2), 243-254.

Husain , H. M., Hamood , M. J., and Sakin, S. (2009). Analysis Up To Failure Of Straight And Horizontally Curved Composite Precast Beam And Cast-In-Place Slab With Partial Interaction. *Engineering and Technology Journal, 27*(13), 2509-2522.

Hobbies

Drawing

GAZİ GELECEKTİR...